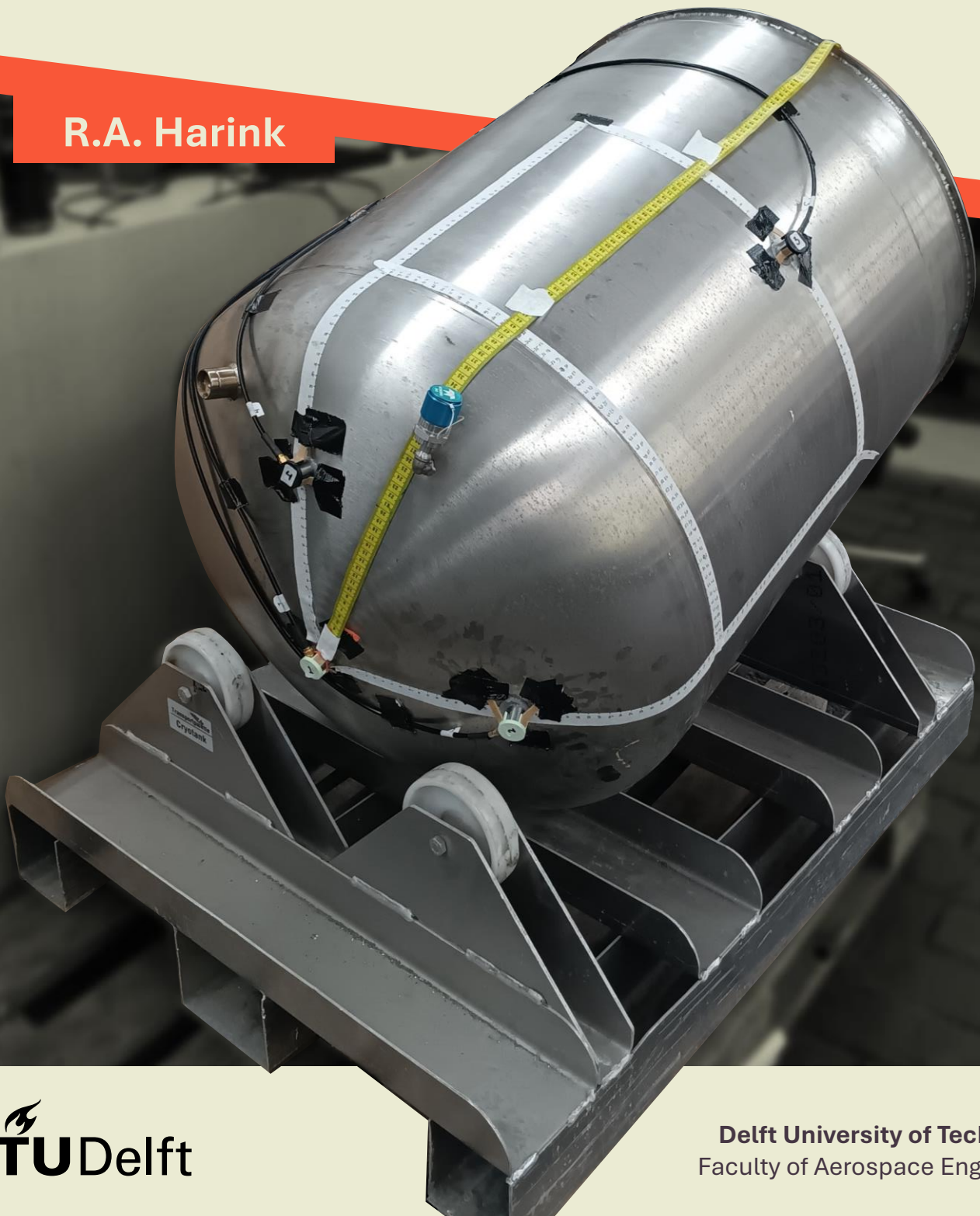


LISTENING TO LIQUID HYDROGEN TANKS

*A feasibility study into localising damage in
double-walled tanks using acoustic emission*

R.A. Harink



Listening to liquid hydrogen tanks

**A feasibility study into localising damage in double-walled tanks
using acoustic emission**

MASTER OF SCIENCE THESIS

For obtaining the degree of Master of Science in Aerospace Engineering
at Delft University of Technology

R.A. Harink

25th of October 2024

The work in this thesis was supported by SHM Next and SAG. Their cooperation is gratefully acknowledged.



Copyright © R.A. Harink
All rights reserved.

DELFT UNIVERSITY OF TECHNOLOGY
FACULTY OF AEROSPACE ENGINEERING
DEPARTMENT OF AEROSPACE STRUCTURES AND MATERIALS

GRADUATION COMMITTEE

Dated: 25th of October 2024

Chair holder:

_____ Dr.ir. J.A. Pascoe

Committee members:

_____ Dr. N. Yue

_____ Dr.ir. O.K. Bergsma

_____ Dr. D. Tajari

Abstract

To facilitate the transition to liquid hydrogen (LH2) as an alternative aircraft fuel, the storage tanks need to be closely monitored to allow for safe operation. This research explores the feasibility of using an acoustic emission-based structural health monitoring method to detect and localise simulated damage on a metal double-walled vacuum insulated tank. The complicated inner and outer tank geometry makes it a novel application of an established method.

To be able to perform experiments, a metal double-walled vacuum insulated tank with a fixed and flexible support was cut in half to make the inner tank accessible. Pencil lead break tests were performed on the inner and outer tank and recorded by lead zirconate titanate (PZT) sensors to assess localisation accuracy. It was found that a pencil lead break (PLB) performed on the inner tank could be detected by a sensor placed on the outer tank. Subsequently, an accuracy of 80% was achieved in making the distinction whether the PLB was located on the inner or outer tank. For the PLBs placed on the inner tank a 1D localisation accuracy of 17 [mm] and 21 [mm] was achievable for the flexible and fixed support respectively. For the outer tank a 1D localisation accuracy of 46 [mm] was achievable, while for 2D localisation this was 41 [mm].

It is concluded that with sensors placed solely on the outer tank, both the inner and outer tank can be monitored. Additionally, simulated damage on the inner and outer tank could be localised with an accuracy below 10% of the tank's dimension. Therefore, based on the feasibility study performed, acoustic emission-based structural health monitoring is deemed a viable method to enhance the reliability and safety of metal double-walled vacuum insulated LH2 tanks.

Table of Contents

Acknowledgments	xix
List of symbols	xxiii
Introduction	xxv
1 Literature Review	1
1.1 The need for cleaner aviation fuels	1
1.2 Hydrogen as a clean aviation fuel	2
1.3 The liquid hydrogen tank	3
1.3.1 Temperature control	3
1.3.2 Cryogenic proof material selection	6
1.4 Challenges for the liquid hydrogen tank	7
1.4.1 General challenges	7
1.4.2 Structural integrity degradation due to the presence of liquid hydrogen	8
1.5 Liquid hydrogen tank inspection	9
1.5.1 Challenges for the inspection and maintenance of liquid hydrogen tanks	10
1.5.2 Structural health monitoring as a solution	10
1.6 Structural Health Monitoring Methods	12
1.6.1 Deformation monitoring	12
1.6.2 Structural damage monitoring	12
1.7 Acoustic Emission Testing	14
1.7.1 The basic principles of acoustic emission testing	15
1.7.2 Acoustic emission detectable events	15
1.7.3 Acoustic emission testing in cryogenic temperatures	16
1.7.4 Acoustic emission sensors	16
1.8 Technical background on Lamb waves	19

1.8.1	S0 and A0 waves	19
1.8.2	Wave attenuation	19
1.9	Acoustic emission testing techniques	22
1.9.1	Signal onset determination techniques	22
1.9.2	Signal end determination	25
1.9.3	Source localisation techniques	25
1.9.4	Source classification principles	28
1.10	Representative experiments	28
1.10.1	Relevant Acoustic Emission Testing Experiments	28
1.10.2	Representative signals	30
1.10.3	Modelling crack growth with Pencil Lead Break tests	33
1.11	Representative environment	34
1.11.1	Sources of noise	34
1.11.2	Liquid hydrogen-related noise	35
1.11.3	Structural noise	36
1.11.4	Solutions to minimize the influence of noise	38
2	Research scope	41
3	Method	43
3.1	Method overview	43
3.2	Experiment setup	45
3.2.1	LH2 tank test setup	45
3.2.2	PLB location measurements	47
3.2.3	Selected frequency for measurements	48
3.2.4	Measuring equipment	48
3.3	Signal onset determination	50
3.3.1	Threshold crossing and AIC method	50
3.3.2	Identifying the signal onset of S0 and A0 waves	51
3.3.3	Used TC and AIC settings	51
3.4	Experiment 1: Signal feasibility	52
3.4.1	Experiment details	52
3.4.2	AE signal attenuation	54
3.5	Noise and signal distinction	55
3.6	Experiment 2: Inner or outer tank distinction	56
3.6.1	Experiment details	56
3.6.2	Influence of noise on distinction accuracy	57
3.7	Experiment 3: Inner tank damage localisation	57
3.7.1	Experiment details	57
3.7.2	Localisation input determination	59

3.7.3	Localisation accuracy	59
3.8	Experiment 4a: Outer tank damage 1D localisation	62
3.8.1	Experiment details	62
3.8.2	Localisation input determination	64
3.8.3	Localisation accuracy	65
3.9	Experiment 4b: Outer tank damage 2D localisation	65
3.9.1	Experiment details	65
3.9.2	Localisation accuracy	66
4	Results and Discussion	69
4.1	Experiment 1: Signal feasibility	69
4.1.1	Feasibility of a signal travel path through the support	69
4.1.2	AE signal attenuation	71
4.1.3	Sensor placement on the complete tank	73
4.2	Experiment 2: Inner or outer tank distinction	74
4.2.1	Simulated damage on the inner tank	74
4.2.2	Simulated damage on the outer tank	75
4.2.3	Method sensitivity, precision and accuracy	75
4.2.4	Influence of noise on method accuracy	76
4.3	Experiment 3: Inner tank damage localisation	77
4.3.1	Localisation input determination	77
4.3.2	Localisation accuracy	78
4.4	Experiment 4a: Outer tank damage 1D localisation	83
4.4.1	Localisation input determination	84
4.4.2	Localisation accuracy experiment part 1	84
4.4.3	Localisation accuracy experiment part 2	87
4.5	Experiment 4b: Outer tank damage 2D localisation	89
4.5.1	Localisation accuracy	89
4.5.2	Localisation accuracy optimisation	90
4.5.3	Sensitivity study	90
4.6	Influence of experiment limitations	91
4.6.1	Effect of an entire tank setup with respect to the half-tank test setup	91
4.6.2	Effect of experiments at room temperature with respect to cryogenic temperatures	92
4.6.3	Effect of simulated damage with respect to real damage	93
4.6.4	Effect of vacuum between the inner and outer tank	93
5	Conclusion	95
5.1	Recommendations for future work	97
	References	97

References	99
A Examples of received AE waves	111
B Examples of signal onset determination	113
C AE characteristics of crack growth in different materials	115
C.1 AE characteristics in aluminium	115
C.2 AE characteristics in steel	116
C.3 AE characteristics in composites	117
D One-way sensitivity studies on inner tank damage localisation	119
E Monte Carlo simulations	121
E.1 Experiment 3: Inner tank damage localisation	121
E.1.1 Flexible support test setup	121
E.1.2 Fixed support test setup	122
E.2 Experiment 4a part 1: Outer tank 1D damage localisation	123
E.3 Experiment 4a part 2: Outer tank 1D damage localisation on a 2D area	123
E.4 Experiment 4b: Outer tank 2D damage localisation	124
F Influence of vacuum on the localisation accuracy	127

List of Figures

1.1	Graphical representation of an LH2 tank proposed by Airbus [1].	5
1.2	Graphical representation of a spring-based flexible support. Adapted from [2]. . .	5
1.3	The effect of temperature on the relative fracture toughness of various materials. Adapted from [3].	8
1.4	The change in Young's modulus with temperature for aluminium alloy 2219. Adapted from [4].	16
1.5	Graphical representation of symmetric and anti-symmetric waves in a plate. Adapted from [5].	19
1.6	The effect of type of insulation adhesion on the wave attenuation [6].	21
1.7	The effect of propagation distance on rise time due to dispersion [7].	21
1.8	Graphical representation of two AE signal localisation techniques. Adapted from [8].	26
1.9	Graphical representation of sensor mounting for double-walled stationary tank. Adapted from [9].	30
1.10	Amplitude and frequency of fatigue crack induced acoustic emission signals (type 1 and type 2). The type 3 signal refers to machine noise. The solid line is the line of interest and refers to the signal that the transducer has registered [6].	32
1.11	Frequency ranges of AE signals generated by aluminium, steel and composites. More information and sources can be found in Appendix C.	33
1.12	Graphical representation of a PLB test. Adapted from [10].	34
1.13	Noise spectrum resulting from a Macchi MB 326 operating at full power [11]. . .	38
1.14	The UniQ of SHM Next applied to a bridge [12].	39
2.1	Flowchart indicating the scope of this thesis.	42
3.1	Flowchart indicating the steps taken in the experiments and other research involved in this thesis.	44
3.2	Graphical representation of the tank used in the experiments. The dotted line indicates where the tank was cut. (Not to scale.)	45

3.3	The tank test setups used in the experiments.	46
3.4	Pipes and other elements on the fixed support test setup.	46
3.5	Graphical representation of the geometry of the two supports (not to scale).	47
3.6	Measurement system used to determine the PLB locations.	48
3.7	Sensitivity per frequency of Mistras' R15 α sensors [13].	49
3.8	Photo of the designed sensor holder in use.	49
3.9	Amplifier gain used in the experiments.	50
3.10	Graphical representation of the test setups for experiment 1 (not to scale).	53
3.11	Graphical representation of the two possible travel paths to sensor 1 (not to scale).	54
3.12	Photo of the welded joint between the half sphere and the cylinder that together make half a tank (flexible support test setup).	55
3.13	Graphical representation of the test setup for experiment 2 (not to scale).	56
3.14	Graphical representation of the test setup for experiment 3 (not to scale).	58
3.15	Graphical representation of the simplified travel path (indicated in red) from a PLB on the inner tank to sensor 1 and 3 (not to scale).	60
3.16	Graphical representation of the test setup for experiment 4a part 1 (not to scale).	63
3.17	Graphical representation of the test setup for experiment 4a part 2 (not to scale).	64
3.18	Graphical representation of the test setup for experiment 4b on a quarter of the half tank test setup (not to scale).	66
3.19	2D localisation examples with graphical representation of time of arrival circles.	67
4.1	Determination whether the signal travels through the flexible support or via the cut edge. Total number of PLBs: 102.	70
4.2	Determination whether the signal travels through the fixed support or via the cut edge. Total number of PLBs: 69.	71
4.3	Maximum amplitude for the different sensors at varying PLB locations on the inner tank.	71
4.4	Sizes of the flexible and fixed supports.	72
4.5	Maximum amplitude for the different sensors at varying PLB locations on the outer tank. Total number of PLBs: 70.	72
4.6	Graphical representation of the sensor placement on the complete tank (not to scale).	74
4.7	Predicted PLB locations (inner (IT) or outer tank (OT)) where the actual location is on the inner tank. Total number of PLBs: 69.	74
4.8	Predicted PLB locations (inner (IT) or outer tank (OT)) where the actual location is on the outer tank. Total number of PLBs: 70.	75
4.9	Influence of signal-to-noise ratio on inner/outer tank distinction accuracy based on A0 waves.	76
4.10	Group velocity diagram for the 4 [mm] thick stainless steel used in the LH2 tank. The A0 and S0 group velocity is indicated and the frequency used in the experiments is indicated with a red vertical line.	77
4.11	Localisation of PLBs on the inner tank on the flexible support test setup. Every point represents the mean of 10 PLBs and the error bar represents the standard deviation.	79

4.12	Localisation using the calculated wave velocity and support travel time. Every point represents the mean of 10 PLBs and the error bars represent the standard deviation.	79
4.13	Localisation of PLBs on the inner tank of the flexible support test setup, using three different rounds of data gathering. In between the rounds the sensors are detached and re-attached. Every point represents one PLB.	81
4.14	Localisation of PLBs on the inner tank based of the fixed support test setup, using two different rounds of data gathering. In between the rounds the sensors are detached and re-attached.	81
4.15	Localisation of PLBs on the outer tank using sensors 1 and 2.	84
4.16	Localisation of PLBs on the outer tank using random PLBs at random locations. Every dot represents one PLB.	86
4.17	1D localisation on a 2D area example using 50 waves.	87
4.18	RMSE optimized 1D localisation error of the PLB on a 2D area.	88
4.19	Optimised 2D localisation.	90
5.1	Graphical representation of sensor placement for the complete tank scenario (not to scale).	96
A.1	Examples of received waves by sensor 1 where the PLB is performed on the inner tank of the flexible support test setup.	111
A.2	Examples of received waves by sensor 3 where the PLB is performed on the inner tank of the flexible support test setup.	112
A.3	Examples of received waves by sensor 1 and 3 where the PLB is performed on the outer tank of the fixed support test setup.	112
A.4	Examples of received waves by sensor 1 and 4 where the PLB is performed on the outer tank of the flexible support test setup.	112
B.1	Examples of signal onset detection (fixed support).	113
B.2	The added accuracy (0.01 [ms]) of using AIC for signal onset determination (flexible support, 50 waves).	114
D.1	One-way sensitivity study to determine the most influential input parameter on the average absolute localisation error of the flexible support test setup.	119
D.2	One-way sensitivity study to determine the most influential input parameter for localisation on the fixed support test setup.	119
E.1	Results (RMSE) of the Monte Carlo simulation for the inner tank damage localisation on the flexible support test setup.	122
E.2	Results (RMSE) of the Monte Carlo simulation for the inner tank damage localisation on the fixed support test setup.	122
E.3	Results (RMSE) of the Monte Carlo simulation for the outer tank 1D damage localisation on the flexible support test setup.	123
E.4	Results (RMSE) of the Monte Carlo simulation for the outer tank 1D damage localisation on a 2D area on the flexible support test setup.	124
E.5	Results of the Monte Carlo simulation for the outer tank 2D damage localisation on the flexible support test setup.	125
F.1	The effect of vacuum between the inner and outer tank on simulated damage on the inner tank of the flexible support test setup.	127

List of Tables

1.1	Overview of possible structural materials for liquid hydrogen tanks.	6
1.2	Overview of possible inspection techniques for structural damage monitoring in-flight.	14
1.3	Overview of possible sensors for acoustic emission sensing.	18
1.4	Acoustic emission parameters associated with crack opening [14].	31
1.5	Acoustic emission parameters associated with damage before the yield load has been reached [15].	31
1.6	Acoustic emission parameters associated with damage after the yield load has been surpassed [15].	31
1.7	Waveform parameters of representative signals in steel.	35
1.8	Types of sloshing noise and the subsequent acoustic frequency range.	36
3.1	Material properties of the materials used in the LNG tank.	47
3.2	TC and AIC settings used to determine the signal onset of S0 and A0 waves.	52
4.1	Confusion matrix for the precision, sensitivity and accuracy determination of inner (IT) and outer tank (OT) distinction based on A0 waves.	76
4.2	Calculated mean inner tank wave velocity including standard deviation per test setup.	77
4.3	Calculated mean support travel time including standard deviation per test setup.	78
4.4	RMSE per test setup determined with S0 and A0 waves.	80
4.5	Results of the optimisation of the localisation accuracy for both the flexible and fixed support. The percentages indicate the relative change with respect to the previously calculated (not optimised) values of those parameters.	80
4.6	Results of repeatability experiments where one PLB is located at random locations along the inner tank.	82
4.7	Results of the Monte Carlo simulations for experiment 3. The reference error refers to the error using the optimised values calculated in the previous subsections. The 90% RMSE refers to the value below which 90% of the calculated errors fall.	83
4.8	Calculated mean outer tank wave velocity including standard deviation.	84

4.9	Localisation accuracy of outer tank 1D localisation, including optimised localisation accuracy. The percentages refer to the relative change with respect to the RMSE using the calculated velocity and sensor 1 and 2 (row 1).	85
4.10	Localisation accuracy for randomly located PLBs.	86
4.11	Results of the Monte Carlo simulations for experiment 4a part 1. The reference error refers to the error using the optimised values calculated in the previous subsections. The 90% RMSE refers to the value below which 90% of the calculated errors fall.	87
4.12	Errors associated with the 1D on a 2D area localisation.	87
4.13	Errors associated with the 1D on a 2D area localisation. The percentages indicate the relative change with respect to the previously calculated (not optimised) values of those parameters.	88
4.14	Results of the Monte Carlo simulations for experiment 4a part 2. The reference error refers to the error using the optimised values calculated in the previous subsections. The 90% RMSE refers to the value below which 90% of the calculated errors fall.	89
4.15	Optimized RMSE associated with 2D damage localisation on the outer tank of the flexible support test setup.	89
4.16	Optimized RMSE associated with 2D damage localisation on the outer tank of the flexible support test setup. The percentages indicate the relative change with respect to the previously calculated (not optimised) values of those parameters.	90
4.17	Results of the Monte Carlo simulations for experiment 4a part 2. The reference error refers to the error using the optimised values calculated in the previous subsections. The 90% RMSE refers to the value below which 90% of the calculated errors fall.	91
4.18	Results of the investigation into the influence of a vacuum between the inner and outer tank on the localisation accuracy of an PLB performed on the inner tank of the flexible support test setup.	94
C.1	Waveform parameters of representative signals in aluminium.	115
C.2	Waveform parameters of representative signals in steel.	116
C.3	Waveform parameters of representative signals in composites.	117
E.1	Settings used in the Monte Carlo simulation for the inner tank damage localisation on the flexible support test setup.	121
E.2	Settings used in the Monte Carlo simulation for the inner tank damage localisation on the fixed support test setup.	122
E.3	Settings used in the Monte Carlo simulation for the outer tank 1D damage localisation on the flexible support test setup.	123
E.4	Settings used in the Monte Carlo simulation for the outer tank 1D damage localisation on a 2D area on the flexible support test setup.	124
E.5	Settings used in the Monte Carlo simulation for the outer tank 2D damage localisation on the flexible support test setup.	124

Acknowledgments

I would like to thank my supervisor Nan for her help and the interesting talks we had. You truly helped me believe that it was all going to work out in the end. I would also like to thank my colleagues at SHM Next for their help, knowledge and optimism. I would especially like to thank my supervisors, Daniel Tajari and Pooria Pahlavan, for their support and insights.

This thesis would also not have become the thesis it is without the generosity and help of the Salzburger Aluminium Group (SAG) in creating the test setup and helping me gain a better understanding about liquid hydrogen tanks. Special thanks goes to Thomas Stepan for arranging this important part of my thesis.

Finally, I want to thank my family and friends for their (moral) support during the ups and downs, not only during my thesis, but also during the years leading up to it. Without you the road would have been less exciting.

Delft, University of Technology
25th of October 2024

R.A. Harink

Acronyms

- AE** Acoustic emission. x–xiii, 12, 13, 15–17, 19, 20, 22, 23, 25–39, 41–43, 45, 46, 48, 50–52, 54, 55, 57, 67, 69, 71–74, 85, 91–93, 95–97, 111, 112, 115–118
- AET** Acoustic emission testing. 12–16, 19, 22, 28–30, 32–34, 36–38, 117
- AF** Average frequency. 28
- AIC** Akaike information criterion. x, xv, xvii, 22–24, 50–52, 113, 114
- CO₂** Carbon dioxide. 1, 2
- DTM** Delta T mapping. 27
- EMI** Electromagnetic interference. 12, 35
- FBG** Fiber bragg grating. 12, 17
- FP** Fabry-perot. 17
- GH₂** Gaseous hydrogen. 2
- HDT** Hit definition time. 25
- HLT** Hit lockout time. 25
- IA** Instantaneous amplitude. 23, 24, 50
- IT** Inner tank. 74
- LH₂** Liquid hydrogen. vii, xiii, xxv, 1–12, 14, 16, 28–30, 32, 34–38, 41, 42, 45, 48, 52, 91–93, 95, 97

- LNG** Liquid natural gas. xvii, 45, 47
- MAE** Modal acoustic emission. 26, 27
- MBFOR** Mandrel-based fiber optic ring. 17
- MLI** Multi-layer insulation. 78
- NO_x** Nitrogen dioxides. 2
- OT** Outer tank. 74
- PLB** Pencil lead break. vii, x, xiii–xv, xvii, xviii, 33, 34, 43, 45, 47, 48, 51–67, 69–75, 77, 79, 81–86, 88–90, 92–94, 97, 111, 112, 121, 123
- PZT** Lead zirconate titanate. vii, 16, 29
- RA** Rise angle. 28
- RMSE** Root mean squared error. xv, xvii, xviii, 60, 61, 65, 79–83, 86, 88–90, 96, 122–124
- SAF** Sustainable aviation fuel. 2
- SHM** Structural health monitoring. 1, 10–12, 15, 28, 34, 41, 73, 75, 97
- SMR** Steam methane reforming. 2
- SNR** Signal-to-noise ratio. 57, 76, 92, 96
- SOFI** Spray-on foam insulation. 3, 4
- STA/LTA** Short term average / long term average. 22–24
- STE-ZCR** Short-term energy zero-crossing rate. 23–25
- TC** Threshold crossing. x, xvii, 22–24, 50–52, 114
- WT** Wavelet transform. 24

List of symbols

A	The signal's amplitude
f	Frequency
t	Time
V_{IT}	Velocity in the inner tank
L_{12}	Distance between sensor 1 and 2
X_{PLB}	X-location of the pencil lead break test
X_{s1}	X-location of sensor 1
Δt_{12}	The signal's time of arrival difference between sensor 1 and 2
$t_{support}$	The time it takes the acoustic emission wave to travel through the support
t_{s1}	Time of arrival of the acoustic emission wave at sensor 1
n	Number of pencil breaks
V_{OT}	Velocity in the outer tank
r	Tank radius

Introduction

To achieve the aviation industry's goal of reaching Net Zero in 2050, a transition to a new energy source is essential [16]. Liquid hydrogen (LH2) is considered a promising, greener alternative. Because of the hazardous nature of hydrogen [17], utilizing LH2 requires a safe storage tank. Current LH2 tanks are designed with an inner and outer tank and in between a vacuum to provide insulation. The inner tank is often supported by a fixed and a flexible support. Because of the inaccessibility of the inner tank, the structural integrity of it remains unknown to the user, which decreases the safety of using the tank. Additionally, safe storage is also inhibited by the low storage temperature (20 [K]) which causes cryogenic embrittlement [2] and by the presence of hydrogen which causes hydrogen embrittlement [18] [19].

The inaccessibility of the inner tank and the risk of cryogenic and hydrogen embrittlement create a hazardous and unpredictable environment. Therefore, predictive maintenance is desired in the form of continuously monitoring the structural health of the tank.

A widely applied method for structural health monitoring is acoustic emission monitoring. This method is chosen to monitor the LH2 tank as is proven to be sensitive enough to register hydrogen induced cracks [20], because it is a passive method that can continuously monitor crack growth (hence focusing on worsening damage) [21] and because it has already been successfully applied to aircraft structures [22] and tanks in the past. For example, this methods has been proven to work on single-walled tanks with relatively high accuracy [23] [24]. However, investigations into the applicability of acoustic emission monitoring on double-walled LH2 tanks (with outside-the-tank sensor placement) is limited [9].

Hence, this research investigates the feasibility of using an acoustic emission-based structural health monitoring method to monitor the structural integrity of metal double-walled vacuum insulated tanks. It will also be investigated if this can be done with sensors placed solely on the outer tank and what localisation accuracy can be obtained.

To do so experiments were conducted on a metal double-walled vacuum insulated tank that was cut in half. This resulted in two test setups: One with a fixed and one with a flexible support. Using pencil lead break tests to simulate damage on the tank, the signal propagation will be investigated to determine a sensor placement that allows for complete tank coverage.

Subsequently, the distinction between inner and outer tank damage will be investigated, even as the localisation accuracy for both inner and outer tank.

The first chapter contains a literature review containing important knowledge to understand the basis of this research. In this chapter relevant experiments and their conclusions are discussed as well, even as the acoustic emission signal characteristics of the expected noise. The second chapter focuses on the method used in the experiments and the data processing. This is followed by a chapter outlining the results and relevant discussions on them ordered by experiment. Finally, the conclusions will be drawn based on those results in the last chapter, followed by supporting work in the appendices.

Chapter 1

Literature Review

To be able to discuss the experiments and their results, it's essential to first understand the context of this research and the existing knowledge in the field. It will do so by first discussing why an alternative fuel is needed and why liquid hydrogen (LH2) has the potential to be that alternative fuel in [section 1.1](#) and [section 1.2](#) respectively. Subsequently, in [section 1.3](#) the storage of LH2 will be discussed and why structural health monitoring (SHM) can help enable the transition to using LH2 in the aviation industry ([section 1.4](#) and [section 1.5](#)). Subsequently, it will be discussed in [section 1.6](#) why acoustic emission testing is a promising SHM technique to monitor LH2 tanks, how it works ([section 1.7](#) and [section 1.8](#)) and how damage can be localised ([section 1.9](#)). Finally, representative experiments and signal parameters will be discussed in [section 1.10](#), even as representative noise in [section 1.11](#).

1.1 The need for cleaner aviation fuels

Even though the aviation industry performs the seemingly impossible on a daily basis, namely flying through the sky, it also has a darker side: The pollution associated to it. Among the harmful emissions is carbon dioxide (CO₂), which amounts for around 3% of the worldwide CO₂ emissions [19] [17]. Additionally, the altitude at which kerosene byproducts are emitted causes not only condensation trails, but also increasing amounts of cirrus cloudiness. Both are associated with climate change [19].

It is not that the aviation industry has been sitting still, on the contrary: The emission of CO₂ per passenger per trip has been decreased by 34% over the last 15 years. However, the amount of people flying has also increased drastically. The International Civil Aviation Organisation expects that the CO₂ emission will be 3-7 times higher in 2050 than was the case in 2005 if the industry continues to grow at the rate it is now [19]. Even if the fuel efficiency is improved every year by 2% the amount of emission will still be doubled by 2050 [16]. Hence, there is a need to decarbonise the aviation industry and to reduce other harmful emissions to keep the climate change effects to a minimum. To do so, the aviation sector needs new energy sources in order to achieve the goal of a Net Zero in 2050 [16].

1.2 Hydrogen as a clean aviation fuel

As the need for a more environmentally friendly aviation fuel is clear, the question remains what that fuel should be. A fuel often linked to the path to sustainable aviation is Sustainable Aviation Fuel (SAF). The fuel is, for example, created from plants [17] which uses CO₂ during their growth, hence making it more sustainable CO₂ emission-wise than kerosene. The main advantage of this fuel is that it is considered a 'drop-in fuel', i.e. there are minimum modifications necessary to the aircraft to be able to use it [17] [25]. However, next to the fact that it is a more expensive fuel compared to kerosene [16], the non-CO₂ effects are barely reduced [25]. For example the nitrogen dioxides (NO_x) that are emitted during flight are actually comparable to those emitted when using kerosene [26]. Additionally, the creation of SAF is a complex and relatively inefficient process. Hence, it is expected that exclusively using SAF to power aircraft will only reduce the climate impact of the aviation industry by 60% in the most optimal scenario [16].

Hence, SAF might be considered to be a good solution in the short term as it is a drop-in fuel, but in the long term an energy source with a lower climate impact is needed. Battery flight is sometimes coined, however due to its low gravimetric efficiency it is mainly limited to short distance flight (max. 500 - 1000 [km] [16]). A promising fuel to revolutionize the aviation industry is hydrogen. The use of hydrogen is not necessarily a new idea, as the first concepts are already almost a century old [16]. There are two methods to use hydrogen as an aviation fuel: In a hydrogen turbine or in a fuel cell. The latter of which has greater prospects as it will only emit water vapor (which is 10x less problematic than the emission of CO₂), whereas the turbine will still emit NO_x, water vapor and create cirrus cloudiness. All in all, this makes the climate impact reduction potential of hydrogen fuel cells 75 to 90% [25]. On top of that, the gravimetric energy density of hydrogen is relatively high [19], namely 2.8x the one of kerosene [16].

For completeness it should be noted that, even though the use of hydrogen is promising, not all hydrogen is environmentally friendly produced. The most used method (used 95% of the time [27]) is steam methane reforming (SMR). In this process fossil fuels (primarily methane) are reformed with steam. For every 1 [kg] of hydrogen that is created with this process, also 13 [kg] of CO₂ are emitted [28]. However, it is important to note that there are also methods that are promising to reduce the climate impact of hydrogen production, like the use of wind energy to perform water electrolysis. This lowers the pollution with respect to SMR with 94% [29]. In short, in order for the aviation industry to truly reach net zero, improvements also have to be made in the production of hydrogen. However, this will be outside the scope of this thesis.

To be able to use hydrogen in a fuel cell it needs to be stored aboard the aircraft. This can be done in gaseous form (GH₂) or liquid form (LH₂). GH₂ takes up significantly more volume than LH₂ (2-3x more) [17], hence it also requires a heavier tank [25]. Additionally, whereas GH₂ needs to be highly pressurized (350 and even 700 bar [17]), LH₂ can be stored near ambient pressure (1-6 bar) [17] [30]. Hence, LH₂ is the more promising fuel for long range aircraft [25].

However, like any relatively new and complex system, LH₂ faces certain challenges that require resolution before it can be widely adopted in the industry. For example, LH₂ needs to be stored around 20 [K] in order for it to remain liquid. Whenever the temperature increases

above this temperature the liquid will vaporize, referred to as 'boil-off'. The boil-off gas in the tank will greatly increase the pressure, causing the necessity for the system to vent hydrogen. This means that valuable fuel will be lost [17]. Additionally, hydrogen is extremely flammable, hence proper safety precautions need to be taken to ensure safe flight [26]. Finally, due to the cryogenic storage requirement and the volume of LH2 it is no longer feasible to store LH2 in the wings like kerosene, therefore an alternative space in the aircraft has to be allocated for hydrogen storage [19]. Hence, it can be concluded that the storage of hydrogen is one of the main issues of the integration of an LH2 fuel cell system [31].

1.3 The liquid hydrogen tank

As it is found that the LH2 is one of the main issues preventing the implementation of LH2 in aviation, it is important to understand how structural design of the tank is determined. It is important to note here that LH2 powered aircraft are not commonly used (yet), which makes the discussed design in this subsection a decision based on currently observed trends. It is observed in literature that the design of an LH2 tank is (among others) dictated by the following two requirements [19]:

- **Temperature control.** The storage tank should be able to maintain the cryogenic temperature (20 [K]).
- **Cryogenic proof materials.** The used materials in the storage tank should be able to withstand the cryogenic temperature.

Hence the most important decisions that need to be made for the tank design is how the temperature is maintained and what materials are used, which will both be discussed in the following two subsections.

1.3.1 Temperature control

The temperature in an LH2 tank can be controlled in two ways: Actively (i.e. with cooling loops) or passively (i.e. with insulation). As active refrigeration is considered to be too heavy and complex relative to its advantages over passive designs [17], only passive designs, i.e. insulation methods, will be discussed here.

The two main passive insulation methods used in aerospace applications are Spray-On Foam Insulation (SOFI) and vacuum insulation. The first method, SOFI, involves an inner tank surrounded by a layer of foam for insulation and an outer skin for protection and rigidity [17]. This method does not need a complex internal tank support system, which minimizes the heat conduction along those supports [19]. The lack of vacuum will also lead to a simpler system. On the other hand, SOFI is prone to cracking if repeated thermal cycles are applied to the storage tank. Hence, regular maintenance is required to check its insulating properties [17]. SOFI has been used in multiple spacecraft applications, like the Space Shuttle [17] and the

DC-XA tank [32]. Also in aviation the SOFI can be found, for example in the unmanned Phantom Eye [17].

Vacuum insulation, on the other hand, bases its insulation on a vacuum layer between an inner and outer tank. On the inner tank there is also a Multi Layer Insulation applied to prevent radiation from heating up the LH2 [17]. This insulation method has better insulating properties than SOFI [31] [17] and is more reliable. Also, the storage tank will become lighter if the LH2 needs to be stored for a longer period of time (due to the reduction of boil-off) [17]. Finally, the outer tank works like a protective layer: If the inner shell cracks and hydrogen can slip through, the outer layer still prevents hydrogen from entering the rest of the aircraft [33]. However, if the vacuum were to fail (e.g. a crack in the outer shell), the tank temperature will rise dramatically fast [17]. Even though there are risk mitigating measures in place to reduce the risk of rapid pressure build-up [17] [2], it is still considered to be a major disadvantage of this insulation method. Also, the supports of the inner tank are major heat sinks [34]. Despite the disadvantages associated with vacuum insulated LH2 tanks, it is (planned to be) commonly used in prototypes for the aviation industry. For example, Airbus aims on using it in their aircraft [1], just as research project COCOLIH2T [35], student team AeroDelft¹ and NLR's Hydra-2 drone [2].

Considering the points mentioned above it can be concluded that the **current trend in the aviation sector is to use vacuum insulated tanks**. SOFI is more often used in the space sector where the tanks are less often thermally cycled and the LH2 is stored for shorter periods of time. Phantom Eye was an exception, as vacuum insulated tanks had not reached a sufficient maturity at that point in time [17].

Inner tank support

Due to the vacuum between the inner and outer tank, there needs to be some sort of support to keep the inner tank in place. The general layout of such a support can be seen in Figure 1.1, but also in [2], [36], or [37]. It can be seen that the inner tank is supported on two sides by cylindrical supports.

¹ AeroDelft, "Our LH2 team has been working with their new double-walled aluminium Cryoworld tank for the scaled powertrain. A cryogenic storage" [Image attached] [Post], LinkedIn, uploaded: January 2024, accessed: February 2024, https://www.linkedin.com/posts/aerodelft_aerodelft-hydrogen-cleanskies-activity-7155941135792631808-0eb0?utm_source=share&utm_medium=member_desktop

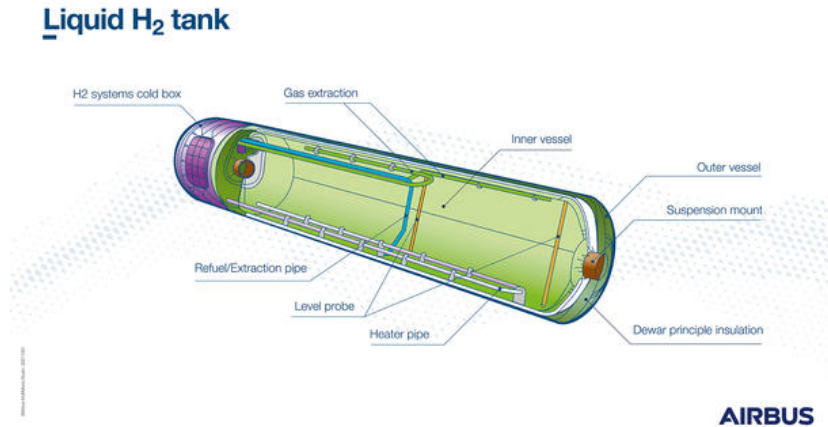


Figure 1.1: Graphical representation of an LH2 tank proposed by Airbus [1].

The specific design of such supports is complicated because of the following two aspects:

- The support design has to **minimize heat conduction**. This design aspect is of great importance, because the support is responsible for the causing the largest heat leakage [34]. To minimize the heat conduction the material should have a high thermal resistance [2]. G-10 CR is a fibre glass material that can be seen often in the use for the support, as it has a low thermal conductivity (0.2-0.3 [W/(m·K)]) [38] and behaves well in cryogenic environments [2]. However, this material is often seen in relatively small tanks, for larger tanks 316L stainless steel is sometimes used. However, the latter does have a larger thermal conductivity [38], but still lower than aluminium [2].
- The second design constraint for the support is that **it should allow for the expansion and contraction** of the different materials due to temperature changes. To do so it is often seen that at least one of the two supports is a flexible support, e.g. using a spring or two cylinder sliding over each other. See Figure 1.2 for a graphical representation of a spring-based flexible support.

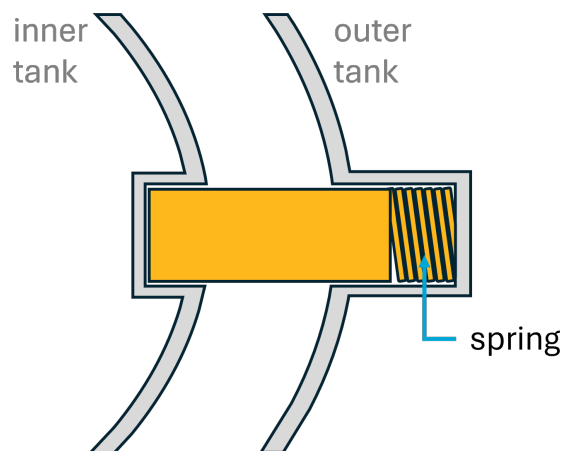


Figure 1.2: Graphical representation of a spring-based flexible support. Adapted from [2].

1.3.2 Cryogenic proof material selection

From literature it can be determined that in the aviation industry most research is focused on the development of aluminium or composite tanks. Occasionally stainless steel or titanium is mentioned, but the former is generally too heavy and the latter too expensive [17]. Therefore, the focus in this research is put on the distinction between aluminium and composite storage tanks. An overview of the advantages, disadvantages and practical examples of both tanks can be found in Table 1.1.

Table 1.1: Overview of possible structural materials for liquid hydrogen tanks.

Material	Advantages	Disadvantages	Practical examples
Aluminium alloy	<ul style="list-style-type: none"> • Relatively low chance of hydrogen embrittlement [17] • Relatively cheap [17] • Proven in cryogenic environments [2] 	<ul style="list-style-type: none"> • The material properties cannot be tailored like is the case for composites, likely resulting in a heavier design. 	<ul style="list-style-type: none"> • H2Fly [39] • NLR's HYDRA-2 drone [2] • Airbus (short term) [1] • AeroDelft¹
Composite	<ul style="list-style-type: none"> • Lighter tank [17] • Able to withstand cryogenic temperatures if right composite is chosen [40] • Can be more cost efficient in the future [1] 	<ul style="list-style-type: none"> • Susceptible to hydrogen permeation (which could be fixed with a metallic liner) [17] • Mismatches in thermal expansion coefficients of the different materials might cause damage [17] • Currently more expensive [17] • Less experience in cryogenic temperatures than aluminium alloys [17] 	<ul style="list-style-type: none"> • COCOLIH2T [35] • Airbus (long term) [1]

Based on Table 1.1 it can be concluded that at this point in time **the tendency of industry is to use aluminium alloy tanks**. However, interesting research is done into the feasibility of composite tanks for future use with promising prospects like lighter structural weight.

The type of aluminium alloy that will be considered in this thesis is AA2219. AA2219 is already used for LH2 tanks since the 1960s for rockets. Until 1998 it was the material of

the Space Shuttle external tank (then it was replaced by the lighter 2195, but this material is very expensive) and the Space Launch System rocket core stage [4]. It is also used in other aerospace propellant tanks, engine castings [14] and in products used for the creation of LH2 [41]. Also [42] recommends the use of AA2219 for cryogenic LH2 or oxygen tanks. The material is used because of its low hydrogen permeability [4] and good weldability [41]. Additionally, another feature of AA2219 is that even at cryogenic temperatures (or high temperatures) the alloy keeps a good (specific) strength. Finally, the alloy also has high ductility and is corrosion resistant [15].

1.4 Challenges for the liquid hydrogen tank

As shown in the previous section, the most promising design of an LH2 tank for aviation purposes is a metal (aluminium) double-walled vacuum insulated tank. In order to use it, it is important to know what the exact challenges are for an LH2 tank. This will be done by first going over the general challenges associated with the operation of an LH2 tank followed by the effect of liquid hydrogen on the tank.

1.4.1 General challenges

The following general challenges can be identified for the operation of an LH2 tank:

- **Space availability.** Even though LH2 takes up significantly less space than GH2, the volume is still 4 times more than that of kerosene [19] [16].
- **Temperature control.** As LH2 needs to be stored at 20 K [17], the tank needs to be properly insulated to prevent boil-off. Also, a loss of vacuum can lead to a rapid increase in temperature, resulting in explosion danger due to the build up of pressure [17].
- **Aircraft safety.** Even at a small concentration, hydrogen can already ignite [17]. Also, a deterioration of the insulation of the tank could cause a rapid boil-off with the potential of tank explosion [19]. It should be noted, however, that hydrogen often quickly dissipates once it leaves the tank. Nevertheless, next to keeping ignition sources (e.g. electrical sparks) far away from the tank, the chance of tank leakage should be minimized [17].
- **Structural integrity degradation.** The LH2 tank is expected to go through a significant amount of thermal cycles. Due to expansion and contraction because of these extreme changes in temperature (from 20K to room temperature) fatigue cracks are expected to form. Additionally, there is a risk of cryogenic and hydrogen embrittlement [19] (discussed in more detail in the next section). This can result in unexpected premature failure of the tank. Especially because of the fact that hydrogen molecules are small and have high diffusivity, the structure becomes prone to leaking [43].
- **Structural weight.** Because of the cryogenic requirements the LH2 system can become heavy [19].

- **Tank placement.** As the volume and tank shape requirements for LH2 are different than those for kerosene, the LH2 cannot simply be stored in the wings. The different placement of the fuel can have significant effects of the c.g. location of the aircraft [19].

1.4.2 Structural integrity degradation due to the presence of liquid hydrogen

The structural integrity degradation discussed above is a significant inhibitor to the implementation of LH2 tanks. Next to the usual culprits of structural degradation, like corrosion, impact damage and part debonds [22], the presence of LH2 can also result in damage. The influence of LH2 on the structure's remaining useful life (and maintenance) is little research in literature [20]. There are two aspects of the presence of LH2 that should be considered with regard to structural integrity: The cryogenic temperature and the presence of hydrogen molecules [44].

This section will dive into how these two aspects affect the structural integrity of an LH2 tank, such that this information can be used in a later stage to understand what kind of damage needs to be monitored.

The influence of cryogenic temperatures

In general materials that are submitted to cryogenic temperatures transition from being ductile to brittle and their resistance to impact goes down. This can lead to premature failure [2] [45] [46]. Cryogenic temperatures can also cause discontinuous yield [45], meaning that due to an abundance or a shortage of mobile dislocations the yield stage is not gradual [47]. However, in contrast to other materials, or even other aluminium alloys, AA2219-T87 actually improves in terms of the toughness [3]. This can be seen in the increase of the relative fracture toughness as the temperature approaches 0 [K] in Figure 1.3.

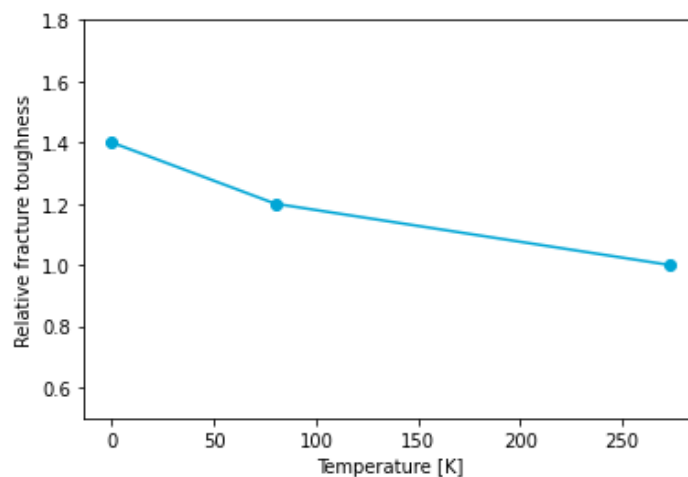


Figure 1.3: The effect of temperature on the relative fracture toughness of various materials. Adapted from [3].

The influence of hydrogen molecules

Just like how cryogenic temperatures can embrittle a material, the presence of hydrogen can also make a material brittle. This happens because the hydrogen molecules find their way into the material [18] [48]. The hydrogen moves towards places with dislocations, promoting propagation of the dislocation and subsequently creating a region with plastic deformation. When this accumulation of dislocation becomes critical, a hydrogen-induced crack starts to form [49].

However, at cryogenic temperatures the process of hydrogen embrittlement is significantly more damped, as molecules move slower and the low temperature raises the barrier to start a chemical reaction [44]. Hence, the hydrogen embrittlement at these low temperatures negligibly affect the material properties of most materials [50] [48]. This is the case for the three forms of hydrogen embrittlement: Hydrogen environment embrittlement (due to high pressure GH2, needs external applied stress), internal hydrogen embrittlement (different H2 source than high pressure GH2, needs external applied stress) and hydrogen reaction embrittlement (material chemically reacts with hydrogen, no externally applied stress needed) [48].

Even though the hydrogen embrittlement is slowed at cryogenic temperatures, it is still important to take the phenomenon into account in the maintenance planning. Namely during maintenance, inspections or long-term storage the tank can be brought back to room temperature and the remaining hydrogen might still embrittle the tank [44]. As a small amount of hydrogen, only a few parts per million, can already cause hydrogen induced cracks [51]. Additionally, the presence of water can make aluminium electrochemically charged, which enables the aluminium to be embrittled by hydrogen, even though it would have a good hydrogen embrittlement resistance otherwise. As water will be frozen at cryogenic temperatures and since there are filters in place to prevent the ingress of water, the chance of embrittlement due to the presence of water at cryogenic temperatures is minimal [4].

In [51] it was experimentally shown that AA2219 is little influenced by hydrogen embrittlement at both room temperature and at cryogenic temperature. Also [4] expects the hydrogen embrittlement susceptibility of AA2219 to be low because of the heat treatment it has received, even as cold working and artificial aging. It should be noted, however, that such experiments are often of relatively short duration. Even though the embrittlement could be insignificant in the short term, it can still be significant in the long term. More research should be performed to determine the long-term effects.

1.5 Liquid hydrogen tank inspection

In order to prevent catastrophic events due to the damage mechanisms discussed in the previous section, a well-defined maintenance plan should be in place. This section will first dive into the challenges associated with the inspection and maintenance of LH2 powered aircraft with respect to those powered by kerosene. Where after, in subsection 1.5.2, it will be explained how structural health monitoring can help to (partially) overcome those challenges.

1.5.1 Challenges for the inspection and maintenance of liquid hydrogen tanks

As the design of an LH2 tank is significantly different from a kerosene tank, the inspection and maintenance (intervals) are expected to be different as well. As LH2 powered aircraft are not commercially in use in general aviation, there are no established standards yet addressing their inspection and maintenance [44]. On the contrary, little research has been done on the impact of LH2 tanks on maintenance (intervals) [20]. However, not only for safety considerations it is important to define the impact, but also to assess the economic viability of LH2 powered aircraft. For example, for a kerosene powered aircraft, maintenance makes up 10-20% of the total operating cost [26]. Additionally, whenever the aircraft is undergoing inspection/maintenance it cannot be used to perform flights, which results in an additional loss of revenue.

Compared to a kerosene powered aircraft the amount of maintenance for an LH2 powered aircraft is expected to increase by 21-32% [26], and also the complexity of said maintenance will most likely increase (due to more thorough inspection (small cracks can already be problematic), small tank openings, etc.). This means that the maintenance cost is also expected to increase for LH2 powered aircraft. It should be noted that for simplicity in-shop maintenance is not included in the maintenance increase. However, it is expected that for a hydrogen system, more parts need to be removed from the aircraft, also increasing the amount of in-shop maintenance [26].

Additionally, the determination of maintenance intervals is a complex task for a novel system like an LH2 powered aircraft, because there is not a significant amount of in-flight data to base the intervals on. Another aspect that complicates the determination of maintenance intervals is that in order to reduce the amount of thermal cycles (and to reduce the amount of times purging of the tank is needed) it is sometimes recommended to leave LH2 in the tank even when the tank is not in use [26]. Hence, during storage the tank might still be exposed to cryogenic temperatures, hydrogen and pressure increase due to boil-off. Thus, the storage time should also be included in the maintenance intervals. As it is expected that, at least initially, using the LH2 system is going to be less reliable than using kerosene [52] it will result in relatively short maintenance intervals.

In short, the maintenance of a LH2 powered aircraft is going to take more time and is of higher complexity. A full inspection is invasive, requires in-shop maintenance, induces additional thermal cycles and requires purging afterwards. Hence, the maintenance/inspection needs to be minimized and simplified.

1.5.2 Structural health monitoring as a solution

The maintenance discussed in subsection 1.5.1 refers to time-based maintenance. This means that the maintenance is scheduled based on time or number of flights irrespective of the experienced loads or performed activities [53]. However, this allows for unexpected failure in between intervals and requires the determination of said intervals. The aviation industry is currently making efforts to shift towards structural health monitoring (SHM) [26]. This means that (part of) the structure is (continuously) monitored by sensors in-flight to assess the structural integrity of the structure. Hence, SHM is a way of predictive or condition-based maintenance, where the actual state of the structure determines the maintenance interval [53].

In general, the usage of an **SHM** system includes the installation of the system, waiting for an indication of damage (carefully filtering out any false-alarms), locating the damage and its severity and based on that assessing the structural integrity of the monitored product. Using this approach has the following main advantages:

- **Increased safety.** The structural integrity of an **SHM** assessed structure is better guaranteed, as a failure between maintenance works is less likely to occur because of the (continuous) monitoring [20]. Especially because the determination of intervals is difficult for a novel system [26]. Also, parts that are obstructed by other parts to be tested properly can in this way be monitored more precisely [54]. Finally, time-based maintenance assumes constant operating conditions, however this is not representative for the actual life of a product [20]. **SHM** allows for the inclusion of incidental high load/impact events.
- **Increased aircraft availability** [20]. As the maintenance is based on the state of the product, only the parts that really need maintaining will be maintained [9]. Hence unnecessary inspections and maintenance are prevented. Additionally, the product can be used longer as the remaining product lifetime (e.g. due to fatigue) can be assessed more accurately [32].
- **Lower maintenance cost** [22] [9]. As the inspections and maintenance will only be performed when needed and because small structural damage can be fixed before it becomes significant, the maintenance cost is expected to go down. For example, in the case of off-shore wind turbines the implementation of **SHM** lowered the maintenance cost by almost 33% [20].

Hence, **SHM** shows promising features to make the **LH2** powered aircraft safer and cheaper to fly. Which is why the use of **SHM** is chosen to investigate in this thesis. However, as **SHM** is not widely implemented yet there are some challenges that need to be mentioned:

- **Expensive system** [26] [20]. Even though the maintenance cost might go down in the long run, the initial investment for the monitoring system is relatively high. However, it can be argued that for a critical systems with large impact on the passenger's safety that it would be worth the cost.
- **False alarms.** **SHM** systems are prone to false alarms, for example due to environmental or structural noise [20] [26]. This could greatly impact the products availability as this means that the product will be taken out of service even though it is not damaged.
- **Certification issues.** For a system to be used in aviation it needs to be properly certified. However, currently the certification authorities do not yet allow to fully rely on automated **SHM** systems [26].

1.6 Structural Health Monitoring Methods

As now the potential of using SHM systems for LH2 tanks is established, this section will elaborate on different monitoring techniques and why this thesis focuses on acoustic emission testing (AET) specifically. The methods to monitor a structure can basically be divided into two categories: One where the deformation of the structure is measured and one where the damage of the structure is observed. The latter category is the most promising for the application at hand, however for completeness the first one will also be shortly discussed.

1.6.1 Deformation monitoring

Deformation, and with that strain, of the structure is often monitored with either Fiber Bragg Grating (FBG) or strain gauges. FBG based monitoring is based on the elongation or contraction of a FBG in a fiber optic cable, which changes how light is refracted in the FBG [55]. This method of monitoring is immune to electromagnetic interference (EMI) and is light weight [32]. Strain gauges, on the other hand, are based on changes in electrical resistance due to the elongation or contraction of the gauges [56]. This way of monitoring a structure is widely used and cheap [57]. However, a major disadvantage of both systems is that they do not provide information about the actual structural integrity of the system. It only provides information on the strain the structure has experienced and additional computationally expensive models are needed to determine the structural integrity. Especially cryogenic and hydrogen embrittlement becomes hard, if not impossible, to monitor. If the actual damage cannot be monitored, it becomes still a matter of estimated guessing whether the structure is still sound.

1.6.2 Structural damage monitoring

The second category of methods to monitor a structure in-flight is of more interest for the LH2 tank application: Monitoring the damage in the structure. Not all methods in this category are suitable for the application at hand. For example, radiography is not sensitive enough to observe the microcracks induced by hydrogen [20], additionally methods like impedance testing, thermography and shearography will not be able to (continuously) monitor the cryogenic or hydrogen induced damage. The two methods that are able to be used in-flight and are sensitive enough to observe hydrogen-induced micro cracks are acoustic emission testing (AET) and ultrasonic testing [58].

Acoustic emission testing

This passive method is based on the fact that nucleating or propagating structural damage emits acoustic emission (AE) waves through the structure. Measuring that wave with multiple sensors allows for the localisation, and to a certain extent characterization, of the material change, also referred to as the AE source [18] [22]. It is important to note that AET is only able to monitor active cracks, as these are the only ones emitting AE waves. This is advantageous as this means that this technique only focuses on worsening damage, which is the one that is relevant for maintenance (e.g. if a crack remains the same length over time,

it is most likely not problematic for the functioning of the structure). This technique has a high sensitivity, such that it can detect microcracking with released energy in the order of atto-Joule [8]. Additionally, with relatively low hardware complexity this method can monitor a relatively large area and has been proven to be effective in aircraft structures [22]. However, the main issue with AET is its sensitivity to noise which can make the interpretation of the data complex [20]. Also structures complex in shape can make the localisation of AE sources difficult due to reflections. Inhomogeneous/Anisotropic materials also complicate the localisation process as the wave speed is not equal in all directions [59]. Due to these issues AET is sensitive to have false alarms or giving inaccurate locations [9].

Ultrasonic testing with guided waves

The second method to detect damage in a structure is ultrasonic testing. This is an active method where a transducer generates a wave through the material. Based on how the wave is reflected back and measured at the sensors, damage localisation can be performed [18] [20]. In contrast to AET which can only measure active cracks, ultrasonic testing measures any crack. This method is able to monitor large areas while experiencing relatively little attenuation [60]. Additionally, it is relatively easy to focus on one area of the structure, whereas with AET there is a larger chance of noise interference from outside the area of interest. However, just like for AET, also this method is prone to false alarms or false negatives in complex structures. This is mainly due to the fact that the geometry can cause AE waves to be reflected back in a complex ways, making the interpretation of the structural integrity complicated. Also, the detection of cracks that are oriented in the direction of the wave's travel direction are difficult to inspect as it barely reflects back AE waves. Finally, when using this method a trade-off needs to be made between the minimum crack detection size and the propagation distance of the wave [21]. An overview of the advantages and disadvantages of AET and ultrasonic testing are given in Table 1.2.

Table 1.2: Overview of possible inspection techniques for structural damage monitoring in-flight.

Inspection technique	Advantages	Disadvantages
Acoustic emission testing	<ul style="list-style-type: none"> • Sensitive to hydrogen induced cracks [20] • Proven in aerospace [22] • Damage can be located [59] • Potential of damage type classification [8] • Large areas can be covered [22] • Passive system • Continuous monitoring possible 	<ul style="list-style-type: none"> • Complex result interpretation [20] • Only active damage [21]
Ultrasonic testing	<ul style="list-style-type: none"> • Sensitive to hydrogen induced cracks [20] • For ultrasonic guided waves large areas can be covered [60] • Experiences relatively little attenuation [60] • Relatively easy to focus on one area 	<ul style="list-style-type: none"> • Trade-off between minimum crack size detection and propagation distance [21] • Complex result interpretation when structures are complex [21] • Cracks oriented along propagation direction can be missed [21] • Periodic monitoring

Even though ultrasonic testing is a promising technique, the passiveness and sensitivity of AET make the latter a better candidate for the application of monitoring LH2 tanks. Additionally, ultrasonic testing is only sensitive to crack presence, whereas AET is sensitive to crack formation and growth which is desirable to monitor the structural integrity changes of the tank. AET as therefore already been used to monitor structures made from AA2219 in the aerospace industry [15].

1.7 Acoustic Emission Testing

Now that the potential of AET is clear, this chapter will focus on the basic principles of it. It will do so by first discussing the basic principles behind it (subsection 1.7.1) and going over the damage types that can be registered in subsection 1.7.2. Finally, the effect of performing AET at cryogenic temperatures and possible AET sensors will be discussed in subsection 1.7.3 and subsection 1.7.4 respectively.

1.7.1 The basic principles of acoustic emission testing

AET is not a newly developed method, but has already been around since the 1940s [61]. The practical applications of the method became known in the work of Joseph Kaiser in the 1950s [15]. The process of AET used for SHM is described below:

1. A material change occurs, e.g. a crack propagates. This is called an AE event [61]. During the AE event energy is released. In total 80% of the energy is used to plastically deform the material [15]. The type of damage that emits detectable AE waves will be further discussed in subsection 1.7.2.
2. The wave travels through the material. Dependent on the type of material and the structure's geometry the wave is changed (e.g. attenuated, dissipated, reflected) [8].
3. The sensors placed on the structure are continuously 'listening' for AE waves in the structure. The decision where to place sensors on the structure is important, but complex. It is dependent the geometry of the structure, the area of interest (as for larger structures it is often recommended to focus on a particular area where damage is expected, a so called 'hotspot' [62]), and the methods used for subsequent AE source localisation. Whenever the wave arrives at the sensor is referred to as a hit [61]. The wave is then transformed into an electrical signal which is pre-amplified and subsequently digitized [8].
4. There after the wave can be analyzed. The arrival time of the wave provides information about the AE source location and the wave shape / number of hits can be used to assess the severity AE event [54]. It should be noted that especially the last part of the wave often contains reflections [8]. The process of localisation and characterisation will be further discussed in section 1.9.

1.7.2 Acoustic emission detectable events

AET is a non-destructive method that is able to register a wide variety of damages. It should be reemphasized that AET can only register active damage. AET can for example monitor (micro) crack growth [63], which can be due to fatigue or hydrogen embrittlement [64]. Even the hydrogen embrittlement itself is measurable in both aluminium alloys [65] and steel [66]. It is also able to measure yielding, corrosion, phase transformations [63], fretting [54], particle fracture/sliding and even the movement of dislocations. In aluminium alloys in particular particle fracture is often observed [8]. For composites it can also measure fibre breakage and matrix debonding [63]. However, the smaller the AE event, the fewer energy is released, the more difficult it becomes to detect it using AET [63].

It should be noted that different events create waves with different characteristics. This will be further discussed in subsection 1.9.4. For now it should be noted that in terms of hydrogen embrittlement the bubble rupture, the accumulation of dislocations and eventually the propagation of cracks are all measurable and have different signal parameters (i.e. frequency, energy, counts, duration, amplitude) [49].

1.7.3 Acoustic emission testing in cryogenic temperatures

Because of the fact that LH2 is stored at such extreme temperatures, it is expected that it will influence the operation of AET. Firstly, changes in temperature of the propagation medium result in changes in the Young's modulus (see Figure 1.4), which in turn results in changes in wave propagation velocity (as the Young's modulus has the largest influence on speed of sound) [67]. Hence, a lower temperature results in a higher speed of sound [68]. As most techniques used for AE source localisation are based on time of arrival of the signal, this change in wave speed can have an influence on for example the beamforming technique (this technique will be discussed in subsection 1.9.3).

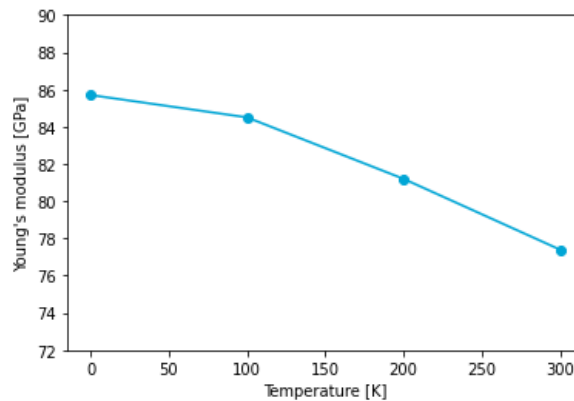


Figure 1.4: The change in Young's modulus with temperature for aluminium alloy 2219. Adapted from [4].

However, cryogenic temperatures also have an advantage: The thermal noise decreases with decreasing temperature [69]. Thermal noise, also known as Johnson noise, is created by resistors. This type of noise has an average value of zero and has "a flat spectral density vs frequency" [70]. Because of the reduction of thermal noise at low temperatures [69] had an improvement of 18 dB in their signal-to-noise ratio when their sensors ($\text{Pb}(\text{Zr}_{0.52}\text{Ti}_{0.48})\text{O}_3$ ceramics AE sensors) were at 4.2 [K].

1.7.4 Acoustic emission sensors

In order to perform AET, sensors need to be placed on the structure. The choice of which has a large impact on the ability to detect and localise damage. The sensors should be able to operate in the designated environment, should not be too heavy or expensive, and the technology should be mature enough for it to be used commercially on a large scale. Table 1.3 shows an overview of sensors and their advantages and disadvantages. There are basically two variants of sensors: Electricity-based and fiber optic-based.

The most well-known electricity-based sensor is the lead zirconate titanate (PZT) AE sensor. These sensors are based on the piezoelectric effect that occurs in piezoelectric materials. This refers to the fact that whenever such a sensor experiences a contraction/extension (due to e.g. an AE), sides of the piezoelectric material will become positively or negatively charged. The amount of charge is proportional to the amount of deformation [71].

A well-known example of a fibre optics-based sensor is one equipped with an **FBG** which can contract/expand. This changes the refraction of the light through the **FBG** which can be translated to a waveform [72].

Another fibre optics-based option is the Fabry-Perot (**FP**) **AE** sensor. In this case light is emitted through a fiber and when it reaches a half mirror part of the light is reflected and another part is let through. The remaining light is later reflected by using a full mirror. The detector can determine, based on the intensity of interference of the two light waves, to what extend the fiber is extended/contracted [73].

Finally, the last fibre optics-based sensor that will be discussed is the mandrel-based fiber optic ring (**MBFOR**), which is a combination of a mandrel with an optical fiber around it. It is an update to the regular fiber optic ring, which, in contrast to the **MBFOR**, cannot be attached to solid object [74]. **AE** waves in the structure deform the mandrel, which deforms the optical fibre. The addition of the mandrel ensures that the sensor does not suffer from the directional sensitivity associated with the **FBG AE** sensor [75].

An overview of the advantages and issues of each sensor type can be found in **Table 1.3**. It can be concluded that the choice of sensor is highly dependent on the application and environment in which it will operate.

Table 1.3: Overview of possible sensors for acoustic emission sensing.

Sensor	Advantages	Disadvantages
PZT AE sensor	<ul style="list-style-type: none"> • Mature [74] • Standard for AE detection [74] [75] • Cheap [74] • High sensitivity [75] • Good stability [75] 	<ul style="list-style-type: none"> • Problems might arise at cryogenic temperatures [76], however there are commercial PZT sensors that can withstand cryogenic temperatures [77] • EMI sensitive [75] • Not operable under high pressure or strong corrosion [75]
FBG AE sensor	<ul style="list-style-type: none"> • High sensitivity [74] [75] • Small [74] [75] • Cheap [72] • Easy to install [72] • EMI immunity [74] • No electricity, hence no electrical spark risk [74] • Functions at low temperatures [74] 	<ul style="list-style-type: none"> • Temperature compensation needed [74] • Limited operating temperature range [74] • Directional sensitivity [74] [75]
FP AE sensor	<ul style="list-style-type: none"> • Sensitive [74] • Wide measurement range [74] [75] • Stable [75] 	<ul style="list-style-type: none"> • Complex manufacturing process [74] [75] • Expensive [74] [75] • Limited signal receiving angle [74]
MBFOR AE sensor	<ul style="list-style-type: none"> • Sensitive [74] • Wide temperature operating range (incl. cryogenic temperatures) [74] • Relatively easy production process compared to FP sensor [75] • Material choice can be tailored to environment [75] 	<ul style="list-style-type: none"> • Not a mature technology [74] • Expensive [74]

1.8 Technical background on Lamb waves

In order to understand AET, it is important to understand Lamb waves. This section will provide the technical knowledge on Lamb waves by first discussing the difference between S0 and A0 waves and thereafter the sources of Lamb wave attenuation.

1.8.1 S0 and A0 waves

Lamb waves (named after Horace Lamb who discovered them in 1917) are ultrasonic elastic guided waves that propagate in plates with thickness similar to or smaller than the wavelength. By interacting with the plates boundaries two modes of the lamb wave exist simultaneously: symmetric waves (S) and anti-symmetric waves (A). Both are visually represented in Figure 1.5. Generally, the symmetric waves have a higher wave velocity [5] [78] [79].

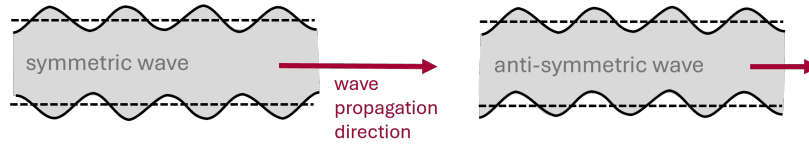


Figure 1.5: Graphical representation of symmetric and anti-symmetric waves in a plate. Adapted from [5].

The symmetric and anti-symmetric waves have multiple modes. However, the frequencies in combination with the plate thicknesses discussed in this research are below the cut-off frequencies of the higher modes of the symmetric (700 [kHz]) and anti-symmetric waves (400 [kHz]). Hence, only the zero-order modes (S0 and A0) will be considered in this research.

1.8.2 Wave attenuation

When an elastic wave travels through a structure it interacts with the medium it travels through, which causes the received signal to be different from the transmitted signal. Knowing how and why the signal changes can help with placing sensors and getting information on the damage. An important phenomenon to take into consideration is wave attenuation, meaning that the peak amplitude will decrease with increasing distance between the AE source and the sensor.

In general, wave attenuation is given by [80] [81]:

$$\frac{A}{A_0} = e^{-\alpha(f)x} \quad (1.1)$$

Where A and A_0 refer to the signal's amplitudes at distances x and $x = 0$ respectively. Also, α refers to the attenuation coefficient expressed in $[dB/m]$ which is dependent on the frequency (f) and is often used in AET to characterize the structure/material [81]. It should be noted that higher frequencies are attenuated more than lower frequencies, hence they will be able to travel less far through a structure while still being detectable [82].

Wave attenuation has three main causes [83] [84] [85]:

- Geometrical spreading
- Material damping / absorption
- Wave scattering
- Dispersion
- Thermoelastic and Akhieser dissipation

Geometrical spreading

The energy of the wave needs to be conserved as it travels through the structure. Over time the wave radially expands, increasing its covered area and hence decreasing the energy (and hence amplitude) per location. This follows the following relationship [86]:

$$I(r) = \frac{I_0}{r^2} \quad (1.2)$$

Where r is the radius, I_0 the intensity 1 [m] from the source and $I(r)$ the intensity of the signal at a given radius. This source of attenuation is mostly not dependent on the material the wave is travelling through. It should be noted that as an anisotropic material influences the propagation pattern of an AE wave, this type of material of attenuation follows a different pattern than the one described by Equation 1.2 [84].

Material damping / absorption

This cause of attenuation entails the conversion of the wave's energy in other energy forms (e.g. heat) [84]. Hence, this cause is material specific. It should be noted that when an insulation layer is glued or sprayed on top of a material, this also influences the attenuation of an AE wave through that material. Figure 1.6 shows the attenuation in [dB/inch] against the frequency for an insulation applied to AA2219. It can be seen that, especially for glued on insulation, the attenuation increases significantly with increasing distance.

Wave scattering

Wave scattering refers to the phenomenon where an AE wave will be refracted or reflected causing attenuation of the signal. The amount of attenuation is dependent on the signal's frequency and size of the discontinuity. Examples of causes of wave scattering are:

- Inhomogeneities in the material (e.g. grain boundaries, cavities) [85].
- Cracks or fractures in the material [84].
- A material boundary [84]. This can for example be a boundary between two materials with an impedance mismatch [87] or between the material and the air. For example, the curvature of a surface can also influence wave's amplitude. It is even possible that the reflections that occur due to the curvature increase the AE wave's amplitude rather than decrease it with increasing distance [84].

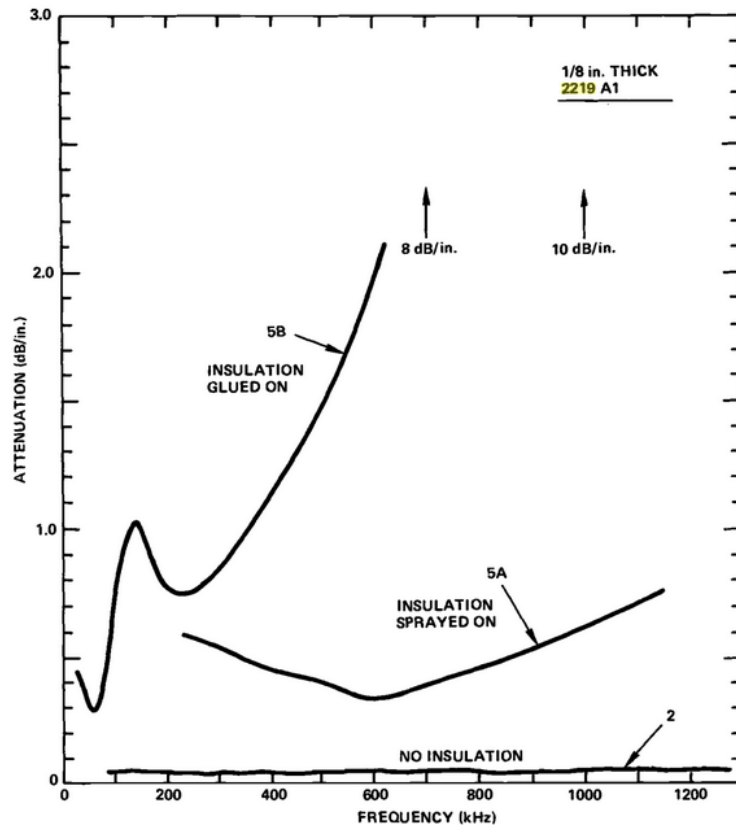


Figure 1.6: The effect of type of insulation adhesion on the wave attenuation [6].

Dispersion

Dispersion refers to the phenomenon that different frequencies travel with different velocities through a plate. This is especially true for thin plates [6]. Due to different frequency parts of the wave separating, the peak amplitude of the wave will decrease with increasing distance due to dispersion. Also, the rise time (the time between the first threshold crossing of the signal and the peak amplitude [8]) will increase [7]. This can be seen in Figure 1.7.

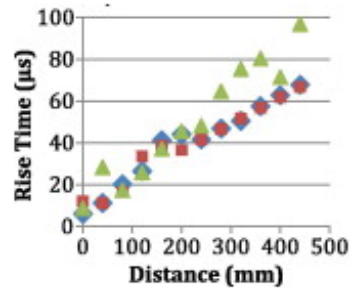


Figure 1.7: The effect of propagation distance on rise time due to dispersion [7].

Thermoelastic and Akhieser dissipation

The AE wave compresses and decompresses the material it travels through. The heat loss that is associated with that causes the thermoelastic dissipation. During Akhieser dissipation, on the other hand, the compressions and decompressions disturb the equilibrium distribution of the thermal vibrations (phonons). This causes the wave to lose energy and hence attenuate. This is especially the case in the far field and with high frequencies [85].

1.9 Acoustic emission testing techniques

This section will dive into the techniques used in AET. First the signal onset determination techniques will be discussed, followed by how the signal end is determined. Subsequently, methods for source localisation will be shown. Finally, it will be discussed how and to what extent the AE source can be classified based on the signal received.

1.9.1 Signal onset determination techniques

Before it can be determined where the signal is located, it first needs to be determined when the signal starts. The more accurately this happens, the more accurately the location determination can be performed [88]. The commonly used techniques are either time-based or time-frequency-based. Purely frequency analysis is not discussed here, as this does not hold any information on the arrival time of the wave [89]. Time domain methods that will be discussed here are: Threshold crossing (TC), cross-correlation, short term average / long term average (STA/LTA) and the Aikake information criterion (AIC). Thereafter the time-frequency analysis will be discussed.

Threshold crossing technique

- **Basic principle.** The most straight forward technique that will be discussed is TC. An operator chooses a threshold and whenever the signal passes that threshold is considered the start of a signal [90].
- **Advantages.** The main advantage is that it is a relatively simple and straightforward method and hence is widely used in AET [90] [88].
- **Issues.** The sensitivity of the technique is highly dependent on the chosen threshold [90]. A too low threshold will result in false alarms (e.g. due to noise), but a too high one causes the technique to miss damage propagation [54]. Additionally, false negatives can be caused by signal attenuation or low signal amplitude at the source [91]. Hence, the use of TC is primarily recommended with constant or gradually changing noise levels [92].
- **Variants.** In order to increase the accuracy of the TC technique multiple updates have been proposed, e.g. using positive and negative thresholds, pre-trigger buffering (which entails considering some data samples before the start of the signal) or changing the threshold over time. However, the latter is especially beneficial if the noise gradually

changes. The threshold crossing technique can also be improved by using the instantaneous amplitude (IA) technique. This technique first creates a characteristic function of the wave envelope. Then the threshold technique is used on that function [88].

Cross-correlation technique

- **Basic principle.** The cross-correlation technique is based on matching the phase difference of a specific frequency at different sensors [91]. The time delay between the sensors can subsequently be determined in finding the point where the cross-correlation function has its maximum value [93].
- **Advantages.** In case the signal-to-noise ratio is relatively low, this method still provides meaningful data. Hence, high background noise is not necessarily an issue for this method [94]. Therefore, this method is considered to often be sufficiently accurate [62].
- **Issues.** If the structure is complex, this method can have difficulty with multiple reflections [54]. The multi-path effect also reduces the accuracy of this method [93].

Short term average / long term average method

- **Basic principle.** This method was originally developed to monitor earthquake onsets [88]. The STA/LTA method is based on the comparison of the average energy of the characteristic function of the AE signal over a short period and a long period of time. Whenever this ratio changes, the signal is considered to start [54]. The latter is done with threshold crossing [88].
- **Advantages.** This method performs well in noisy data [54] and is considered to be more accurate than TC [90]. Additionally, background noise has a relatively low influence on signal onset determination [88].
- **Issues.** A threshold still needs to be set and exact signal onset determination is difficult because of the use of averages [54] as the long term average part induces a delay [88]. Also, this technique requires the most amount of parameters to be tuned, making it a complex method to use.
- **Variants.** A variant on the STA/LTA, which is also based on energy, is the Short-term energy zero-crossing rate (STE-ZCR) method. The origin of this method can be found in speech processing, or more specifically voice activity detection. The method is based on determining a short term energy function and short term zero crossing function of the signal. An AE event has in general a relatively high energy and low zero crossing. Based on two thresholds (the identification upper threshold and the identification zero crossing threshold) the signal onset and end can be determined. This method is accurate and performs well in the presence of noise [95].

Akaike information criterion method

- **Basic principle.** The AIC method bases the signal onset on a change in entropy of the signal. Noise has a high entropy, whereas the AE signal has a relatively low entropy. Hence, that change in entropy indicates signal onset. The AIC function is minimum at that point [54] [91].
- **Advantages.** This method is considered to be more accurate than TC [90] [54] and STA/LTA [88]. Additionally, it performs good compared to hand picked signal onsets.

This method is also robust enough to perform well with a variety of signal-to-noise ratios [91].

- **Issues.** The **AIC** method is based on the selection of a window length. The window selection is a complex task, because a too long window means multiple signals are within one window and a too short window means that one signal is divided up and considered as multiple signals. There have been successful attempts at using **TC** to give a first estimation of the signal onset and using the **AIC** subsequently on a window around the **TC** signal onset to get to a more accurate arrival time [91].
- **Variants.** A similar method is based on the Hinkley criteria. This method is based on the application of a negative trend on the partial energy which is computed for each point. The signal is considered to start when the trend achieves its minimum. However, this criteria will not be further discussed in this thesis, as it is shown to be inferior to the **AIC** method [91].

Time-frequency distribution analysis

- **Basic principle.** In a time-frequency analysis the waveform in the time dimension is converted using a wavelet transform into a 3D space, with on its axis time, frequency and wavelet amplitude. Hence, in contrast to the frequency method using a simple Fourier transform, now the time dimension is still maintained [96] [89] [88]. To do the wavelet transform (**WT**) a mother wavelet has to be chosen, e.g. Gabor's **WT**, Mexican hat, Shannon **WT**, etc. Because of its good resolution (in the domain of both time and frequency) Gabor's **WT** is often used [96] [97]. The time of arrival of a mode of the wave can subsequently be found with a peak in **WT** amplitude [97].
- **Advantages.** It is an accurate method [88] and it can reveal more about the source than only time analysis can [97], e.g. the failure mode [96].
- **Issues.** The resolution of time and frequency is bound by Heisenberg's uncertainty, resulting in complex synchronization between the two [98] [99].

Comparing the above-mentioned methods was done in multiple researches. For example, in [88] it was found that all methods were able to achieve absolute errors of 20 [μ s] or less. **IA** and **STA/LTA** were the most accurate in "quality of detection", where **IA** was more responsive and **STA/LTA** was more accurate. **AIC** and time-frequency distribution analysis are more accurate in determining the beginning of the signal than the **TC**. However, both are dependent on an initial detection of a signal, adding a degree of uncertainty [88].

Secondly in [59] it was observed that in a plate with holes **TC** was significantly less accurate than **AIC** (especially the dispersed signals).

Finally, [95] compared the **STE-ZCR** method to the **IA**, **STA/LTA**, **AIC** and time-frequency methods. They performed pencil lead break tests and an uniaxial tensile test. In both tests the **STE-ZCR** was found to be the most accurate and precise and to have the lowest false positive/negative rate, all while also being the fastest method. However, it should be noted that the **STE-ZCR** was introduced by this paper, so some bias might be in place.

All in all, the choice for the signal onset determination method is greatly dependent on the received signals and how they are affected by the structure and its environment (e.g. noise) [88].

1.9.2 Signal end determination

In a real use case, multiple **AE** signals happen short after each other or even simultaneously. It is therefore important to be able to distinct between the different signals. This part of the **AE** analysis is much less researched than the signal onset determination [95]. A method often used is based on amplitude and time. This method is based on hit definition and hit lockout time (**HDT** and **HLT**). The **HDT** is a timer that is restarted every time the signal crosses a threshold. Whenever the **HDT** is over, the signal is considered to have ended. **HLT**, on the other hand, refers to the time after the signal end in which no new signal will be registered to prevent the registration of reflections. It should be noted that the determination of the length of the **HDT** and **HLT** should be done carefully in order not to split up or miss signals [88]. There are methods like the **STE-ZCR** that aim to improve the signal end determination [95]. Also, frequency analysis can be used to separate signals. For example, in [96] they were able to distinct signals of two different failure modes based on the different frequencies associated with those failure modes.

1.9.3 Source localisation techniques

Just like for signal onset determination, there are also multiple methods do determine the location of the **AE** source. These methods are based on different principles, do or do not require to know the material properties, and require a different number of sensors. Commonly used techniques and their (dis)advantages will shortly be discussed in this subsection. It should be noted that for all methods reflections and attenuation are an issue [8].

Triangulation

- **Basic principle.** This method is based on the time difference between the wave arrival time at different sensors. From that time difference and the wave propagation speed the distance to the sensors can be determined. A minimum of three sensors is needed to determine the location of the **AE** event [8]. See [Figure 1.8a](#) for a graphical representation of this technique.
- **Advantages.** Because of the relative simplicity of the technique, it is widely used [54].
- **Issues.** The method is based on the assumption that the wave speed should be known and be equal in all directions [8] [91], which makes it a particularly popular technique for isotropic materials [62]. However, even in structures made of isotropic materials, the wave speed is rarely exactly known and constant, e.g. due to thickness changes [54]. It should be noted that even a small deviation in the estimated wave speed from the actual wave speed can have a large effect on the source localisation accuracy [62]. Finally, the method assumes that the wave can travel in a straight line from the source to the sensor. However, in complex structures this is not always possible, due to, for example, the presence of holes [54] A solution could be to place a large number of sensors, however in literature this technique is mostly used on plate-like structures [62], hence it is uncertain what accuracy can be achieved on more complex structures.

Beamforming method

- **Basic principle.** The beamforming method is based on the delay-and-sum algorithm where signals registered by different sensors are adjusted to the same datum [64]. In essence the sensors 'sweep' the monitored area for AE source location possibilities, by means of applying signal delays [8].
- **Advantages.** Exact signal onset determination for a particular wave mode is not needed to determine the damage location, which is beneficial if noise is present [62]. A high localisation precision can be achieved [100].
- **Issues.** This method requires a significant amount of closely spaced sensors. Also, the material properties need to be known [8] (although there have been variations of the beamforming method developed where the wave propagation speed could be an unknown [100]). Also, the distance to the source should be large relative to the distance between the sensors [8]. This method is mostly used for plate-like structures [62].

Clustered sensors

- **Basic principle.** For this method three (or more) sensors are closely spaced, most often in an L-shape. The time delay between the received signals can be used to determine the incidence angle and wave speed of the received wave. The combination of these two parameters can be used to determine the location of the AE source [8]. See Figure 1.8b for a graphical representation of this technique.
- **Advantages.** The material properties of the structure do not need to be known [8].
- **Issues.** This method is also dependent on the wave being able to travel in a straight line. Additionally, when the source is far away from the sensor cluster, the incidence angles become similar, hence the AE source localization becomes less accurate. Additionally, the complexity of the method increases significantly when it is used for anisotropic materials [8].

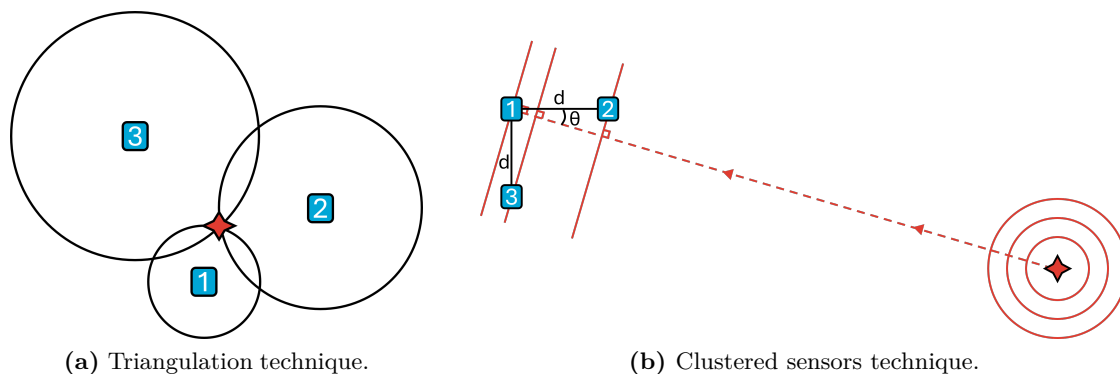


Figure 1.8: Graphical representation of two AE signal localisation techniques. Adapted from [8].

Modal acoustic emission method

- **Basic principle.** The modal acoustic emission (MAE) method is based on the analysis of different modes (extensional, flexural) of the received wave. The location of the damage can be determined in comparing the arrival times of different modes [101]. This

can be done in two ways for one dimensional source localisation: Using two sensors (examining the same or different modes and frequencies) or to use one sensor and determine the wave speed based on the arrival of different modes (as the difference in arrival time is proportional to the distance travelled) [97].

- **Advantages.** The MAE method needs less sensors than other methods. The method is based on analysing different wave modes, hence this method theoretically also allows for gaining extra information on for example the source's strength [100] [62].
- **Issues.** This method is computationally intensive [100]. Additionally, the plate properties (e.g. thickness) need to be known in advance and the method only works for relatively thin plates [62].

Delta T mapping (DTM)

- **Basic principle.** The first step in this method is to create artificial AE events (e.g. pencil lead break tests). The time differences observed at the sensors are recorded and used to make a training map. When a real AE source is detected, the time difference can be cross-referenced to the training map and hence the location of the AE source can be determined [54]. This technique was specifically developed for complex structures [91].
- **Advantages.** No knowledge is needed about the material properties or the structure in advance [62]. Due to the fact that it accounts for complex shapes and differences in wave speed it can obtain high accuracy on complex structures (and on anisotropic materials) [54]. Finally, the strength of the source can also be determined [62]. Even though the creation of a training map is labor intensive, once one is made it can be used for other structures that are the same as the one on which the training map was made [59].
- **Issues.** Even though this technique is promising for complex structures, it is a very time-consuming process to collect all the training data [54]. Hence, this technique is often used to monitor smaller regions of interests, also referred to as 'hotspots' [91]. Also, the operator needs to select the right data and parameters for the training map, which requires experience [54]. Finally, the training map for DTM is made in certain environmental conditions. If these conditions change, e.g. the structure is heated up or cooled down, the wave speed in the material changes and could therefore influence the accuracy of this method.
- **Variants.** A variant of DTM is automatic DTM introduced in [54]. This method is slightly faster than regular DTM and takes away part of the human intervention by using a clustering algorithm to sort the received waves. This data is subsequently used to create a training map. Also, linking waves to sensors is done automatically with this method [54]. Another localisation technique that uses training data are neural networks. This method is for example used in [24], which will be further discussed in subsection 1.10.1. Even though the method has promising features like a relatively high accuracy [24], its practical application is limited due to its computational complexity [54].

It should be noted that when a structure is sufficiently complex, the only methods that remain decently accurate are the DTM method and placing a large number of sensors such that e.g. triangulation can be used. However, if another method than DTM or a large number of sensors can be chosen, it is recommended to choose another method because of the labor and computational power that is required for using that many sensors or the DTM method [62].

1.9.4 Source classification principles

Often it is sufficient for an SHM system to determine the location of a damage such that the maintenance crew can focus on a specific area rather than the entire structure. However, if an AE source can be classified (e.g. determine the failure mode or severity) it can be determined more accurately whether maintenance is really necessary. Source classification can be based on parameter analysis (used most often, based on e.g. amplitude, rise time, duration) or based on waveform analysis in the time-frequency domain (gives a more in-depth image of e.g. failure modes) [102].

A parameter that is often investigated in the parameter analysis is the signal's amplitude. The magnitude of the amplitude is dependent on the size of the crack propagation, if the crack propagates with a large surface a large amplitude is expected and vice versa [8]. Also, a combination of parameters can be investigated. For example, the rise angle (RA, signal rise time divided by peak amplitude) and average frequency (AF, threshold crossings divided by signal duration), can indicate the type of crack propagation. If the signal has a low RA and high AF this refers to tensile crack propagation, whereas a high RA and low AF is often indicative of shear crack propagation [103] [102]. Also, in [49] they were able to make distinctions between hydrogen bubbles, hydrogen permeation and hydrogen-induced cracking based on energy, counts and amplitude range.

For the waveform analysis the frequency spectrum of a signal can be analysed. The frequency of a signal can tell something about the size of the created area. A high frequency is associated with a small crack propagation, often at the beginning of the damage process. Whereas a large crack propagation is often associated with a relatively low frequency, happening near final failure. Additionally, in [96] they were able to, based on the frequencies measured, predict the failure mode of a composite. This can be done as different failure modes of composites (e.g. fibre break and matrix crack) have different associated frequencies. This will be further discussed in subsection 1.10.2.

However, just as is the case for localisation methods, also source classification is influenced by noise, attenuation and dispersion. Also, it assumes that a singular event happens in time, such that a clear distinction can be made between different signals to localise and classify them. However, in real structures this is not always the case [8].

1.10 Representative experiments

This section will first go over relevant AET experiments to get an idea as to what has been done in the field of AET and LH2 tanks. Subsequently, representative signals will be discussed that can be used as a basis for this research.

1.10.1 Relevant Acoustic Emission Testing Experiments

This section aims to give an overview of experiments performed that can be related to using AET to monitor LH2 tanks. As no research had been found on AE-based SHM for aluminium vacuum-insulated LH2 tanks, the following subsections will dive into the separate

aspects. These aspects includes the liquid hydrogen conditions, the effect of the outer tank geometry and finally the possibility of monitoring the inner tank through supports. Every subsection discusses the experiment itself and which lessons can be drawn from it.

Liquid hydrogen conditions: DC-XA spacecraft

In the 1990s the liquid hydrogen tank of McDonnell Douglas' DC-XA spacecraft [104] was tested using acoustic emission testing. The purpose of the test was to determine the structural integrity specifically in the central joint and the forward dome where a repair area was located. Additionally, it aimed to determine whether AET could be used for cryogenic tanks [105].

The tank in question was made of composite and had internal insulation [104]. The sensors were selected based on their ability to withstand low temperatures and the working of those sensors was verified with pencil lead break tests. The tests that were performed can be organised into three categories: Loads at ambient temperature, loads at cryogenic temperature and "fill, pressurize, and drain tests using liquid hydrogen" [105].

The conclusion of the experiment was that the tank was structurally sound and that the sensors withstood the temperatures. When a stable pressure was achieved in the tank AEs were still detectable. This, according to the researchers, could mean that there was interaction between the liquid and the insulation. Additionally, during the test the researches wondered if the adhesive itself, even though it was not visibly damaged, caused some of the measured AEs [105].

A conclusion that can be drawn from this experiment is that sensors are able to measure AE events in cryogenic temperatures to a good extent. However, careful consideration has to be made for sources of AE that are not the ones of interest (e.g. sensor adhesive or insulation interaction).

Outer tank geometry: Pressure vessels

Localizing damage on a tank similar to the outer tank of an LH2 tank has been researched, for example, by [23]. In that research the clustered sensor method was used to localise artificial damage on a cylindrical pressure vessel. They were able to accurately predict (max error = 49.2 [mm]) the AE source location. In [24] they also placed sensors on a pressure vessel, but used the triangulation method to localise simulated damage. Their classic-average deviation in the tank filled with water from the actual pencil lead break location was 60 ± 62 [mm] and for the PZT induced signals was 149 ± 129 [mm].

The conclusion that can be drawn from experiments done on pressure vessels is that it is shown in multiple researches that the AE source localisation on cylindrical objects is doable with multiple methods with differences in computational complexity and accuracy.

Inner tank geometry: double-walled stationary tank

In contrast to the outer tank geometry, methods to monitor the inner tank are much less researched. In [9] the aim was to monitor the inner tank bottom of a double-walled tank storing ammonia with a diameter of 22 [m]. Between the two tanks is granular insulation, inert gas and rigid insulation between the floors. It should be noted that ammonia is stored at -33 [°C] [106], hence significantly warmer than LH2. However, because of the double-walled geometry it is still an interesting case to include.

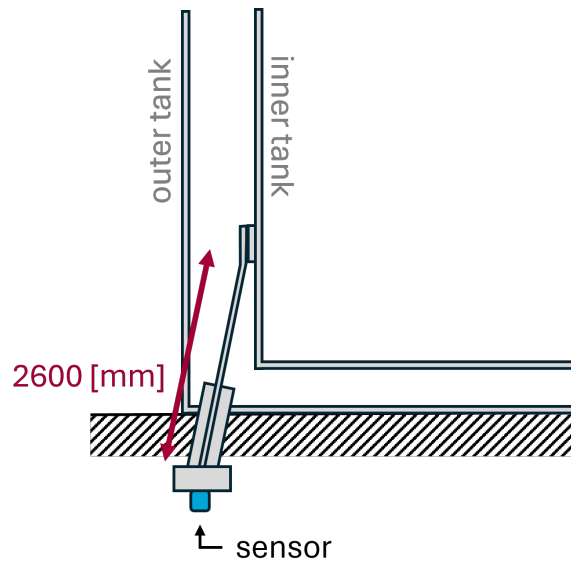


Figure 1.9: Graphical representation of sensor mounting for double-walled stationary tank. Adapted from [9].

To measure **AE** of the inner tank sensors were placed at the end of supports, see [Figure 1.9](#). However, due to the length of the supports a significant amount of attenuation was perceived. The researchers also investigated which couplant to use. They found that regular vacuum grease caused high attenuation at cryogenic temperatures: A 10 dB decrease in mean amplitude was observed. Hence, it was found that water, which froze, was a good alternative as it had the attenuation values of vacuum grease at room temperature. It should be noted, however, that there is also research that does recommend the use of silicone vacuum grease as a couplant at cryogenic temperatures, because it did not crack and protected the sensors against moisture ingress before the experiment [69]. The conclusion of the research was that it was feasible to detect **AE** events in the bottom of the inner tank with the method described in [9].

Conclusions that can be drawn are that it is possible to determine and localise **AE** events via a supporting structure. However, attenuation has to be taken into account at signal evaluation. Additionally, the sensor couplant needs to be carefully chosen.

1.10.2 Representative signals

In order to perform a representative **AET** experiment, it is important to understand the wave parameters of a representative **AE** source. This subsection will first dive in the characteristics of crack growth in AA2219, the material that is often used for **LH2** tanks. Thereafter, for completeness, the **AE** characteristics of other materials are shown. Finally, it will be discussed why and how pencil lead break tests can be used to simulate crack growth for **AET**.

AE characteristics of crack growth in AA2219

In [14] the **AE** associated with crack propagation in AA2219-T87 was investigated. This was achieved by loading a compact tensions specimen and measuring the **AEs** that were produced.

Pattern recognition was used to distinct the noise from the AE signals. They found that the parameters as shown in Table 1.4 are indicative of crack opening in AA2219.

Table 1.4: Acoustic emission parameters associated with crack opening [14].

Parameter	Value
Amplitude [dB _{AE}]	70
Duration [ms]	8
Energy [-]	100

After the compact tension specimen test a pressure tank was monitored for AE using as a threshold the amplitude mentioned in Table 1.4. They tested two tanks: For one tank the AE remained under the threshold, for the other tank the thresholds were surpassed. Even though there was no repeated emission from a specific location, further non-destructive tests were performed to verify the structural integrity of the tank. The tank was found to have no cracks. Hence, it was concluded that the set thresholds were somewhat conservative [14].

Also [15] investigated the AE signal characteristics of 2219-T87. They did so by loading a plain 2219-T87 specimen and a 2219-T87 specimen with a weld in the middle. For both specimens they performed five tests. The average parameters of the received signals (when the load is below the yield strength) are given in Table 1.6. It should be noted that for the plain specimen in three cases no hits were recorded.

Table 1.5: Acoustic emission parameters associated with damage before the yield load has been reached [15].

Parameter	Plain specimen	Welded specimen
Amplitude [dBdB _{AE}]	36	71
Duration [ms]	0.3	1.15
Energy [-]	1	15

The AEs after the yield strength has been surpassed show the average parameters as seen in Table 1.5.

Table 1.6: Acoustic emission parameters associated with damage after the yield load has been surpassed [15].

Parameter	Plain specimen	Welded specimen
Amplitude [dBdB _{AE}]	50	63
Duration [ms]	0.350	1.5
Energy [-]	15	8

Finally, [6] has investigated the amplitude and frequency of an **AE** signal generated by fatigue cracks in AA2219-T87. They recorded the fatigue crack growth in a 0.63 [cm] thick plate. Three types of signals were noticed: Type 1, type 2 and type 3. Their frequency spectra can be seen in [Figure 1.10](#). Type 1 and type 2 were associated with fatigue crack growing, whereas type 3 was associated with machine noise.

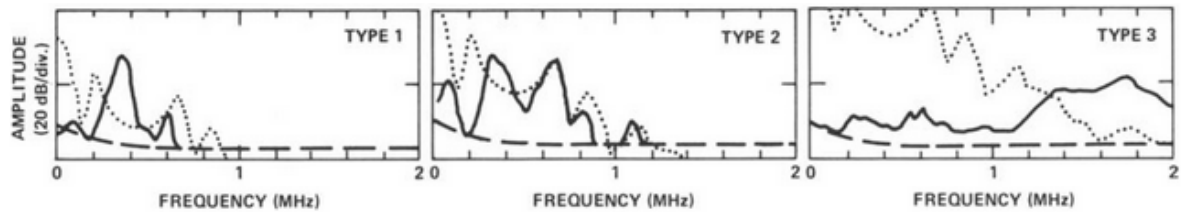


Figure 1.10: Amplitude and frequency of fatigue crack induced acoustic emission signals (type 1 and type 2). The type 3 signal refers to machine noise. The solid line is the line of interest and refers to the signal that the transducer has registered [6].

As can be seen in [Figure 1.10](#), the noise has a significantly higher frequency than the useful **AE** signals. The **AE** signals of type 1 and 2 had frequencies in the range of 0-1 [MHz], with peaks in the frequency spectrum around 0.35 [MHz] for type 1 and around 0.1, 0.35, 0.65 [MHz] for type 2.

AE characteristics of other materials

As the use of **LH2** tanks in aviation is still premature and the material choice can change, it is important to see whether a material change will still allow for **AET** of the tank. Hence, an investigation has also been done into representative crack growth signals in other materials: Other aluminium types, steel and composites. The results of this investigation can be found in [Appendix C](#).

[Figure 1.11](#) shows a summary of the frequency ranges of common **AE** signals based on the research shown in [Appendix C](#). From this graph it can be concluded that for aluminium the frequency range goes from 50-700 [kHz]. For steel the frequencies are lower, from 50 to 400 [kHz]. Finally, the composites range from 30 to 500 [kHz]. It should be noted that for composites there is a clear distinction between the relatively low frequency matrix cracking and the higher frequency associated with fiber breakage.

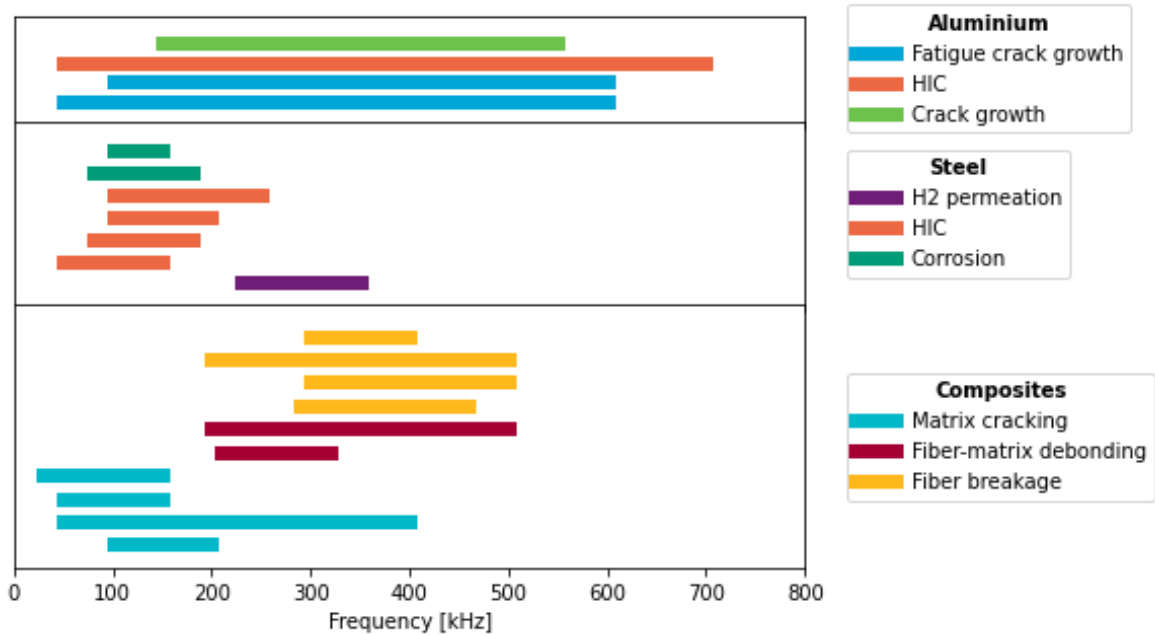


Figure 1.11: Frequency ranges of AE signals generated by aluminium, steel and composites. More information and sources can be found in [Appendix C](#).

1.10.3 Modelling crack growth with Pencil Lead Break tests

In order to assess the localisation accuracy of a proposed method, AEsources have to be placed at known locations. As this is complex to do with real growing damage (especially in the case of hydrogen induced cracking) a simulated source is needed. A method often used in AET is performing pencil lead break test (PLB, also known as Hsu-Nielsen source) [107] [108] [109]. Using PLBs is an accepted means to simulate an AE source according to ASTM E976-15 [10]. The PLB is performed with a mechanical pencil where the breaking of the lead causes a sudden release of energy into the structure where the lead of the pencil touches the structure [10].

The PLB test is used because the wave characteristics generated by a PLB test are similar to those generated by a real AE source [108] [109] and because it is easily repeatable [10]. Additionally, because of the variability of the generated signal, it also gives an idea on how the measurement system responds to different wave shapes. The method described in the ASTM E976-15 dictates the following prescriptions [10]:

- **Lead diameter:** 0.3 [mm] (occasionally 0.5 [mm] is used [110])
- **Lead hardness:** 2H
- **Pencil angle:** 30 [°]
 - The use of a guide ring (also known as the Nielsen shoe) is recommended. This is a ring around the tip of the mechanical pencil that will allow for a consistent pencil angle [10]. Additionally, it prevents the pencil tip from hitting the surface after the lead breaks [110]. See figure [Figure 1.12](#) for a graphical representation of a PLB test.
- **Free lead length:** 2-3 [mm]

- It should be noted that both the free lead length and pencil angle influence the load applied to the structure [108].
- **Pencil orientation:** Should remain the same for all tests.
- **PLB distance to sensor:** A distance less than 100 [mm] to the sensor complicates getting consistent results

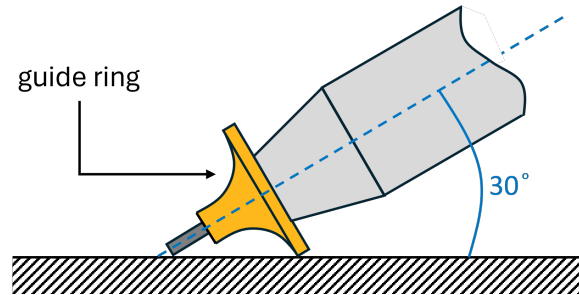


Figure 1.12: Graphical representation of a PLB test. Adapted from [10].

In literature the PLB test are used for the following:

- **Measurement system calibration:** E.g. testing the functioning and coupling of the sensors and determining the effectiveness of the band-pass filter [109].
- **Characterize the signal:** E.g. investigating the signal's frequency (change), wave modes, attenuation and length of the signal [107] [109].
- **Localisation accuracy:** E.g. calculating the wave velocity and determining how accurate the measurement system can localise the PLB [109].

1.11 Representative environment

To be able to place AET experiments performed in a lab in context, it is important to understand the environment in which the product will eventually be used. Especially the effect of noise on AET is of importance to investigate, as the technique's sensitivity to noise is a significant drawback [21], so it is important to understand this environmental parameter on AET. It is important to know what kind of noise can be expected (subsection 1.11.1, 1.11.2 and 1.11.3) and what to do about it to prevent false alarms or missed damage (subsection 1.11.4) [88].

1.11.1 Sources of noise

During operation an AE-based SHM system experiences noise from a variety of sources. Below a list of expected noise sources is given.

- **Operational noise** is noise created due the operation of the structure, in this case the LH2 tank. For example, sloshing, vibrations or actuated valves [8]. For sloshing the emptier the tank the longer the impact of the sloshing will be [111]. In [112] the liquid

settling noise (which can be compared to sloshing to a certain degree) could be observed in the obtained **AE** data. Additionally, boil-off occurs in the tank. The bubbles that form during this process were measured in [49] using **AE** in steel. These signals were different than those of hydrogen permeation and micro cracking. The characteristics of **LH2**-related noise will be further discussed in subsection 1.11.2. Hence, the boil-off does not necessarily need to interfere with the **AE** signals of interest. Also, in [113] it was found that the boil-off of liquid nitrogen did not interfere with their measurements.

- **Structural noise** is generated by the structure itself, for example due to friction between the tank and its supports or vibrations in the structure. This noise source causes a lot of **AE** activity [8]. Structural noise will be further discussed in subsection 1.11.3.
- **Electromagnetic interference (EMI)** can be created due to nearby cables or electronic equipment. The **EMI** might induce spikes in the signal traveling through the cables of the sensors, resulting in false positives. This can be minimized by careful cable placement, grounding and amplifying the signal at the sensor itself [8].
- **Sensor noise** is noise induced due by the sensor. For example, due to internal noise, noise because the sensor itself affects the wave signal [114] (especially in cryogenic applications [9]), or the sensor adhesive induces noise [105]. Hence, source of noise should be taken into account during the sensor and adhesive selection.
- **Thermal noise** is noise due to resistors and is dependent on temperature. This was discussed in more detail in subsection 1.7.3.

1.11.2 Liquid hydrogen-related noise

The two main sources of noise specifically related to the use of **LH2** tanks are: Bubble rupture and sloshing. Both will be briefly described below including their **AE** wave parameters.

Explanation of bubble rupture

As discussed before, bubble rupture refers to the rupture of bubbles created during boil-off. Table 1.7 shows typical **AE** wave parameters for this type of noise in a steel structure.

Table 1.7: Waveform parameters of representative signals in steel.

Material	Frequency [kHz]	Amplitude [dB _{AE}]	Energy [eV]	Source
4130X steel	50-150	40-45	0-10	[49]
A516 carbon steel	50	X	X	[115]
09GSF pipeline steel	30-60	X	X	[116]

Hence, as bubble rupture is a low energy event and likely at a different frequency than hydrogen induced cracking, it is not expected to interfere with **AE** measurements. All sources listed in Table 1.7 were able to distinct the bubble rupture from hydrogen induced cracking

based on its [AE](#) signal.

Sloshing

Sloshing occurs due to the movement of liquid in a container. In this case the [LH2](#) is free to move within the tank. Three types of sloshing noise can be identified. These are detailed in [Table 1.8](#).

Table 1.8: Types of sloshing noise and the subsequent acoustic frequency range.

Sloshing type	Description	Frequency [kHz]	Source
Splash	Two wave fronts hitting each other	0.5-10	[117]
		<2	[118]
Hit	A wave front hits the side of a tank	0.2-2	[117]
		< 4	[118]
Clonk	An impact air bubble is created by trapping and compressing air abruptly	0.15-0.5	[117]
Combination of splash, hit and clonk	X	< 5	[119]

It should be noted that all sources mentioned in [Table 1.8](#) aimed to find the audible noise, e.g. to investigate the influence on passenger comfort. Hence, the sloshing noise was recorded with a microphone rather than with transducers on the structure.

Comparable to sloshing is the noise that a fluid produces when flowing through a pipe. This flow causes a noise lower than 20 [kHz]. A flow containing bubbles causes a slightly higher frequency in the range of 20-80 [kHz]. These values were obtained using a transducer [120]. However, both are still below the expected frequency for hydrogen induced cracking.

1.11.3 Structural noise

Next to noise coming from the [LH2](#) itself, structural noise is also expected to have a significant influence on [AET](#). Possible sources of structural noise are:

- Structural rubbing [121] [122]
- Fretting [121] [122]
- Noise due to airflow [122]

Especially the fretting and rubbing noise have similar characteristics to fatigue growth [AE](#) signals [121] [122]. The amount of noise is dependent on the structure and materials, but also on the flight conditions. For example, an increase in altitude and/or Mach number correlates to more [AE](#) hits [121]. This can be due to more crack growth due to the higher loads, but can also be due to increased noise with these higher and continuously changing loads.

To determine the influence of the structural noise on the functioning of [AET](#) in an aircraft, four in-flight [AET](#) experiments on different aircraft were gathered and compared.

- Lockheed C-5A Galaxy
 - **Component material:** Aluminium 7075-T6 [123].
 - **Flight profile:** Flights at 10 000 and 20 000 [ft] [123].
 - **Results:** During the flight at 10 000 [ft] the maximum noise was registered at 100 [kHz] (120-380 [μ V] dependent on the sensor location) and a signal over noise ratio of 2/1 was achieved from 400-750 [kHz] upwards (assuming that fatigue cracks generated a 65 [μ V] signal). With an increase in altitude, the structural noise increases slightly, most likely due to the lower temperature effects on the structure. However, a similar frequency range was obtained to obtain a signal over noise ratio of 2/1 as for a flight at 10 000 [ft]. It should be noted that the highest noise was recorded in the main landing gear area [123].

- Aermacchi MB-326
 - **Component material:** 4340 Steel [11].
 - **Flight profile:** Formation, circuits and landing, aerobatics and low flying [11].
 - **Results:** The experiment was focused on monitoring a known defect. A band-pass filter was applied at a frequency of 400 [kHz] \pm 25 [kHz]. A peak in noise was detected below 400 [kHz] as can be seen in Figure 1.13. However, in the frequency window selected, it was possible to detect AE hits [11].

- Avro Canada CF-100 Canuck
 - **Component material:** 7075-T6 [124].
 - **Flight profile:** Climb to 4000 [ft], right and left turns of +2g, +3g and +4g (all for 1 [min]). In total the test flight took about one hour [124].
 - **Results:** The part under investigation was the forward wing trunnion. As this part is meant to transfer loads, it is expected to be an acoustically noisy area. A transducer was used that operated between 300 and 1000 [kHz]. The paper states that it is possible to detect AE hits over the noise when data is only gathered during constant G conditions [124].

- Cessna T-303 Crusader
 - **Component material:** 7075-T6 [125].
 - **Flight profile:** Flight including "taxi, take-off, steady level flight, rolls, and Dutch rolls" [125].
 - **Results:** Using neural networks, the paper was able to identify AE signals resulting from a fatigue crack. No information on the frequency range of the signals and the noise was provided [125].

It can be concluded from the experiments mentioned above that in-flight AET is not as straight forward as testing in a laboratory environment. It should be noted, however, that the majority of the examples (except the Cessna T-303 Crusader) are from before the year 1985, hence technological advancements (e.g. neural networks, more sensitive transducers) could ease the AE detection process now. Nevertheless, the examples show a need to either minimize the amount of noise arriving at the LH2 tank or finding more accurate methods to distinct noise from AE sources.

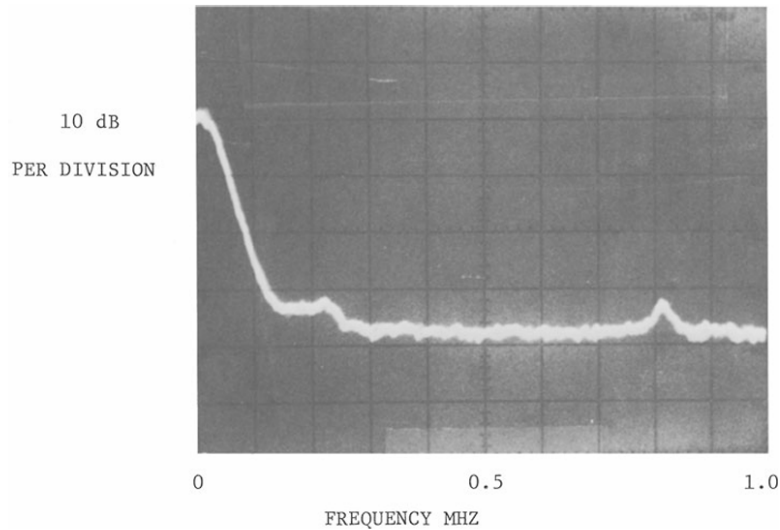


Figure 1.13: Noise spectrum resulting from a Macchi MB 326 operating at full power [11].

1.11.4 Solutions to minimize the influence of noise

There are two methods to minimize the influence of noise on the [AET](#). On one side the noise itself can be minimized and on the other side the noise can be filtered out post-processing.

Minimizing noise at the source

To minimize structural noise, the [LH2](#) tank can be vibrationally isolated from the main structure. This will dampen the incoming noise, hence making [AET](#) easier. This can be done, for example, by using materials with an impedance mismatch to reflect noise signals [126].

Another source of structural noise is friction. This can be minimized by for example adding a lubricant [8]. Also, to minimize the sloshing noise, baffles can be installed [127], however this will not prevent all sloshing.

It is also possible to extract noisy periods from the obtained data. For example, strain gauges and/or accelerometers could be used to identify times during the flight where, for example, sharp turns were performed and hence a lot of noise is expected. These periods can subsequently be excluded from the [AE](#) analysis. The other periods could then be used to listen for crack growth [124]. However, a drawback of this method is that important crack growth can be missed.

Removing noise post-processing

The second method to minimize the effect of noise is to filter out the noise after the signal has been recorded. A method sometimes used to determine whether signals come from the part of the structure of interest or from other parts is the use of so-called guard sensors. These sensors are strategically placed in such a way that if the signal is received by them first, it means that it is from a part of the structure outside the field of interest, hence it can be ignored [128].

Another method to identify an **AE** hit amidst noise, is cross-correlation. When there are no hits all sensors will only receive noise. When a hit occurs the correlation coefficient shall change, hence an **AE** hit can be identified [122].

A system that is able to distinguish between noise and **AE** hits well is UniQ developed by SHM Next (see **Figure 1.14**). The UniQ houses four sensors and uses above mentioned cross-correlation to match the signal arrival times between the sensors and filters are used to filter out the noise. Subsequently a quasi-beam forming method (a variant on the beam forming method mentioned in **subsection 1.9.3**) is used to localise the damage, for which no calibration of the system is needed. The system can monitor an area of 50 [m²] of steel, concrete or composite (e.g. bridges, pipelines) [12].



Figure 1.14: The UniQ of SHM Next applied to a bridge [12].

Chapter 2

Research scope

From the literature review it can be concluded that **LH2** is a worthwhile option to investigate as a more sustainable alternative to kerosene. However, as [section 1.2](#) suggests: The storage of **LH2** poses a barrier to the implementation of this alternative fuel. Because of the cryogenic and hydrogen embrittlement, the difficult to inspect geometry and the disastrous effect of failure, there is a need to closely monitor the structural integrity of the tank, such that the safety of the operation can be guaranteed. Multiple methods and their advantages and disadvantages have been researched, but the conclusion of [section 1.6](#) is that acoustic emission monitoring is the most suitable solution to continuously monitor the tank's integrity in use.

As is discussed in [subsection 1.5.2](#) the main steps of using an **SHM** system are installing the system, distinguishing if the **AE** response is associated with damage or noise, locating the damage and finally assessing the structural integrity of the product. The flow of these steps are shown in [Figure 2.1](#).

From the flow chart it is decided that the main focus of this thesis will be put on the feasibility of localising damage of the **LH2** tank. However, the determination of noise and sensor placement will also be discussed in this thesis. Hence, the main research question that will be investigated in this thesis becomes:

To what extent is it feasible to monitor the structural integrity of a metal double walled vacuum insulated liquid hydrogen tank in room temperature with an acoustic emission-based structural health monitoring system?

To answer this question, the following sub-research questions will be investigated:

RQ 1 Where do sensors need to be placed such that simulated damage can be identified in room temperature on a metal double walled vacuum insulated **LH2** tank?

RQ 1.1 To what extent is it possible to monitor the inner tank of an **LH2** tank with outside-the-tank sensor placement in room temperature?

- RQ 1.2** How does the inner tank support affect the amplitude of an **AE** signal in room temperature?
- RQ 1.3** How does the inner tank affect the amplitude of an **AE** signal in room temperature?
- RQ 1.4** How does the outer tank affect the amplitude of an **AE** signal in room temperature?
- RQ 2** How accurately can the distinction be made in room temperature between simulated damage from the inner and outer tank?
- RQ 3** How accurately can the proposed sensor placement localise simulated damage in an **LH2** tank in room temperature?
- RQ 3.1** How accurately can the proposed sensor placement localise simulated damage in the inner tank in room temperature?
- RQ 3.2** How accurately can the proposed sensor placement localise simulated damage in the outer tank in room temperature?

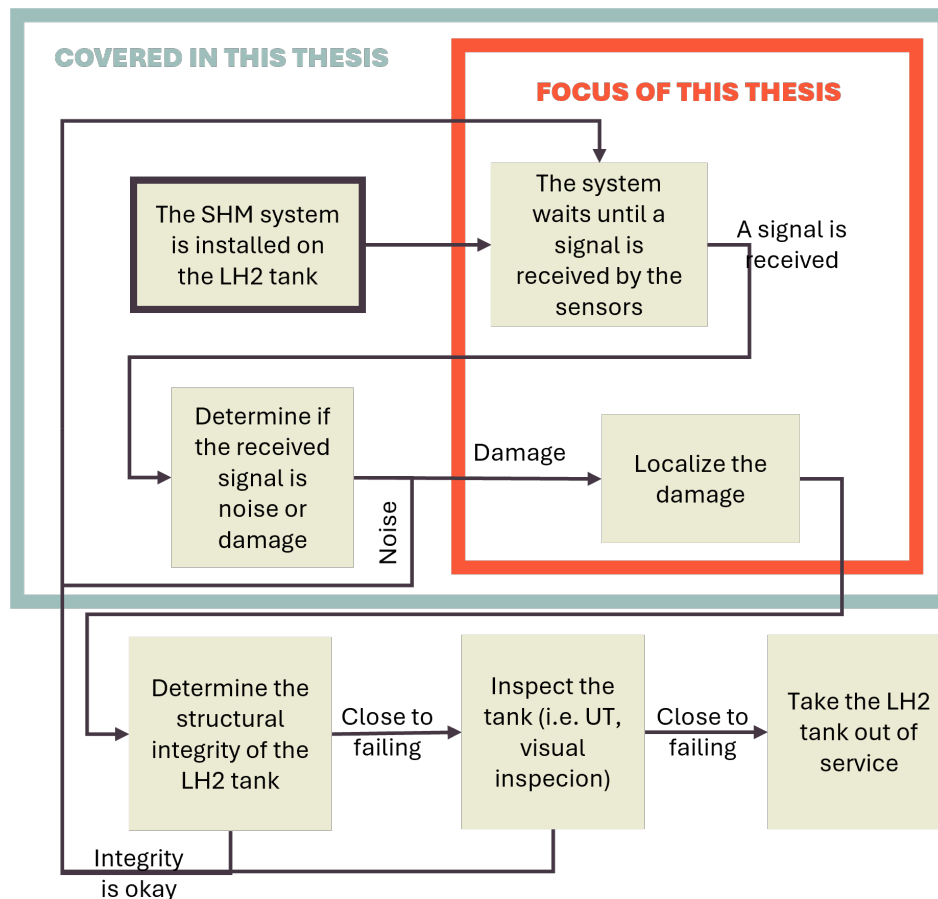


Figure 2.1: Flowchart indicating the scope of this thesis.

Chapter 3

Method

As the research aim and questions are now laid out, the method to answer them will be discussed. First an overview of the method is given to provide clarity to the reader on how the method is structured. Thereafter the experiment setup will be discussed and how the signal onset determination was performed in [section 3.2](#) and [section 3.3](#) respectively. Finally, the experiments and research methods will be discussed per experiment in the final sections of this chapter.

3.1 Method overview

In [chapter 2](#) the high-level steps that will be covered in this thesis were laid out. These steps can be divided up into smaller steps and experiments as can be seen in [Figure 3.1](#).

The first step is to receive a signal. The feasibility of receiving an [AE](#) signal caused by a [PLB](#) will be investigated in experiment 1 ([section 3.4](#)). The representativeness of a [PLB](#) as an [AE](#) source is already discussed in [subsection 1.10.3](#). Then it has to be determined whether the signal originates from damage or noise. This is not investigated in-depth in this research with experiments, but rather with a literature review ([section 1.11](#)). Subsequently it has to be determined whether the signal that is received originates from the inner or outer tank. This is investigated in experiment 2 in [section 3.6](#). Finally, the simulated damage ([PLBs](#) in this research) has to be localized for the inner tank (experiment 3 in [section 3.7](#)) and for the outer tank (experiment 4a in [section 3.8](#) and experiment 4b in [section 3.9](#)). It should be noted that important inputs for the localisation process are the [AE](#) wave's travel speed and sensor locations.

For the sake of optimally using time and other available resources, some experiments were combined while performing them. However, for the sake of clarity they will be treated separately in this thesis.

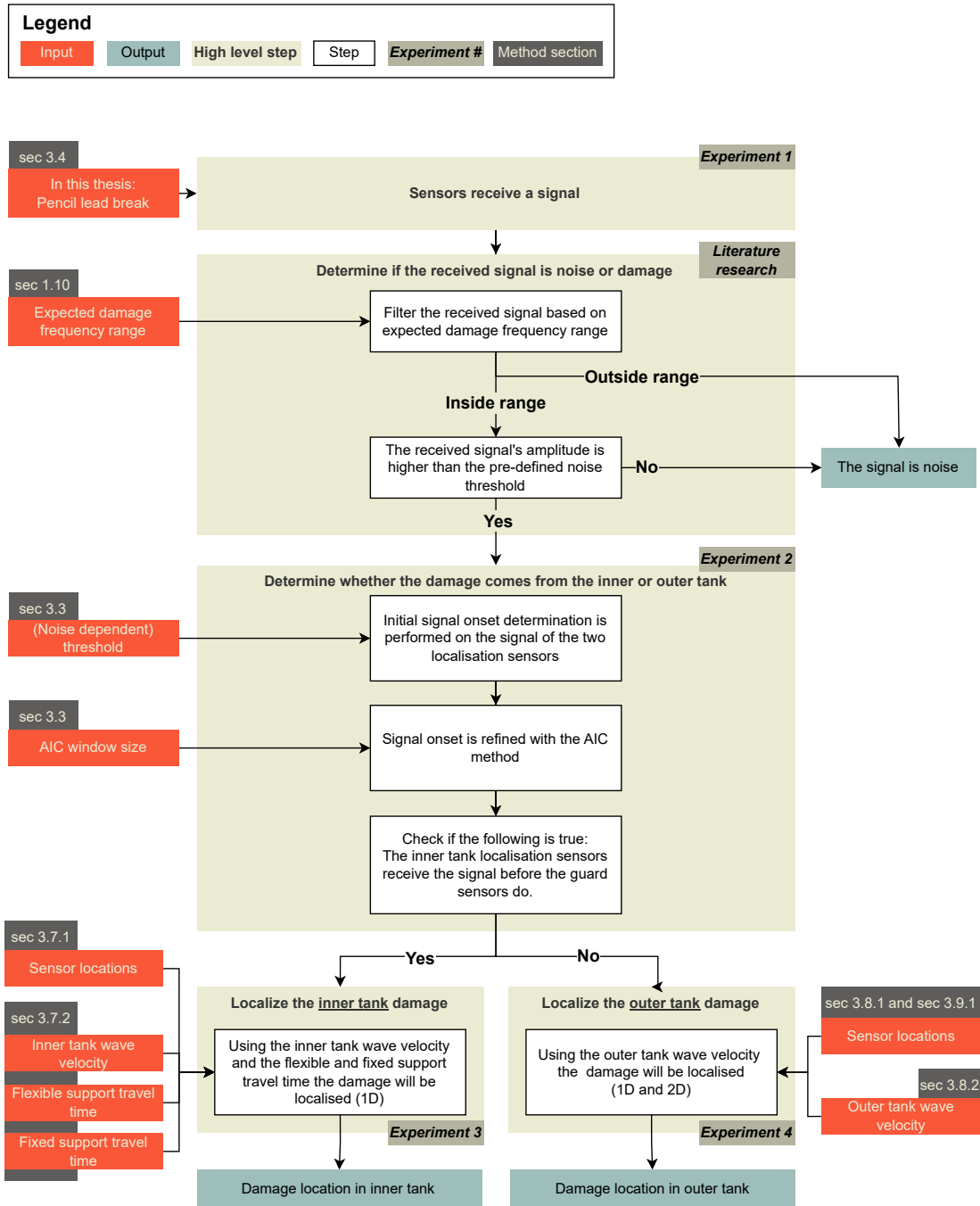


Figure 3.1: Flowchart indicating the steps taken in the experiments and other research involved in this thesis.

3.2 Experiment setup

In this section the setup of the experiment will be discussed. First the tank setup will be explained, where after the coordinate system used to measure the location of the PLBs will be shown. Then it will be discussed which frequency will be investigated, such that the equipment used to measure the AE waves can be chosen in the next section.

3.2.1 LH2 tank test setup

In order to perform experiments, a representative test setup had to be made. A tank was gratefully borrowed from the company SAG¹ (Salzburger Aluminium Group). It should be noted that the tank is not an LH2 tank, but a liquid natural gas tank (LNG). The main difference between the two tanks is the fact that the LNG tank inner and outer tank was made of stainless steel rather than aluminium (the stainless steel properties can be found in Table 3.1). However, as the structure (e.g. the support design) of the LH2 and LNG tank are the same and because stainless steel is still an isotropic material, the tank was deemed representable enough for a feasibility study.

As can be seen in the graphical representation of the tank in Figure 3.2, the tank has a flexible support and a fixed support (which will be discussed in more detail later in this section). For the experiments in this thesis the inner tank needed to be reachable to perform PLBs on it. Hence, the tank was cut into two parts (as can be seen in Figure 3.2): One half-tank containing the flexible support and one half-tank containing the fixed support.

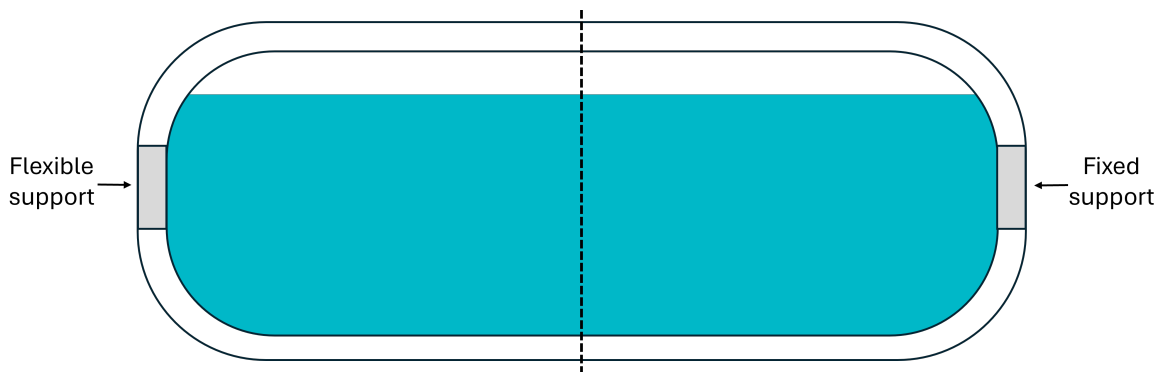


Figure 3.2: Graphical representation of the tank used in the experiments. The dotted line indicates where the tank was cut. (Not to scale.)

The two test setups and their dimensions can be seen in Figure 3.3. The inner tank has a length along the tank of around 1000 [mm]. The average thickness of the tank is 4 [mm].

¹More information on the company at <https://sag.at/nl/>

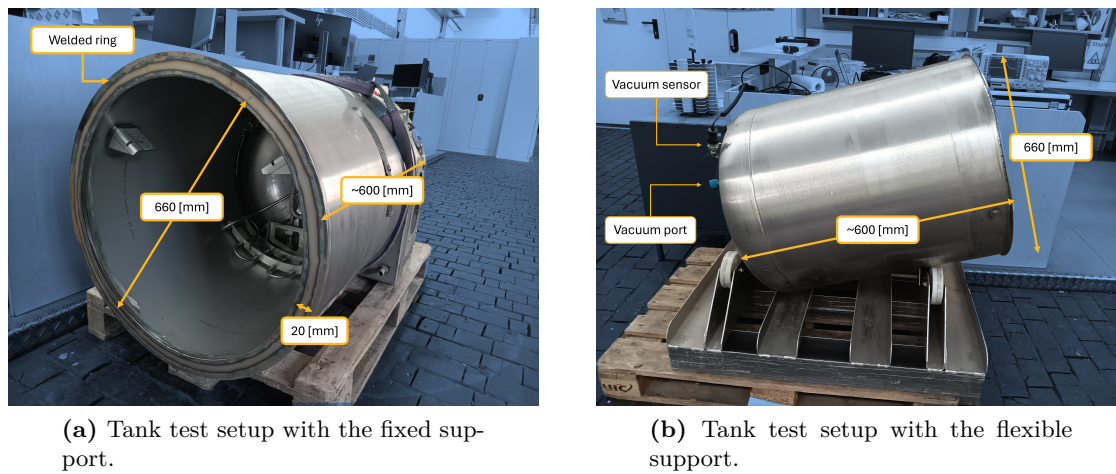


Figure 3.3: The tank test setups used in the experiments.

It should be noted that, whereas the flexible support setup is almost purely the tank itself, the fixed support has a significant number of pipes and other elements as can be seen in Figure 3.4.

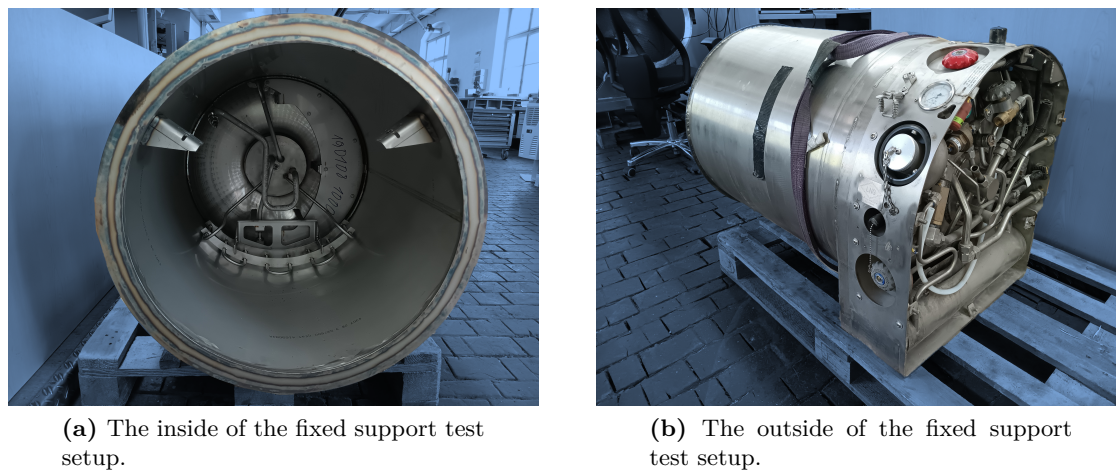


Figure 3.4: Pipes and other elements on the fixed support test setup.

To ensure that there remained a vacuum between the inner and outer tank shells, a ring was welded at the cut edge to close the gap (see Figure 3.3a). Restoring the vacuum is important to mimic the in-use conditions of the tank, as AE signals cannot travel through a vacuum, but can through air. The air pressure in between the inner and outer tank for the flexible and fixed support were 0.02 [mbar] and 0.06 [mbar] respectively (measured via the vacuum sensor port shown in Figure 3.3). It should be noted that the air pressure in the actual tank would be even lower, however due to time constraints the air pressures reached were deemed sufficient for the measurements to be performed.

Another important element to discuss is the support design. The fixed and flexible supports used in the tank are graphically represented in Figure 3.5. The longitudinal glide surface of the flexible support allows for movement of the inner/outer tank due to e.g. thermal expansion. The cylinder is made of a glass fibre composite, which properties can be found in Table 3.1.

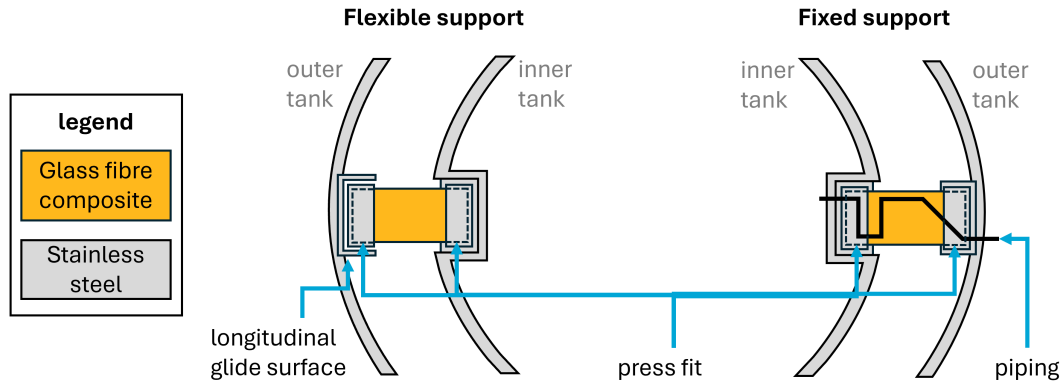


Figure 3.5: Graphical representation of the geometry of the two supports (not to scale).

Table 3.1: Material properties of the materials used in the LNG tank.

Material	Young's modulus [GPa]	Density [kg/m ³]
Stainless steel (1.4301)	200	7.9
Glass fiber composite (0/90)	28	2

3.2.2 PLB location measurements

In order to know where the PLBs are placed, a coordinate system for the tank has to be established. This was done by making and applying an adhesive flexible ruler to the tank as is shown in Figure 3.6. For the inner tank a single ruler is applied as all measurements will be performed in a line (the reason for this will be explained subsection 3.4.1). The 0 measurement is located at the edge of the support. For the outer tank, on the other hand, a 2D coordinate system is needed. This is achieved by measuring how far the PLB is along the circumference of the tank (the a-coordinate) and by measuring how far it is from the sensor located at the middle of the tank (the b-coordinate).

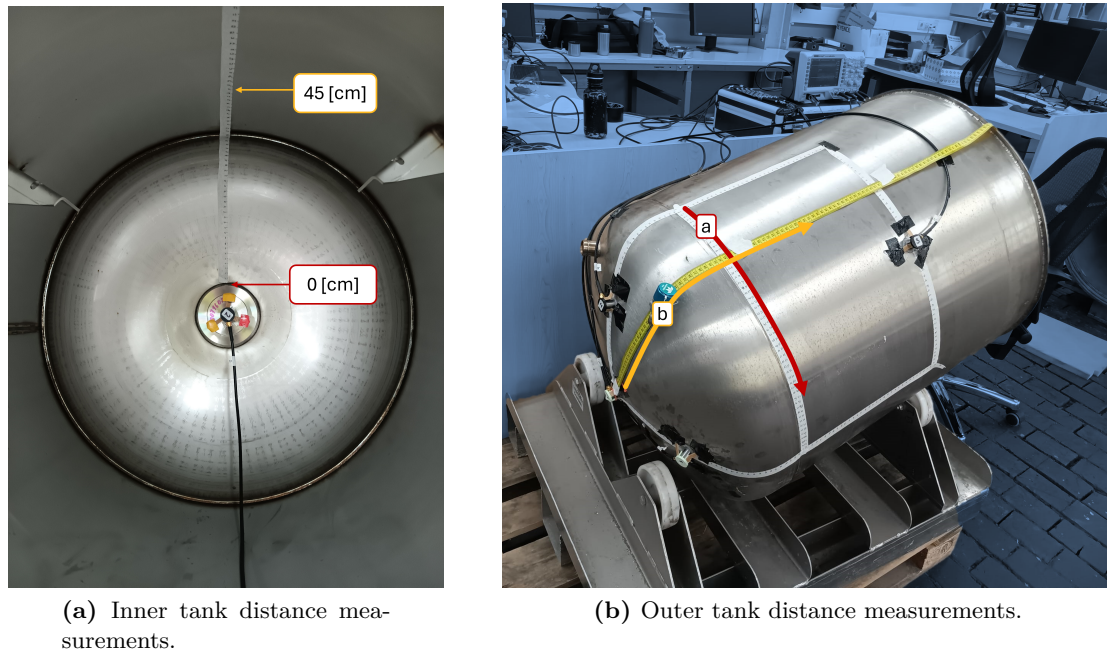


Figure 3.6: Measurement system used to determine the PLB locations.

3.2.3 Selected frequency for measurements

Before the measuring equipment can be selected, first the frequency of interest needs to be determined. Based on the literature research performed in subsection 1.10.2 a frequency of 100 [kHz] is selected. This is not only indicative of crack growth in AA2219 (which is often used in LH2 tanks), but falls within the ranges of the other materials investigated in subsection 1.10.2 as well. However, for composites 100 [kHz] is only indicative of matrix cracking.

3.2.4 Measuring equipment

In order to measure the AE waves generated by the PLBs the following is used: Sensors, amplifiers and an oscilloscope.

Sensors

First, the sensors used were Mistras' R15 α . The sensor sensitivity can be found in Figure 3.7. The sensor has an operating frequency range of 50 to 400 [kHz] and a temperature range of -65 to 175 [°C].

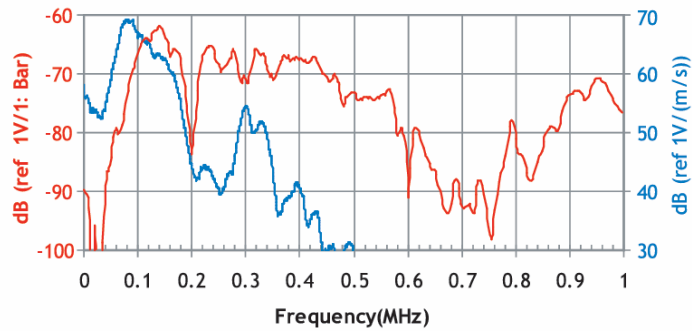


Figure 3.7: Sensitivity per frequency of Mistras' R15 α sensors [13].

Because of the different curvatures of the tank and the fact that the material was not magnetic, a new adaptable and easily removable sensor attachment method had to be developed. This resulted in the design that can be seen in Figure 3.8. The sensor holder is attached to the tank with strong double-sided tape. Before the experiments, the sensor holder was tested for its ability to hold the sensor firmly to the structure of different curvatures/angles, which was deemed sufficient.



Figure 3.8: Photo of the designed sensor holder in use.

Amplifiers

The used amplifiers were developed in-house by SHM Next². The specifications of the amplification achieved by the amplifiers (4 in total) can be seen in Figure 3.9. The max amplification of amplifier 1 is 67 [dB] whereas that of amplifier 2, 3 and 4 is 66 [dB]. Amplifier 1 has a slightly higher amplification to allow for smaller waves to be detected. It should be noted that in this thesis amplifier 1 is always connected to sensor 1, amplifier 2 to sensor 2 etc.

²More information on the company at <https://shmnext.com/>

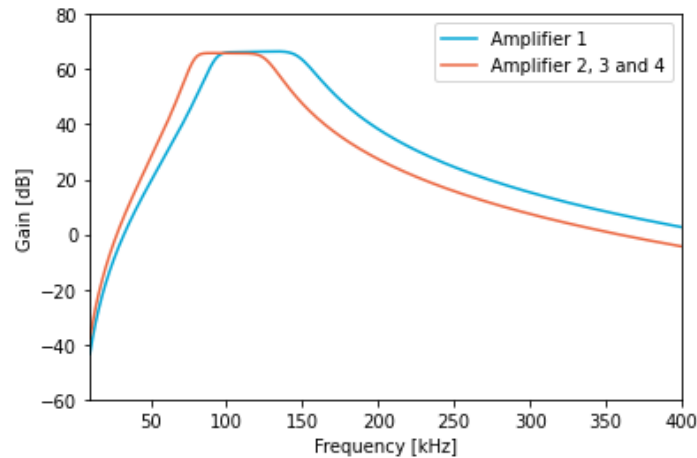


Figure 3.9: Amplifier gain used in the experiments.

Oscilloscope

The oscilloscope used to process the received signals is the Rigol DS1104Z+ with four channels. It has a 100 [MHz] bandwidth and is able to make 1000 [MSa/s] [129].

3.3 Signal onset determination

Before the damage localisation can be discussed, it is important to establish a method to determine the signal onset of an **AE** wave. This is due to the fact that most localisation methods mentioned in subsection 1.9.3 rely on the wave's time of arrival difference between sensors. To do so first the method to determine the signal onset will first be discussed. Then the difference in method to find **S0** and **A0** waves will be discussed. Finally, the settings used in this thesis will be shown.

3.3.1 Threshold crossing and **AIC** method

Because of its simplicity, promising results and the fact that the majority of the frequencies are already damped out by the amplifier, **TC** in combination with **AIC** was selected from the methods mentioned in subsection 1.9.1.

The **TC** method dictates that the signal has started whenever the signal crosses a predefined threshold. To increase accuracy the **IA** method was used. This means that the signal onset was defined based on the wave envelope crossing the threshold rather than the waveform itself. The **IA** was obtained by using the Hilbert transform on the signal [130]. To be able to use the lowest threshold possible, a variable threshold was used based on the noise in the signal. It was assumed (and visually verified) that for the first 0.1 [ms] the signal that was received did not contain an **AE** hit. Hence, the maximum value obtained in that time period will be used as a basis to add the threshold to.

As mentioned in subsection 1.9.1, the TC method has some drawbacks (large dependency on chosen threshold, sensitive to varying noise, can miss AE events if the threshold is too high). To overcome those, the AIC was performed based on a window around the signal onset determined by the TC method. The AIC method is based on the difference in entropy between the noise and the signal. The signal onset can be determined by finding the minimum of the AIC formula [131]:

$$AIC(i) = i \cdot \log(\text{var}(A[1, i])) + (M - i - 1) \cdot \log(\text{var}(A[i + 1, M])) \quad (3.1)$$

Where $A = [A_1, A_2, \dots, A_M]$ represents the signal data, M the number of samples, $\text{var}(A)$ refers to the signal amplitude variance and i ranges between 1 and M . It should also be noted that \log refers to the natural logarithm [131]. The improvement of signal onset determination due to AIC with respect to only using TC can be seen in Appendix B.

3.3.2 Identifying the signal onset of S0 and A0 waves

As discussed in subsection 1.8.1, whenever a PLB test is performed on a thin plate S0 and A0 waves travel through the structure with different speeds. As both waves have different properties, it was decided to look into both in this thesis to determine if one results in a better localisation accuracy for the problem at hand.

To determine the signal onset of S0 waves, the first crossing of the lowest possible threshold (i.e. such that it will not catch the noise) will be used, where after the AIC method will be used to improve the signal onset even more.

To find the signal onset of the A0 waves it is assumed that the amplitude of the A0 wave is larger than that of S0 waves at 100 [kHz] [132]. Hence, the threshold to detect A0 waves is set significantly higher than that of S0 waves. Subsequently, the AIC method will be used to find its signal onset more accurately. It should be noted that not in all cases it will accurately catch the A0 waves. However, as long as the method will accurately catch the same 'part' of the wave consistently, it will still be usable for damage localisation. For simplicity, however, it will be referred to in this thesis as the A0 wave. A drawback of differentiating between S0 and A0 waves is that when the PLB is performed close to the sensor, the S0 and A0 waves have not separate significantly, hence differentiating between the two will be less accurate.

3.3.3 Used TC and AIC settings

Based on trial and error, comparing the automatically determined signal onset with the manually selected onset and consistency of signal onset for PLBs on the same location the settings as shown in Table 3.2 were chosen. It should be noted that for damage localisation purposes the received signals were normalized against their maximum value, such that the waves were easily comparable. Additionally, there are separate thresholds for the fixed and flexible support setup, e.g. because of attenuation. These separate thresholds resulted in more accurate signal onset determination and hence better localisation accuracies.

Table 3.2: TC and AIC settings used to determine the signal onset of S0 and A0 waves.

Parameter	S0 waves	A0 waves
Threshold flexible support [-]	Max. noise + 0.03	0.45
Threshold fixed support [-]	Max. noise + 0.025	0.24
AIC window size [samples]	3000	3000

3.4 Experiment 1: Signal feasibility

The first experiment is focused on determining whether it is possible for a representative AE signal to travel through the entire tank and how its amplitude is affected by doing so. First the experiment will be detailed where after the method for attenuation determination will be discussed.

3.4.1 Experiment details

This experiment focuses on two aspects:

- **Part 1** focuses on whether it is possible for an PLB AE signal to travel through the support.
- **Part 2**, on the other hand, investigates the attenuation through the support, inner tank and outer tank. This is done to establish to what extent the signal changes with increasing propagation distance.

Associated research questions

Part 1 of this experiment aims to answer the following research question:

- RQ 1.1** To what extent is it possible to monitor the inner tank of an LH2 tank with outside-the-tank sensor placement in room temperature?

Part 2 of this experiments aims to answer:

- RQ 1.2** How does the inner tank support affect the amplitude of an AE signal in room temperature?
- RQ 1.3** How does the inner tank affect the amplitude of an AE signal in room temperature?
- RQ 1.4** How does the outer tank affect the amplitude of an AE signal in room temperature?

Test setup

To measure whether an AE signal can travel through the support (part 1 of this experiment), sensor 1 is placed at the end of the outer tank (see Figure 3.10a), while PLBs are performed on the inner tank. All PLBs are placed in a straight line next to the measuring tape that could be seen in Figure 3.6. This is done, because in the "entire tank with outside-the-tank

sensor placement" scenario there would only be two points of access to the inner tank: The two supports. Hence, only 1D localisation is possible. Therefore, to simplify the experiment (especially for inner tank localisation in experiment 3) all PLBs were placed on one line.

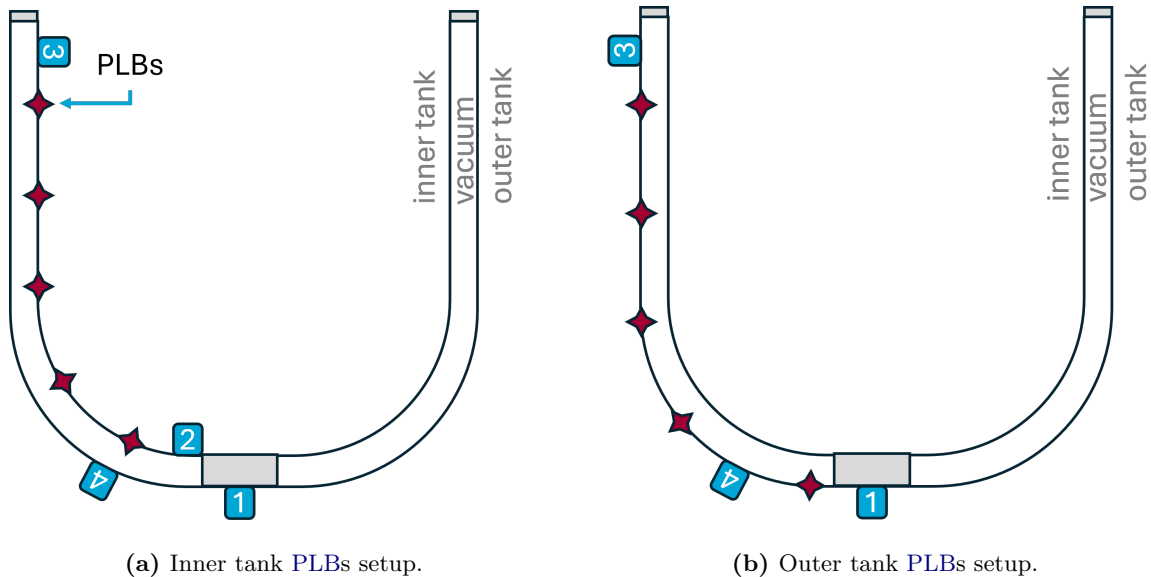


Figure 3.10: Graphical representation of the test setups for experiment 1 (not to scale).

However, it should be noted that due to the required accessibility of the inner tank, the signal now has two ways of travelling to sensor 1. These two paths can be seen in [Figure 3.11](#): Via the support (the red path) or via the cut edge (the green path). To verify that the (beginning of the) signal received at sensor 1 travelled via the support, sensor 4 is placed as shown in [Figure 3.10a](#). Whenever the signal reaches sensor 1 before it reaches sensor 4, the signal is considered to have travelled via the support. When, on the other hand, sensor 4 receives the signal first then the signal travelled via the cut edge (the green path).

Part 2 uses sensor 1, 2 and 3 as indicated in [Figure 3.10a](#) to investigate the amplitude change for PLBs placed on the inner tank. This part of the experiment also uses sensor 1 and 3 as indicated in [Figure 3.10b](#) to investigate the signal change for outer tank PLBs. In an entire tank scenario sensor 1 and 3 would both be placed on the ends of the tank. However, because the test setup is only half a tank sensor 3 is placed on the edge of the inner tank.

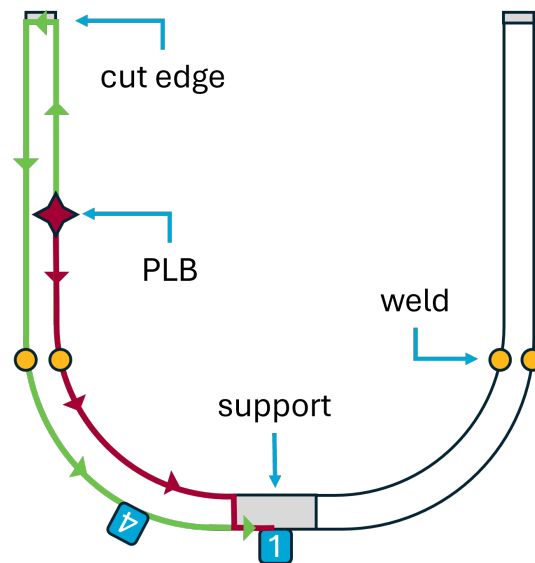


Figure 3.11: Graphical representation of the two possible travel paths to sensor 1 (not to scale).

PLB locations

The PLB locations for part 1 of this experiment are located such that they are along the entire line specified, but with more located near the cut edge to determine from where the signal travels along the cut edge rather than the support. The following PLBs were performed (5-10 PLBs per indicated location):

- **Flexible support, inner tank:** At 10, 40, 100, 200, 300, 400, 500, 550, 650, 700, 750 and 790 [mm]
- **Fixed support, inner tank:** At 0, 30, 200, 150, 300, 450, 500, 550, 600, 650 and 720 [mm]

Part 2 of this experiment uses a lower number of relatively evenly spaced PLB locations. At every locations 10 PLBs were performed to obtain an average maximum amplitude per PLB location. The following locations were used:

- **Flexible support, inner tank:** At 40, 100, 200, 300, 400, 500, 650 and 790 [mm]
- **Flexible support, outer tank:** At 10, 70, 150, 300, 450, 600 and 730 [mm]
- **Fixed support, inner tank:** At 30, 150, 300, 450, 600 and 720 [mm]

3.4.2 AE signal attenuation

The signal attenuation for part 2 of this experiment will be determined for the support, inner and outer tank.

Support attenuation

Once it is established whether an AE signal can travel through the support, it will be determined how the signal's amplitude has changed because of it. The change in amplitude due to the support is of interest as it will help understand what the minimum signal is that can travel through the support while still being detectable. The amplitude change will be

determined by subtracting the maximum values of the signals. The maximum amplitudes will be given in $[dB_{AE}]$, which uses a reference voltage of $1 [\mu V]$. It should be noted that for every signal the same window (starting from the measured signal onset) is looked at. This is done to minimise the influence of reflections.

Inner and outer tank attenuation

To understand how the AE signal is affected by travelling through the inner and outer tank, the amplitude change for PLBs at different locations is studied. This is again done by looking at the maximum amplitude in a given fixed window. To determine the inner tank attenuation signals from sensor 2 and 3 will be investigated. For the outer tank, the data obtained by sensor 1 and 3 will be used. Because of the logarithmic nature of decibels, the relation between PLB distance to the sensor and signal amplitude is expected to be linear [133].

It is important to note here that both the inner and outer tank consist of a dome and a cylinder welded together (see Figure 3.12). Figure 3.11 shows the locations of the welds. It is expected that these welds will cause additional refraction/scattering of the signal [134]. Hence, the presence of the weld will be taken into account while determining the attenuation.



Figure 3.12: Photo of the welded joint between the half sphere and the cylinder that together make half a tank (flexible support test setup).

3.5 Noise and signal distinction

When it is verified that the signal can travel through the inner and outer tank and the support, according to the flowchart in Figure 3.1 the next step is to determine if a received signal is noise or an AE signal originating from growing damage. As the focus of this thesis is on the feasibility of damage localisation, the research into the feasibility of using AE in the intended aviation environment is a literature review. The results of this review were summarised in section 1.11.

It should be noted, however, that the influence of noise on the inner and outer tank distinction accuracy will be discussed in section 3.6.

3.6 Experiment 2: Inner or outer tank distinction

The next step in the process, according to the flowchart in [Figure 3.1](#), is to determine whether a received signal came from the inner or outer tank.

3.6.1 Experiment details

The associated research questions to this experiment will be discussed where after the test setup will be elaborated upon. Finally, the positioning of the [PLBs](#) will be justified.

Associated research questions

The aim of this experiment is to answer the following research question:

- RQ 2** How accurately can the distinction be made in room temperature between simulated damage from the inner and outer tank?

Test setup

The test setup for this experiment can be seen in [Figure 3.13](#). Similar to experiment 1 ([section 3.4](#)) sensor 4 plays an important role. If a [PLB](#) is performed on the inner tank, the signal will travel via the support and reach sensor 1 before it will reach sensor 4. On the other hand, when a [PLB](#) is performed on the outer tank, sensor 4 will receive the signal before sensor 1.

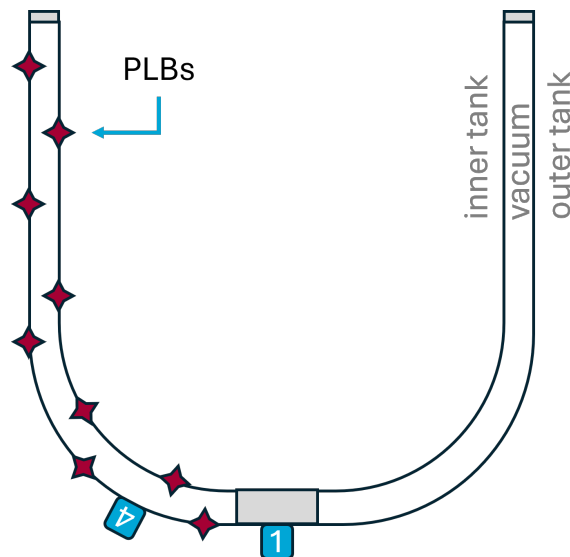


Figure 3.13: Graphical representation of the test setup for experiment 2 (not to scale).

It should be noted that this experiment will only be performed on the flexible support test setup. This is done because the outside of the fixed support test setup is difficult to reach, because of pipes and other elements as can be seen in [Figure 3.4](#).

PLB locations

The PLBs used in this experiment are:

- **Flexible support, inner tank:** At 40, 100, 200, 300, 400, 500, 650 [mm]
- **Flexible support, outer tank:** At 10, 70, 150, 300, 450, 600, 730 [mm]

The inner tank PLB locations mentioned above are based on the results of experiment 1. Hence, all inner tank locations are sufficiently far from the cut edge, such that the AE wave will travel faster through the support.

3.6.2 Influence of noise on distinction accuracy

To determine the effect of noise on the inner/outer tank distinction accuracy artificial noise is added to the received signal. This is done for a range of signal-to-noise ratios (SNRs). The noise added is a sinusoidal noise with constant amplitude and a frequency similar to the received signal (100 [kHz]). This is not necessarily the expected type of noise but does give an indication of the influence on the accuracy. The noise added is given by:

$$f_{noise}(t) = A_{max,signal} \sin(200000\pi t) \quad (3.2)$$

Where $A_{max,signal}$ is the maximum amplitude of the received signal. It should be noted that for all SNRs (except SNR=2) the algorithm still uses the threshold set to 0.45 of the maximum received amplitude. However, for an SNR of 2, this would mean that the threshold is below the noise, hence the threshold is raised to 0.51 of the maximum received amplitude.

3.7 Experiment 3: Inner tank damage localisation

The aim of this experiment is to determine the location of simulated damage on the inner tank. This section will first elaborate on the performed experiment and how the inputs needed to localise damage (wave speed and support travel time) are calculated. Finally, the localisation accuracy will be determined.

3.7.1 Experiment details

This subsection covers the details concerning experiment 3, which includes the associated research question, the test setup and PLB placements.

Associated research questions

The research question that will be answered with this experiment is the following:

- RQ 3.1** How accurately can the proposed sensor placement localise simulated damage in the inner tank in room temperature?

Test setup

For inner tank localisation sensor 1 and 3 are used, which are placed as indicated in Figure 3.14. In an entire tank scenario sensor 1 and 3 would both be placed on the "ends" of the tank. However, because the test setup is only half a tank sensor 3 is placed on the edge of the inner tank. To mimic the 1D nature of the inner tank localisation, all PLBs will be placed on a line between sensor 3 and sensor 1/the support. The experiment will be performed on the fixed and flexible support test setup.

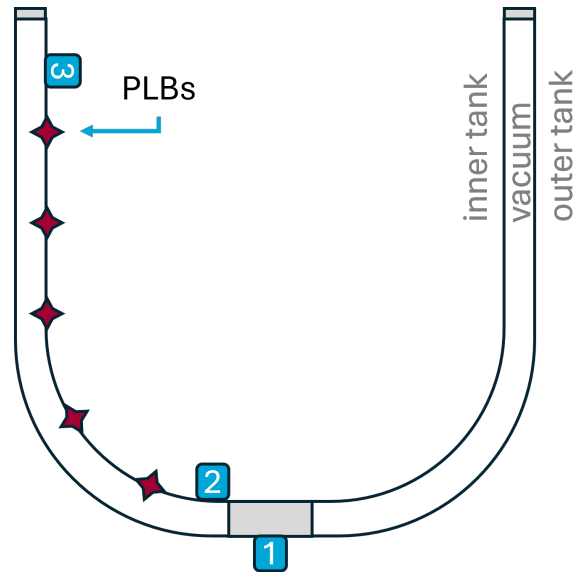


Figure 3.14: Graphical representation of the test setup for experiment 3 (not to scale).

PLB locations

For this experiment two datasets per test setup are gathered referred to as the 10 PLB dataset and the repeatability dataset. All PLBs were performed on the inner tank on one line between sensor 2 and 3.

The 10 PLB dataset consists of 10 PLBs at every location indicated below. This is done such that an average difference in arrival time can be obtained per location. This reduces the effect of outliers.

- **Flexible support:** At 40, 100, 200, 300, 400, 500, 650 and 790 [mm]
- **Fixed support:** At 30, 150, 300, 450, 600 and 720 [mm]

The repeatability dataset, on the other hand, has one PLB per indicated location. These locations are randomly selected, but different from the locations in the 10 PLB dataset. This dataset is gathered three (for the flexible support setup) or two (for the fixed support setup, due to resource constraints) times per test setup and in between the sensors were taken off and reattached again. This was done to determine the repeatability of the experiment and to see the influence of the sensor placement. The following locations were used:

- **Flexible support:** At 70, 120, 250, 290, 380, 420, 430, 510, 590 and 630 [mm]
- **Fixed support:** At 70, 120, 170, 250, 290, 310, 350, 380, 390 and 420 [mm]

3.7.2 Localisation input determination

As can be seen in the flowchart in [Figure 3.1](#), to be able to perform inner tank damage localisation, the inner tank wave speed and support travel time have to be determined.

Inner tank wave speed determination

To determine inner tank wave speed sensor 2 and 3 will be used in combination with the PLBs from the 10 PLB dataset. The inner tank velocity will be determined using the difference in time of arrival between sensor 2 and 3. The inner tank velocity (V_{IT}) is subsequently determined using [\[135\]](#) [\[136\]](#):

$$V_{IT} = \frac{L_{23} - 2(X_{PLB} - X_{s2})}{\Delta t_{32}} \quad (3.3)$$

Where L_{23} is the distance between sensor 2 and 3, X_{PLB} and X_{s2} the location of the PLB and sensor 2 respectively, and finally Δt_{32} the arrival time difference between sensor 3 and 2. The mean of the velocities obtained will be used for localisation of the PLB.

Support travel time determination

To determine the time it takes a signal to travel through the support the time difference between sensor 2 and sensor 1 is used (travel path indicated in green in [Figure 3.15](#)). Hence, the support travel time is given by:

$$t_{support} = t_{s1} - t_{s2} \quad (3.4)$$

Where t_{s1} is the signal's arrival time at sensor 1 and t_{s2} the arrival time at sensor 2. The mean of the travel times obtained will be used for localisation of the PLB.

3.7.3 Localisation accuracy

This subsection will dive into the steps needed to localise the PLBs. To do so first the localisation algorithm will be discussed, where after it will be investigated to what extend the inputs for the localisation can be optimised based on the localisation accuracy. Finally, the experiment repeatability and sensitivity will be investigated.

Localisation algorithm

To be able to localise the PLBs the path that the signal travels is of importance. The path of an arbitrarily placed PLB can be seen in [Figure 3.15](#). As can be seen the path consists partly of travelling through the inner tank (stainless steel, path indicated in red) and partly through the support (stainless steel and glass fibre, path indicated in green).

For localisation on a flat plate consisting entirely of the same material, [Equation 3.3](#) can be rewritten to find the PLB location based on the observed time difference between sensor 1 and 2. This results in the following equation:

$$X_{PLB} = \frac{L_{13}}{2} - \frac{V_{IT}\Delta t_{13}}{2} + X_{s1} \quad (3.5)$$

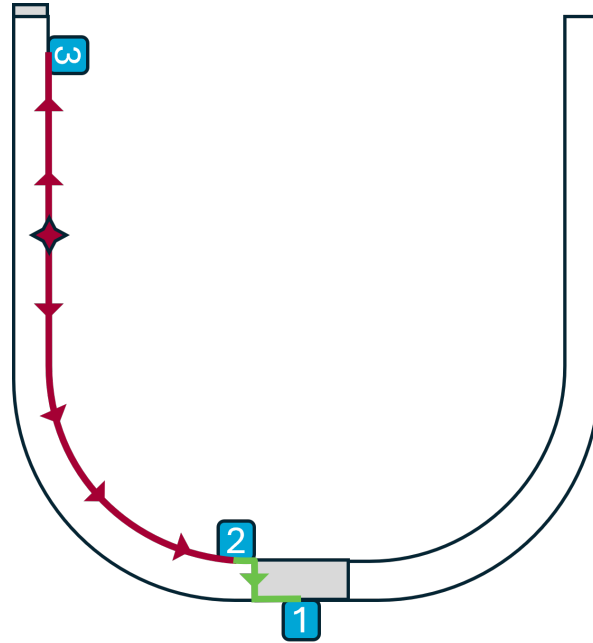


Figure 3.15: Graphical representation of the simplified travel path (indicated in red) from a PLB on the inner tank to sensor 1 and 3 (not to scale).

However, in reality the signal will travel through multiple materials and through a complex structure. Hence, Equation 3.5 no longer holds. Instead, the equation can be updated by realising that $\frac{L_{13}}{2}$ stands for the time-wise middle³ between sensor 1 and 3 (which in the case of a plate made of one isotropic material would be equal to the distance-wise middle⁴). The time-wise middle (X_{middle} , assuming that it is located on the inner tank) for the situation at hand can be determined by:

$$X_{middle} = X_{s3} - V_{IT} \frac{t_{support} + \frac{L_{23}}{V_{IT}}}{2} \quad (3.6)$$

Where $t_{support}$ refers to the time it takes the signal to travel through the support. Subsequently, knowing that sensor 1 is placed at $X=0$ [mm], the PLB location can be determined using:

$$X_{PLB} = X_{middle} - \frac{\Delta t_{13} V_{IT}}{2} \quad (3.7)$$

The predicted PLB locations will be compared with the actual PLB locations to determine the accuracy of the monitoring system. The localisation accuracy for S0 and A0 waves will be compared based on their root-mean-square error (RMSE). This error is relatively easy to interpret as it is in the same units as the original variable. Additionally, it is sensitive to large

³The time-wise middle refers to the location where a PLB would result in the same time of arrival at both sensors.

⁴The distance-wise middle refers to the location where the PLB is located the same distance from both sensors.

errors. Hence, during input optimization it penalizes possibilities with large outliers more. The **RMSE** can be determined using [137]:

$$RMSE = \sqrt{\frac{\sum_{i=1}^n (\hat{X}_i - X_i)^2}{n}} \quad (3.8)$$

Where X_i refers to the predicted location, \hat{X}_i to the actual locations and n to the number of **PLBs**.

Input optimisation to improve localisation accuracy

The inputs used in the localisation algorithm (V_{IT} and $t_{support}$) were calculated based on the experiments performed (see subsection 3.7.2). However, the determination of these inputs has uncertainty (signal onset determination, distinction between S0 and A0 waves, etc.). Hence, it will be investigated if there is a V_{IT} and $t_{support}$ combination that would result in a higher localisation accuracy. This will be done by inputting a range of values for V_{IT} and $t_{support}$ (1% to 200% of the original V_{IT} value and 1% to 300% of the original $t_{support}$ value) and comparing the subsequent **RMSE** to find the most optimal combination.

Experiment repeatability

To determine whether the experiment is repeatable, ten **PLBs** were performed on random locations on the inner tank. Subsequently the sensors were removed and reattached and on the same 10 random locations a **PLB** was performed. For the flexible tank this was also done a third time (due to time constraints this was not possible for the fixed support tank). The localisation accuracy was then determined based on those two or three rounds using the optimised velocity and support travel time.

These rounds of **PLBs** had two main reasons:

- By removing and reattaching the sensors there will be a **deviation in the sensor location and how well it is attached** to the structure. This deviation can also exist in real life use. Hence, this method will allow for a more realistic localisation accuracy.
- This allows for determination of localisation accuracy of **data points that were not used to optimise the inner tank velocity and support travel time**. Hence, it will give a more realistic image of expected localisation accuracy.

Sensitivity study

Finally, a sensitivity study will be performed. This is done to determine the sensitivity of the method to changes of the input variables. The two types of sensitivity studies that were performed are: A one-way sensitivity analysis and a Monte Carlo analysis.

The aim of the one-way sensitivity analysis (also known as one-at-a-time analysis) is to find the parameter in the method that has the largest influence on the localisation accuracy. This is done by changing one parameter at a time and determining its influence on the localisation accuracy [138]. The changed parameters were: Sensor location, Δt_{13} , inner tank wave velocity and the support travel time. All these parameters were changed with +10% and -10%. The parameter that changes the output the most is considered to be the parameter the method is the most sensitive to.

The Monte Carlo analysis investigates the influence of the same parameters as in the one-way sensitivity analysis. However, instead of changing them one by one they will all be changed at the same time. The choice for parameter values are based on a normal distribution of those parameters [138]. The standard deviations for the inner tank wave velocity and the support travel time are the standard deviations from the localisation input determination. The standard deviations used for the sensor locations are 10 [mm] based on the estimated expected difference between actual and measured sensor placement. Lastly, the wave arrival time differences' standard deviation is set to 20 [μs]. The number of iterations is chosen such that the analysis is converged. An overview of the inputs and their standard deviations is given in [Appendix E](#).

3.8 Experiment 4a: Outer tank damage 1D localisation

After the localisation of [PLBs](#) on the inner tank, it is determined how accurately [PLBs](#) on the outer tank can be localised. The focus of this experiment is on determining the 1D localisation accuracy of simulated damage on the outer tank.

3.8.1 Experiment details

This experiment is focused on determining the 1D localisation accuracy of simulated damage on the outer tank. It consists of two parts, which (because of accessibility) will both only be performed on the flexible support test setup.

- **Part 1** performs the outer tank localisation similar to the inner tank localisation. This means that all sensors and [PLBs](#) are located on the same line in between the sensors. This experiment allows for localisation accuracy comparison with localisation on the inner tank, hence the influence of the support can be determined.
- **Part 2** of the experiment still has the sensors on one line, but the [PLB](#) will no longer be performed on that line. It is essentially a 1D localisation on a 2D plane. This experiment is more representative of the in-use scenario and hence gives a better representation of the actual expected accuracy.

Associated research questions

The research question that will be answered with this experiment is:

- RQ 3.2** How accurately can the proposed sensor placement localise simulated damage in the outer tank in room temperature?

Test setup for experiment part 1

The test setup for experiment 4a part 1 can be seen in [Figure 3.16](#). Sensor 1 is again placed on the end of the tank. Also, the guard sensor 4 is placed on the same location as is done in experiment 1 and 2. Sensor 3 is placed relatively close to the cut edge (200-300 [mm] distance). The placement of sensor 3 has the same reasoning as the placement of sensor 3 experiment 3.

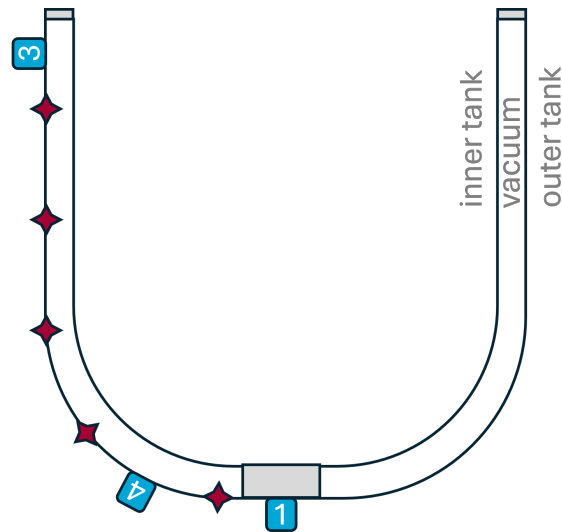


Figure 3.16: Graphical representation of the test setup for experiment 4a part 1 (not to scale).

Due to the accessibility of the outer tank, this experiment (both part 1 and part 2) will only be performed on the flexible support test setup. As the outer tank material for both test setups is the same, it is assumed that the flexible support test setup will provide an indicative accuracy result for the entire outer tank.

PLB locations for experiment part 1

For the same reasons as discussed in experiment 3 there will be two datasets: The 10 PLB and the repeatability dataset. In both cases all PLBs will be performed on the outer tank on one line between sensor 1 and 3. The 10 PLBs dataset will contain the following locations: 10, 70, 150, 300, 450, 60 and 730 [mm].

In contrast to experiment 3, the repeatability dataset is only gathered once. This was done due to the limitation of resources. Hence, this dataset cannot be used to determine the influence of the sensor placement but can give an indication on the localisation accuracy based on one PLB that was not used in the optimisation of the localisation accuracy. The following locations were used for the repeatability dataset: 10, 60, 100, 150, 280, 360, 470, 530, 540, 640 and 720 [mm].

Test setup for experiment part 2

As can be seen in Figure 3.17, the setup for part 2 of this experiment is similar to the setup of part 1. Again sensor 1 is placed at the end of the tank and sensor 3 near the cut edge (200-300 [mm] distance). However, in part two a 2D area covering a quarter of the half tank test setup is used (with the flexible support). The area under consideration is assumed to be a flat plate for simplicity.

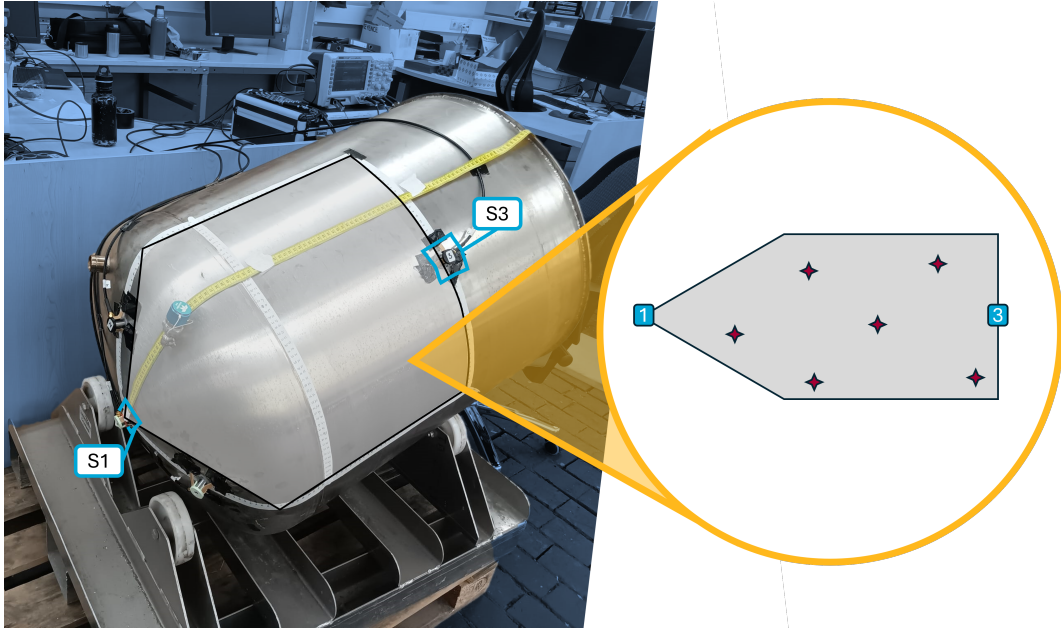


Figure 3.17: Graphical representation of the test setup for experiment 4a part 2 (not to scale).

PLB locations for experiment part 2

As the PLBs are now placed on a 2D area the a,b-coordinate system as explained in [subsection 3.2.2](#) will be used. The semi-random choice for locations follows the following pattern: At every randomly selected a-coordinate, 5 PLBs are performed at different b-coordinates (of which 2 on the dome part and 3 on the cylinder part of the setup). The following locations are used (a [mm], b [mm]):

- (80,120) • (200,150) • (320,70) • (410,170) • (500,40)
- (80,300) • (200,320) • (320,280) • (410,340) • (500,260)
- (80,390) • (200,400) • (320,410) • (410,370) • (500,400)
- (80,540) • (200,500) • (320,490) • (410,620) • (500,450)
- (80,720) • (200,600) • (320,730) • (410,700) • (500,600)

3.8.2 Localisation input determination

Both part 1 and part 2 of this experiment need the signal's outer tank velocity to be able to localise the PLBs. This will be done using the 10 PLB dataset from part 1 of the experiment as it is the most extensive dataset that allows for averaging the wave velocity at different locations to minimize the effect of outliers. The equation used to determine the outer tank wave velocity (V_{OT}) is similar to [Equation 3.3](#) and can be stated as follows:

$$V_{OT} = \frac{L_{13} - 2(X_{PLB} - X_{s1})}{\Delta t_{31}} \quad (3.9)$$

Where L_{13} is the distance between sensor 1 and 3, X_{PLB} and X_{s1} the location of the PLB and sensor 1 respectively, and finally Δt_{31} the arrival time difference between sensor 3 and 1. The mean of the velocities obtained will be used for localisation.

3.8.3 Localisation accuracy

To determine the localisation accuracy first the localisation algorithm used and how it can be optimised is discussed. Thereafter the sensitivity of the proposed method is investigated. The discussed methods are valid for part 1 and 2 of this experiment.

Localisation algorithm

As outer tank localisation does not have to take into account the influence of the support, the localisation of the PLBs can simply be done by rewriting Equation 3.9 to:

$$X_{PLB} = \frac{L_{13} - \Delta t_{31} V_{OT}}{2} + X_{s1} \quad (3.10)$$

The calculated X_{PLB} will be compared to the b-coordinate of the actual PLB location to determine the RMSE.

Input optimisation to improve localisation accuracy

The minimisation of the RMSE will be done in two ways: Optimising the outer tank wave velocity and by using sensor 4 (as indicated in Figure 3.16) to divide up the 1D line in two parts, such that there are two parts that are a bit curved instead of one really curved one. Finally, these two optimisation methods will be combined to determine the lowest RMSE obtainable.

To perform the optimisation using sensor 4 the following method is used:

- Use sensor 1 and 2 to make a first location estimation.
- If the first estimation results in a damage location between sensor 1 and 4, use sensor 1 and 4 to localise the damage.
- If the first estimation results in a damage location between sensor 4 and 3, use sensor 4 and 3 to localise the damage.

Sensitivity study

The Monte Carlo sensitivity study will be performed similarly to experiment 3 (subsection 3.7.3). The inputs of the sensitivity study are given in Appendix E.

3.9 Experiment 4b: Outer tank damage 2D localisation

Because of the accessibility of the outer tank, more sensors can be placed, making 2D localisation is possible. Hence the aim of experiment 4b is to assess the 2D localisation accuracy of simulated damage on the outer tank.

3.9.1 Experiment details

Before the localisation can be discussed, first the details of the experiment will be given. This entails the associated research question, test setup and PLB placements.

Associated research questions

The research questions that will be answered with this experiment is:

- RQ 3.2** How accurately can the proposed sensor placement localise simulated damage in the outer tank in room temperature?

Test setup

Figure 3.18 shows the test setup for experiment 4b, which is again a quarter of the half tank test setup (with the flexible support). Sensor 1 and 3 are placed at the same location as is the case in experiment 4a part 2. Sensor 2 and 4 are located such that they represent guard sensors (as for an entire tank monitoring system three to four guard sensors are needed around sensor 1 for inner/outer tank distinction). All four sensors will be used to localise damage.

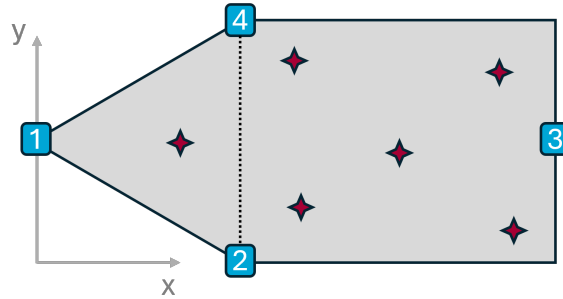


Figure 3.18: Graphical representation of the test setup for experiment 4b on a quarter of the half tank test setup (not to scale).

PLB locations

The same PLBs will be used in this experiment as were used in experiment 4 part 2.

3.9.2 Localisation accuracy

To determine the localisation accuracy of outer tank 2D localisation, the method used to determine the PLB locations will first be discussed. Thereafter it will be shown how the method will be optimised and how the sensitivity will be assessed.

Localisation algorithm

Similarly to experiment 4a part 2, the quarter tank will be assumed to be a flat plate. In order to compare the PLB locations (a,b-coordinate system) to the predicted locations (x,y-coordinate system), the used a,b-coordinate system of the tank has to be converted to the x,y-coordinate system of the flat plate (indicated in Figure 3.18). For PLBs located in the left triangle in Figure 3.18 the following coordinate system conversion can be used:

$$x = b\cos(\theta) \quad (3.11a)$$

$$y = y_{s1} + b\sin(\theta) \quad (3.11b)$$

Where:

$$\theta = \frac{a}{r} - 0.25\pi \quad (3.12)$$

Where r refers to the radius of the tank. Similarly, for the PLBs located in the rectangle on the right in Figure 3.18:

$$x = r\cos(\theta) + b - r \quad (3.13a)$$

$$y = y_{s1} + r\sin(\theta) \quad (3.13b)$$

The next step is to predict the PLB location based on the time of arrival differences between sensors. To determine the PLB location the unknowns in the following equations (X_{PLB} , Y_{PLB} and t_{PLB}) are iterated upon to reduce the errors ($\epsilon_{1,2,3,4}$).

$$V_{OT}(t_{s1} - t_{PLB}) = \sqrt{(X_{s1} - X_{PLB})^2 + (Y_{s1} - Y_{PLB})^2} + \epsilon_1 \quad (3.14a)$$

$$V_{OT}(t_{s2} - t_{PLB}) = \sqrt{(X_{s2} - X_{PLB})^2 + (Y_{s2} - Y_{PLB})^2} + \epsilon_2 \quad (3.14b)$$

$$V_{OT}(t_{s3} - t_{PLB}) = \sqrt{(X_{s3} - X_{PLB})^2 + (Y_{s3} - Y_{PLB})^2} + \epsilon_3 \quad (3.14c)$$

$$V_{OT}(t_{s4} - t_{PLB}) = \sqrt{(X_{s4} - X_{PLB})^2 + (Y_{s4} - Y_{PLB})^2} + \epsilon_4 \quad (3.14d)$$

Where $X_{s\#}$ (and $Y_{s\#}$) and $t_{s\#}$ refer to the location and signal arrival time of a certain sensor. Additionally, X_{PLB} (and Y_{PLB}) and t_{PLB} refer to the AE source location and time of the initiation of the signal which are unknown. The errors ($\epsilon_{1,2,3,4}$) in the above equations are due to, for example errors in the signal onset determination or due to structural differences between the test setup and an isotropic flat plate (for which the equations are derived). The combination of X_{PLB} , Y_{PLB} and t_{PLB} that result in the lowest average error for all four equations above is the predicted PLB location. A visual representation of above method (a good and bad example) can be seen in Figure 3.19.

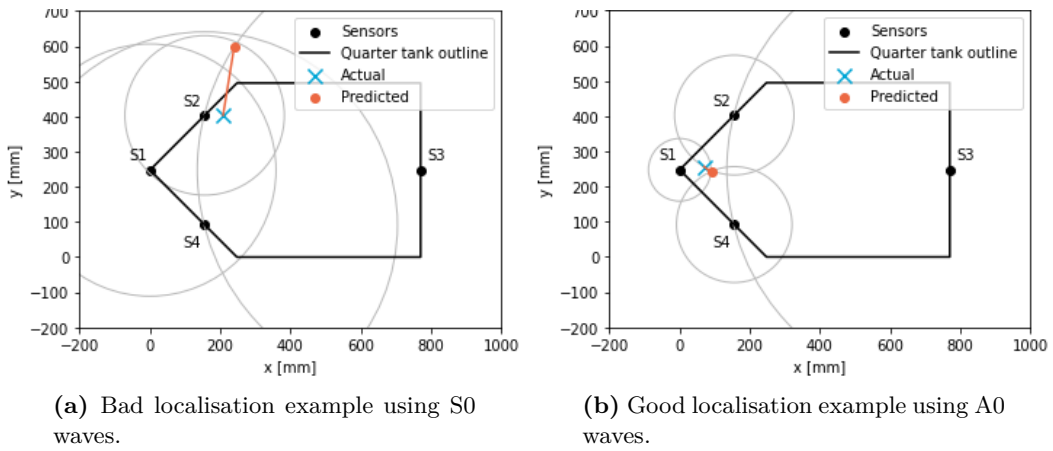


Figure 3.19: 2D localisation examples with graphical representation of time of arrival circles.

Input optimisation to improve localisation accuracy and sensitivity study

To optimise the localisation accuracy the outer tank wave velocity will be iterated upon to find the most optimal value in terms of localisation accuracy. For the sensitivity analysis a Monte Carlo simulation was performed using the method explained in [subsection 3.7.3](#). The inputs of the Monte Carlo simulation can be found in [Appendix E](#).

Results and Discussion

This chapter dives into the results of the performed experiments following the same order as indicated in the method flowchart ([Figure 3.1](#)). It should be noted that all results are divided into those of the flexible and those of the fixed support setup results and those based on S0 and A0 waves. First the feasibility of the signal travelling through the support and its attenuation will be discussed in [section 4.1](#). Thereafter it will be discussed in [section 4.2](#) whether and to what extent the distinction between inner and outer tank damage can be made. Subsequently, the 1D localisation accuracy of inner tank damage and outer tank damage are shown in [section 4.3](#) and [section 4.4](#) respectively. In the last experiment section, the 2D localisation accuracy of outer tank damage will be discussed ([section 4.5](#)). Finally, this chapter is ended with a discussion in [section 4.6](#) about the limitations of the experiments and how they are expected to influence the discussed results.

4.1 Experiment 1: Signal feasibility

In order to facilitate the outside-the-tank sensor placement as discussed in [chapter 2](#), the AE signal has to be able to travel through the support. The results as to whether this is possible will be discussed first. Thereafter it will be discussed how the support and other structural parts influenced the signal's amplitude.

4.1.1 Feasibility of a signal travel path through the support

First the flexible support results will be discussed, thereafter the fixed support results. Examples of received signals can be found in [Appendix A](#).

Flexible support

The results of whether the signal would travel through the support from PLBs at multiple distances from the support can be found in [Figure 4.1](#).

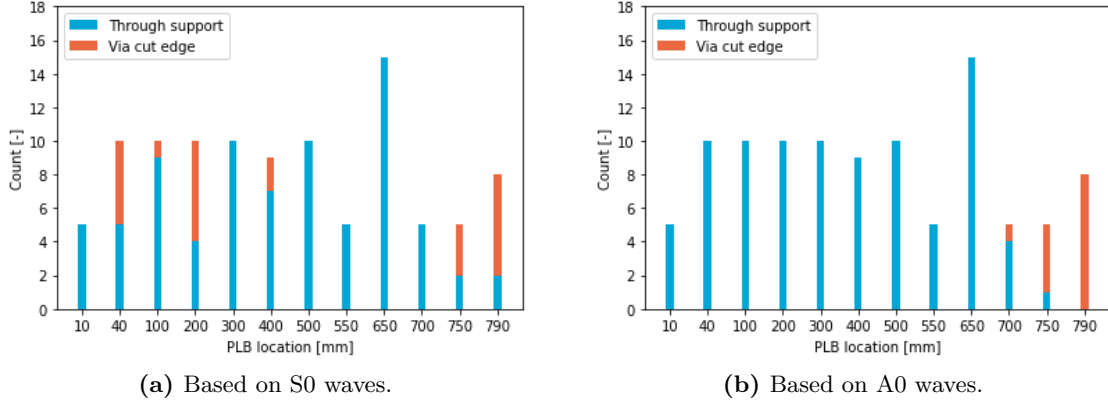


Figure 4.1: Determination whether the signal travels through the flexible support or via the cut edge. Total number of PLBs: 102.

It can be seen that, especially for the A0 waves, the signal travels through the support up to a distance of 700 [mm] from the support. From there onwards the wave travelling through the support and via the cut edge arrive around the same time. If the PLB is placed even further away from the support (e.g. 790 [mm]) the signal travels via the cut edge faster than it travels via the support. The S0 waves does not give such a clear-cut view as the A0 graph does. However, further investigation into the S0 waves shows that the signal onset determination method sometimes catches a bit of noise, or the noise itself makes it difficult to find an accurate S0 onset.

Hence, it can be concluded that an PLB signal can travel through the flexible support and that A0 waves outperform the S0 waves in determining so. However, in further experiments the PLBs should not be placed further away than 650 [mm] to ensure that the signal travels via the flexible support faster.

Fixed support

Whether or not a signal travelled through the fixed support faster than via the cut edge can be seen in Figure 4.2.

In contrast to the flexible support results, for the fixed report results the S0 and A0 waves both indicate that a PLB further away than 500 [mm] results in a signal travelling via the cut edge faster. This distance is significantly shorter than the 650 [mm] that was found for the flexible support. This can be explained by the fact that for the fixed support test setup sensor 4 is placed further away from sensor 1 than is the case for the flexible support test setup. This is due to the presence of pipes and valves on the fixed support setup. Hence, sensor 4 on the fixed support setup will catch the wave travelling via the cut edge sooner, which results in the 500 versus 650 [mm] distance difference.

Therefore, it can be concluded that an PLB signal can travel through the fixed support. However, in further experiments the PLBs placed on the inner tank should be at most 500 [mm] away from the support to be sure that the received signal travels via the support faster.

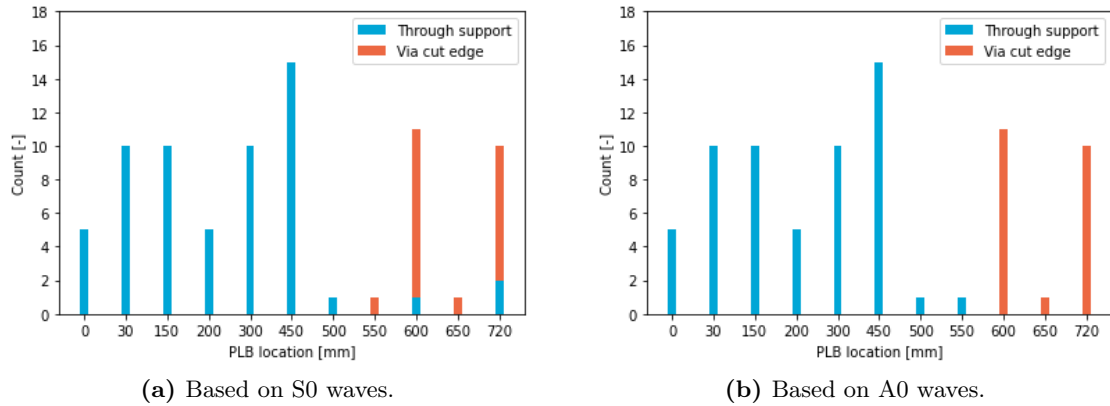


Figure 4.2: Determination whether the signal travels through the fixed support or via the cut edge. Total number of PLBs: 69.

4.1.2 AE signal attenuation

The change in maximum wave amplitude per sensor is illustrated in Figure 4.3. In these figures it is also illustrated whether the PLB is placed on the cylinder part of the test setup, or the dome part.

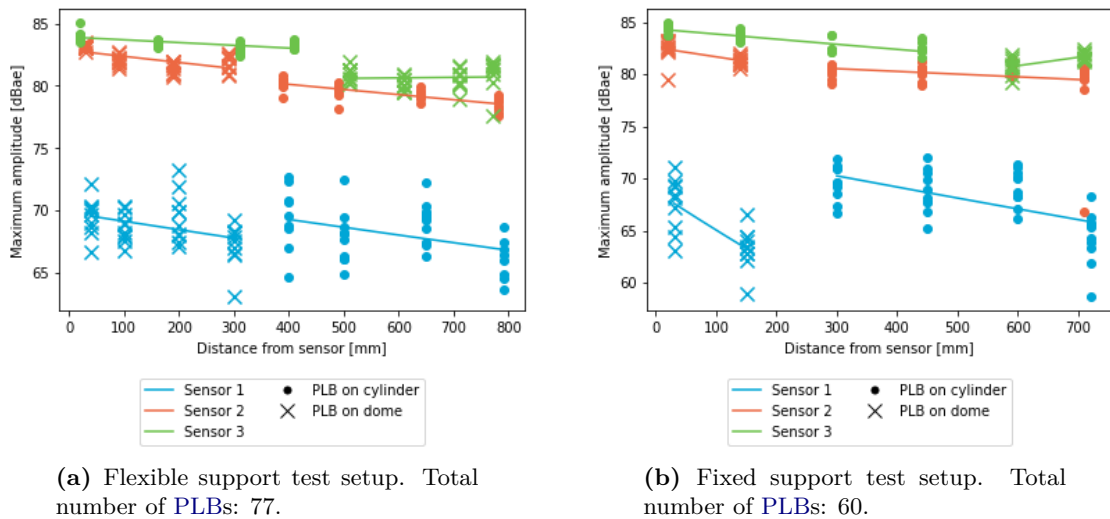


Figure 4.3: Maximum amplitude for the different sensors at varying PLB locations on the inner tank.

For both the flexible and fixed support it can be seen that sensor 2 and 3 give similar values and trends, as is expected as they are both located on the inner tank. For sensor 2 and 3 on the flexible support an average attenuation of $-2.70 \cdot 10^{-3}$ [dB_{AE}/mm] is measured, whereas for the fixed support setup an attenuation of $-2.06 \cdot 10^{-3}$ [dB_{AE}/mm] is measured. Amplitude differences between the sensors could be attributed to differences in how well the sensors are attached and/or the amount of Vaseline used. Hence it is recommended for future research

to perform the attenuation experiment multiple times while detaching and re-attaching the sensors in between the experiments. Also, a slight change in amplitude can be observed as the signal passes the weld between the dome and the cylinder part of the tank due to scattering of the signal.

Sensor 1, on the other hand, has a significantly lower maximum amplitude for both test setups. This can be explained by the attenuation (flexible support: -12.01 [dB_{AE}], fixed support: -13.68 [dB_{AE}]) as a result of the AE signal travelling through the support. The difference between the flexible and fixed support attenuation can be attributed to the distance between sensor 1 (on the outer tank) and sensor 2 (on the inner tank against the support). This distance is larger for the fixed support than for the flexible support due to a difference in support size, see Figure 4.4). Also, as the fixed support holds the pipes, it can be argued that their presence could also lead to additional reflections and scattering. Hence, the presence of the pipes could increase the attenuation between sensor 1 and 2.

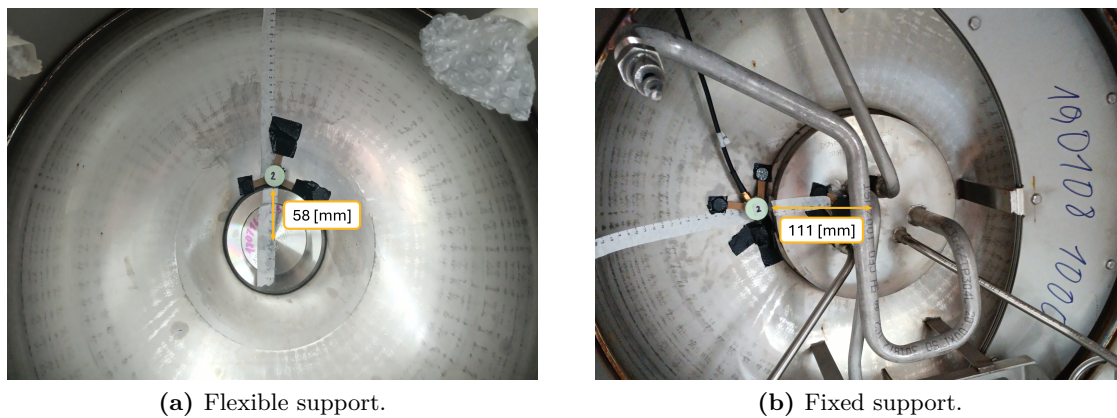


Figure 4.4: Sizes of the flexible and fixed supports.

For the outer tank, the results can be found in Figure 4.5.

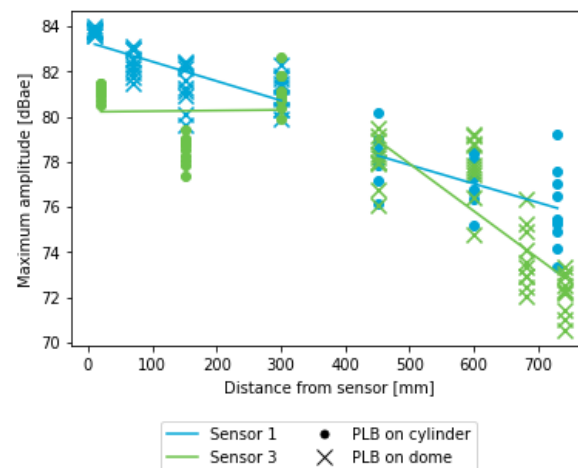


Figure 4.5: Maximum amplitude for the different sensors at varying PLB locations on the outer tank. Total number of PLBs: 70.

For sensor 1 on the outer tank an attenuation of $-8.47 \cdot 10^{-3}$ [dB_{AE}/mm] can be observed, with a slight additional drop (1.15 [dB_{AE}]) in maximum amplitude as the weld between the dome and the cylinder part of the tank is passed. Sensor 3 on the other hand has an attenuation of $2.95 \cdot 10^{-4}$ [dB_{AE}/mm] for the PLBs on the cylinder and an attenuation of $-2.10 \cdot 10^{-2}$ [dB_{AE}/mm] for those placed on the dome.

For both the inner and outer tank attenuation on both setups there are certain locations where the maximum amplitude goes unexpectedly up rather than the expected downwards trend. There are multiple reasons as to why this is the case:

- **Location accessibility.** Due to the size of the test setup, not all locations were easily accessible. This could lead to differently performed PLBs at different locations (e.g. different pencil angle, position or force). Additionally, because of the fact that some locations were difficult to reach, noise was created (i.e. a zipper of a jacket rubbed against the setup). Hence, a variation in maximum amplitude could be a result of the lack of accessibility.
- **Reflections.** Due to the geometry of the tank, reflected waves could influence the maximum wave amplitude. For example, the weld between the dome and the cylinder part of the tank leads to scattering of the wave, hence reducing the wave's maximum amplitude [134]. Additionally, the reflections could lead to superposition or cancelling out of the wave, hence resulting in higher or lower maximum amplitudes than would be expected based on the distance from the sensor. To minimize the effect of reflections, the window of the wave that is looked at is kept consistent for all received signals and is tuned such that the number of reflections is minimized.

4.1.3 Sensor placement on the complete tank

As the AE waves can travel through both supports, all sensors can be placed on the outer tank, still allowing inner tank monitoring. This outside-the-tank sensor placement has the following advantages:

- The sensors can be placed after the tank has been manufactured, hence it will not interfere with the tank design or the manufacturing process. This also means that the SHM system can be applied to already existing tanks.
- If a sensor fails it can easily be replaced.

A sensor placement as shown in Figure 4.6 is proposed. The placement of sensor 1 and 2 is based on the inner tank damage localisation. They are placed on the outer tank in the center of the support, such that they are at the symmetry line of the tank to allow for 1D localisation in the inner tank. The sensors around sensor 1 and 2 are guard sensors and are used to determine whether damage is located on the outer or inner tank (discussed further in the next section). These guard sensors will also be used for outer tank damage localisation. Dependent on the size of the tank a required outer tank damage localisation accuracy more sensors could be placed halfway the tank.

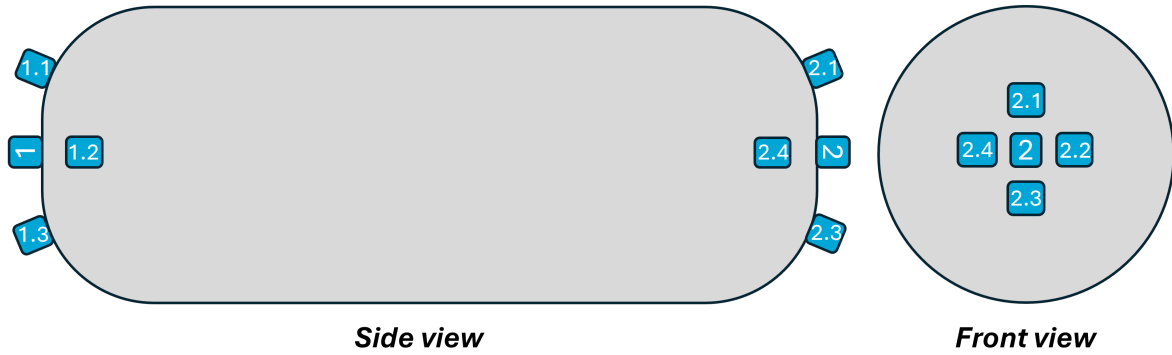


Figure 4.6: Graphical representation of the sensor placement on the complete tank (not to scale).

4.2 Experiment 2: Inner or outer tank distinction

Now that it has been established that a PLB AE signal can travel through the support, the next step is to determine whether that signal originates from the inner or outer tank. To do so the ability to accurately predict simulated damage on the inner tank will be investigated and subsequently the outer tank damage. Thereafter, the overall accuracy of the proposed method will be discussed. Finally, the influence of noise on the accuracy will be investigated.

4.2.1 Simulated damage on the inner tank

First it was determined how accurate the proposed method can predict that inner tank (IT) PLBs are indeed inner tank PLBs and not outer tank (OT) ones. The results are shown in Figure 4.7. It can be seen that the S0 waves are correct the majority of the times and the A0 waves' prediction is even correct 100% of the time. This difference can again be attributed to the S0 waves mistakenly identifying noise as the signal start.

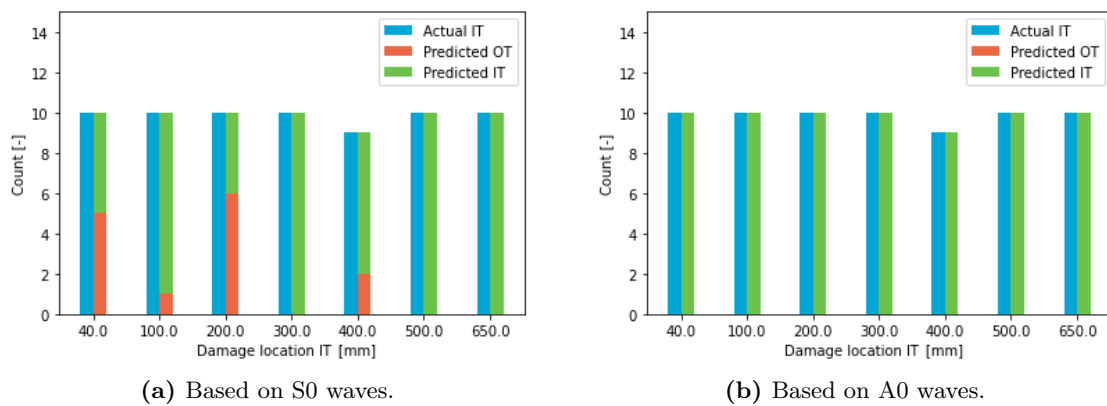


Figure 4.7: Predicted PLB locations (inner (IT) or outer tank (OT)) where the actual location is on the inner tank. Total number of PLBs: 69.

4.2.2 Simulated damage on the outer tank

Secondly, PLBs were performed on the outer tank. Figure 4.8 shows that the prediction is slightly better for S0 waves than it is for A0 waves. What is noticeable in both cases is that the PLBs located at 10 and 70 [mm] on the outer tank are systematically categorised as inner tank damage. This is due to the fact that these locations are in between sensor 1 and 4, but closer to 1 than to sensor 4 (referred to as the 'grey area'). Hence, as sensor 1 will receive the signal first, the proposed method will categorise this damage as inner tank damage. Possible solutions to overcome this problem:

- **Sensor 4 can be placed closer to sensor 1.** For this feasibility study it was desired to have a relatively large distance between sensor 1 and 4, such that the signal's arrival time difference would be significant. By placing sensor 1 and 4 closer together, the gray area where outer tank damage is mistaken for inner tank damage becomes smaller.
- **More sensors available on the entire tank.** When the SHM system is used on a entire tank, more (guard) sensors will be in place to monitor the entire tank. These additional (guard) sensors can be used to further narrow down the actual damage location.

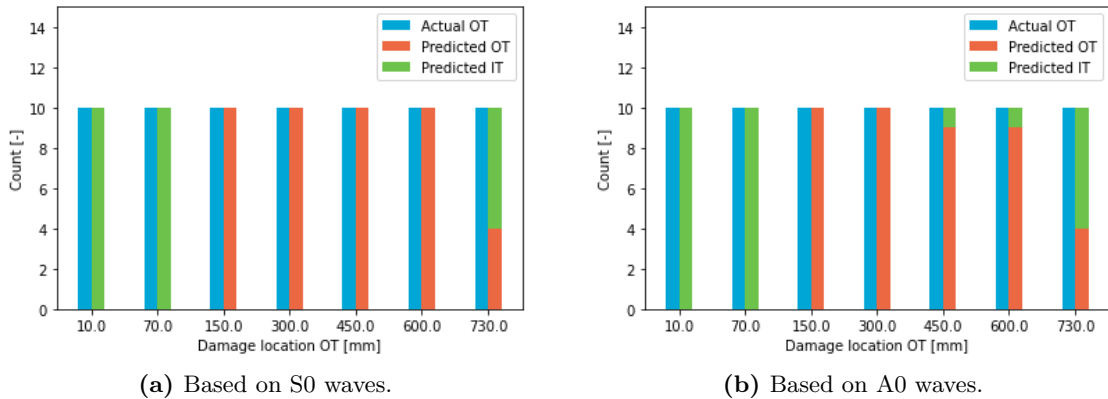


Figure 4.8: Predicted PLB locations (inner (IT) or outer tank (OT)) where the actual location is on the outer tank. Total number of PLBs: 70.

4.2.3 Method sensitivity, precision and accuracy

Based on the results discussed above, a confusion matrix can be composed to determine the sensitivity, precision and accuracy of the method used. The A0 wave-based inner/outer tank distinction outperforms the S0 wave-based distinction on sensitivity, precision and accuracy. Hence, a confusion matrix is only shown for A0 waves in Table 4.1.

Table 4.1: Confusion matrix for the precision, sensitivity and accuracy determination of inner (IT) and outer tank (OT) distinction based on A0 waves.

		Predicted		
		Inner tank	Outer tank	
Actual	Inner tank	69	0	Sensitivity IT 100%
	Outer tank	28	42	Sensitivity OT 60%
		Precision IT 71%	Precision OT 100%	Accuracy 80%

This difference in accuracy for S0 and A0 waves can be explained with the fact that for example the support attenuates the already small amplitude S0 wave. That in combination with (electronic) noise, it becomes difficult to systematically distinct the signal onset of the S0 wave.

4.2.4 Influence of noise on method accuracy

The influence of SNR on the inner/outer tank distinction accuracy based on A0 waves can be seen in Figure 4.9. As can be expected with an increasing noise level (hence decreasing SNR), the localisation accuracy goes down.

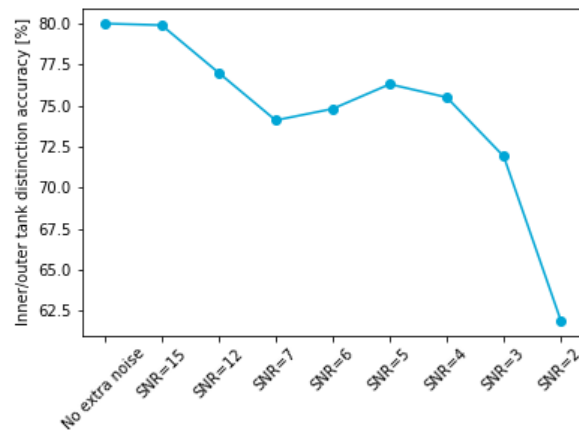


Figure 4.9: Influence of signal-to-noise ratio on inner/outer tank distinction accuracy based on A0 waves.

4.3 Experiment 3: Inner tank damage localisation

After the distinction is made whether the simulated damage is originating from the inner or outer tank, the next step is to localise the simulated damage on the inner tank. This section will first discuss the calculated localisation inputs required for PLB localisation, where after the localisation accuracy will be discussed. The latter includes repeatability experiments and sensitivity analyses.

4.3.1 Localisation input determination

Before localisation can be performed on the inner tank the localisation inputs have to be calculated as laid out in the flow chart in Figure 3.1. First the inner tank wave velocity will be calculated, where after the support travel time will be determined.

Inner tank wave velocity

The average inner tank wave velocity per test setup can be found in Table 4.2.

Table 4.2: Calculated mean inner tank wave velocity including standard deviation per test setup.

Test setup	Inner tank wave velocity [m/s]	
	Based on S0 waves	Based on A0 waves
Flexible support	4077.85 ± 296.51	2759.96 ± 193.82
Fixed support	4132.6 ± 418.5	2827.3 ± 200.2

As the inner tank is the same for the flexible and fixed support the calculated velocities are expected to be similar, which is the case as the S0 and A0 wave speeds differ less than 2.5% between the test setups. The expected inner tank velocity based on used 4 [mm] thick stainless steel can be seen in Figure 4.10. This indicates that for the S0 and A0 waves a velocity of 5100 and 1800 [m/s] respectively is expected.

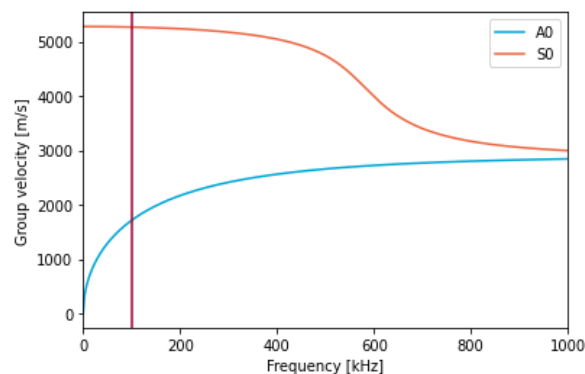


Figure 4.10: Group velocity diagram for the 4 [mm] thick stainless steel used in the LH2 tank. The A0 and S0 group velocity is indicated and the frequency used in the experiments is indicated with a red vertical line.

The differences between the expected velocities and the measured velocities can be explained as follows:

- The group velocity is a theoretical value for the travel speed of a wave in a flat plate. However, the setup at hand is heavily curved and includes a weld along the wave's travel path. Additionally MLI is added in between the inner and outer tank for insulation. These parts make the test setup different from the flat plat on which the theoretical values are based.
- The dome part of the setup does not have a completely uniform thickness. This is due to the fact that the dome part is cold formed (deep drawn). This deformation process leads to non-uniform deformation of the material, resulting in thickness variations (i.e. at the edges). This could result in different velocities at different locations.
- As indicated in subsection 3.3.2 the aim is to catch the S0 and A0 waves. However, as indicated in that same section, due to e.g. (electronic) noise this becomes challenging. As a result not always the actual S0 or A0 wave is selected, causing a deviation (plus or minus) from the expected wave velocity. This results, most likely, in calculated velocities in between the theoretical S0 and A0 wave velocity.

Support travel time

The calculated average support travel time and the standard deviations can be found in Table 4.3. As the supports for the two test setups are different, the support travel time is also expected to be different.

Table 4.3: Calculated mean support travel time including standard deviation per test setup.

Test setup	Support travel time [μs]	
	Based on S0 waves	Based on A0 waves
Flexible support	83.32 \pm 14.49	85.08 \pm 10.76
Fixed support	119.95 \pm 24.40	130.57 \pm 13.83

As can be seen the fixed support travel time is significantly larger than that of the flexible support. This difference can largely be attributed to the fact that the inner tank protrusion around the support is significantly larger as it also has to contain the piping. This difference is also discussed in subsection 4.1.2 can be seen there in Figure 4.4 (flexible support radius: 58 [mm], fixed support radius: 111 [mm]). Hence, regardless of the fact whether the support has a longitudinal glide surface, the wave has to travel further in the fixed support setup than on the flexible support setup (as sensor 2 is placed next to the protrusion). Hence, the fact that the fixed support has a larger travel time is as expected.

4.3.2 Localisation accuracy

The location accuracy is first determined with the calculated inputs. Thereafter the location accuracy results will be shown with optimised inputs. Finally, the results of the repeatability experiments and sensitivity analyses will be shown.

Localisation accuracy based on calculated input values

The predicted locations based on the 10 PLB dataset for the flexible support can be seen against the actual PLB locations in Figure 4.11. It should be noted that the predicted locations are the mean value of 10 PLBs performed at the same location. The predicted locations are calculated using the mean inner tank wave velocity and support travel time shown in Table 4.2 and Table 4.3 respectively.

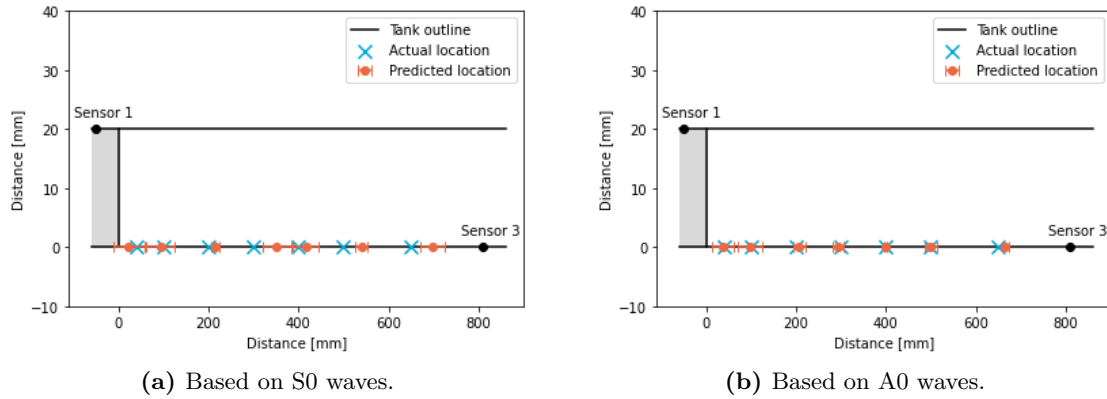


Figure 4.11: Localisation of PLBs on the inner tank on the flexible support test setup. Every point represents the mean of 10 PLBs and the error bar represents the standard deviation.

Similarly, for the fixed support the results of the PLB localisation can be seen in Figure 4.12.

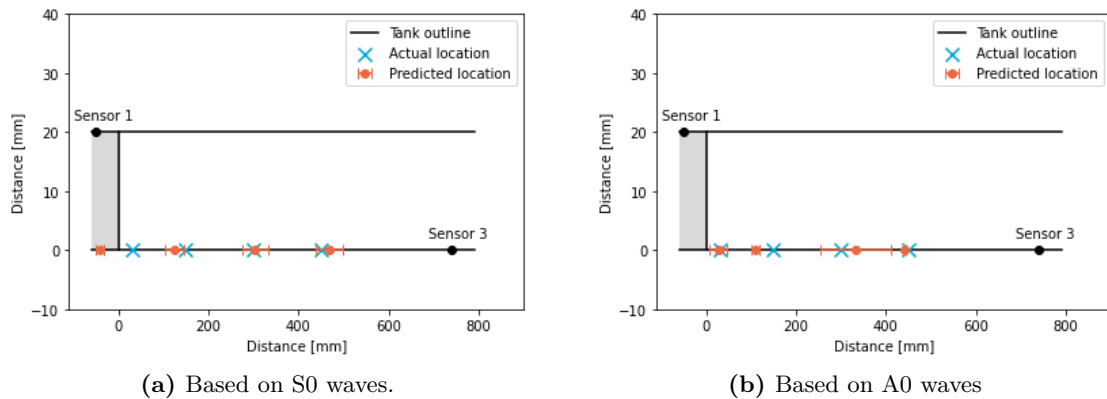


Figure 4.12: Localisation using the calculated wave velocity and support travel time. Every point represents the mean of 10 PLBs and the error bars represent the standard deviation.

The RMSE of the localisation for both the flexible and fixed support can be seen in Table 4.4.

Table 4.4: RMSE per test setup determined with S0 and A0 waves.

Test setup	RMSE [mm]	
	Based on S0 waves	Based on A0 waves
Flexible support	32.63	7.06
Fixed support	38.71	26.56

Based on [Table 4.4](#) the A0 wave-based localisation outperforms the S0 wave-based localisation for both the flexible and fixed support for the same reasons as mentioned in [section 4.2](#). Additionally, the flexible support allows for more accurate localisation than the fixed support. This could be attributed to the extra parts and piping that are attached to fixed support test setup (shown in [Figure 3.4](#)), as this could lead to a significant amount of reflections and attenuation, complicating the localisation. Additionally, the placement of sensor 1 on the fixed support was difficult to perform exactly and securely because of the presence of those parts and pipes.

Input optimisation to improve localisation accuracy

The results of the optimisation of the input parameters and the resulting localisation RMSEs can be found in [Table 4.5](#). It also includes the relative change with respect to the calculated wave velocity, calculated support travel time and the RMSE based on those original values.

Table 4.5: Results of the optimisation of the localisation accuracy for both the flexible and fixed support. The percentages indicate the relative change with respect to the previously calculated (not optimised) values of those parameters.

Parameter	Flexible support		Fixed support	
	Based on S0 waves	Based on A0 waves	Based on S0 waves	Based on A0 waves
Optimised inner tank wave velocity [m/s]	3691 (-9.5%)	2711 (-1.8%)	3411 (-17.5%)	2641 (-6.6%)
Optimised support travel time [μ s]	99.1 (+18.9%)	87.5 (+2.8%)	126.2 (+5.2%)	134.8 (+3.2%)
Optimised localisation RMSE [mm]	12.81 (-60.7%)	5.7 (-19.3%)	7.61% (-80.4%)	23.84 (-10.3%)

It can be seen that the A0 waves still outperform the S0 waves for the flexible support, however for the fixed support it is the other way around. Additionally, the optimisation has resulted in a much greater accuracy improvement for S0 waves than it had for A0 waves. This could be attributed to the fact that in the inner tank wave velocity and support travel time determination the standard deviations were larger for S0 waves than for A0 waves for reasons mentioned in [subsection 4.3.1](#). Hence, it was expected that there is more optimisation possible for S0 waves than for A0 waves. Finally, it should be noted that the inner tank accuracy is can only be obtained whenever the inner/outer tank distinction is made correctly. As that distinction has an accuracy of 80% the inner tank localisation error of the system as a whole is considered to be higher than the ones mentioned in [Table 4.5](#).

Experiment repeatability

The predicted PLB location against the actual location of the repeatability dataset for the flexible support test setup can be seen in Figure 4.13. Every data point predicted location represents one PLB.

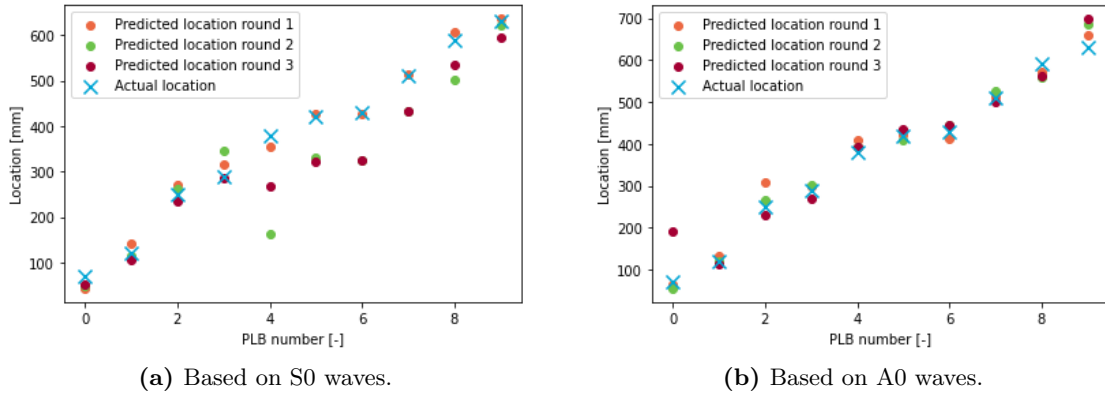


Figure 4.13: Localisation of PLBs on the inner tank of the flexible support test setup, using three different rounds of data gathering. In between the rounds the sensors are detached and re-attached. Every point represents one PLB.

Figure 4.14 shows the predicted and actual PLB locations for the fixed support test setup. As explained in subsection 3.7.1 only two rounds are performed on this test setup.

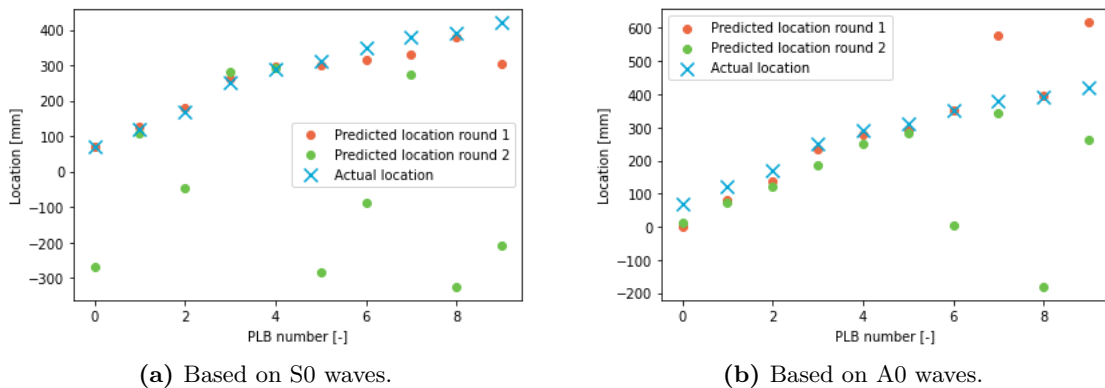


Figure 4.14: Localisation of PLBs on the inner tank based of the fixed support test setup, using two different rounds of data gathering. In between the rounds the sensors are detached and re-attached.

The RMSE per round and the average RMSE over the rounds performed can be found in Table 4.6. This table includes two entries for the 10 PLB dataset for comparison with the repeatability dataset. The first one is the "10 PLB (mean) dataset". The RMSE calculated with this dataset is determined the same way as in the previous subsection about input optimisation, resulting in the same RMSE. The second entry is referred to as the "10 separate PLBs dataset". This dataset uses the same PLB signals as the first entry, but to determine

this **RMSE** there was no calculation of mean predicted location. Hence, every predicted location is compared to the actual location separately. This allows for better comparison with the repeatability dataset, which is based on a single **PLB** per location.

Table 4.6: Results of repeatability experiments where one **PLB** is located at random locations along the inner tank.

Parameter	Flexible support		Fixed support	
	Based on S0 waves	Based on A0 waves	Based on S0 waves	Based on A0 waves
10 PLB (mean) dataset RMSE [mm]	12.81	5.7	7.61	23.84
10 separate PLBs dataset RMSE [mm]	27.27	17.29	21.15	44.77
Round 1 RMSE [mm]	17.83	24.97	41.54	93.12
Round 2 RMSE [mm]	91.78	23.23	403.34	220.29
Round 3 RMSE [mm]	66.36	46.65	X	X
Average RMSE round 1, 2 and 3 [mm]	58.66	31.62	222.44	156.71

It can be seen that for both the flexible and fixed support the repeatability experiments have a higher **RMSE** than the one calculated using the 10 **PLB** dataset. There are multiple reasons for this:

- **Not an average value.** The repeatability dataset exists of only one **PLB** per location per round, whereas the localisation accuracy of the 10 **PLB** (mean) dataset is based on the average location of 10 **PLBs** in the same location. Hence, outliers in the repeatability dataset have much more influence on the overall localisation accuracy. This can also be seen in the fact that the 10 separate **PLB** dataset has **RMSE** values significantly closer to the repeatability dataset **RMSEs**.
- **Inputs not optimised for the repeatability dataset.** The inner tank wave velocity and the support travel time are both optimised for the 10 **PLB** (mean) dataset, which did not include the repeatability dataset. This is not expected to have a large influence, but can have an influence nonetheless.
- **Sensor placement.** Even though the measurement tape allowed for precise sensor placement, the sensors could still be inaccurate and subsequently affecting the localisation accuracy of the different rounds.
- **Sensor attachment.** For the creation of the 10 **PLB** dataset and round one of the repeatability dataset the sensors were securely attached to the structure. However, after taking them off the coupling grease was still on the structure, making the reattachment using tape difficult. This was especially the case for round 2 for the fixed support, where also the most significant increase can be seen. The location of sensor 1 on the fixed support setup was difficult to reach and subsequently difficult to clean.

Even though the localisation accuracy drastically increased during the repeatability experiments, especially for the flexible support the average **RMSE** is still relatively low.

Sensitivity study

The graphically represented one-way sensitivity study results can be found in [Appendix D](#). The results show that accurate sensor placement had the largest influence on the localisation accuracy. Hence, it is important to accurately measure the locations of the sensors. Due to the fact that the location of sensor 1 is already accounted for in the determination of the support travel time, the placement of sensor 3 had the largest influence.

Additionally a Monte Carlo simulation was performed. The results of 10^5 iterations can be found in [Appendix E](#). It should be noted that the calculated reference error in those Monte Carlo simulations are not based on the mean locations of the 10 PLBs at the same location, but an average RMSE of all predicted locations separately. The values of interest from the Monte Carlo simulation are shown in [Table 4.7](#). In this table the reference error refers to the error using the optimised values calculated in the previous subsections using the "10 separate PLB dataset". The 90% RMSE refers to the value below which 90% of the calculated errors fall. It can again be seen that the A0 waves outperform the S0 waves.

Table 4.7: Results of the Monte Carlo simulations for experiment 3. The reference error refers to the error using the optimised values calculated in the previous subsections. The 90% RMSE refers to the value below which 90% of the calculated errors fall.

Parameter	Flexible support		Fixed support	
	Based on S0 waves	Based on A0 waves	Based on S0 waves	Based on A0 waves
Reference RMSE [mm]	27.27	17.29	21.15	44.77
Mean RMSE [mm]	53.95	37.56	59.30	57.45
90% RMSE [mm]	81.29	58.16	95.08	73.36
90% RMSE as percentage of inner tank length (=1000 [mm]) [%]	8.1	5.8	9.5	7.3

4.4 Experiment 4a: Outer tank damage 1D localisation

After the localisation of inner tank damage, the outer tank damage localisation will be investigated. This experiment will focus on 1D localisation. Similar to the previous section first the localisation inputs will be calculated where after the localisation accuracy will be determined and optimised. It should be noted that for the localisation accuracy the experiment is divided into two parts. The first one performs 1D localisation on a 1D line. The second part, on the other hand, investigates the accuracy of 1D localisation on a 2D plane. In the rest of this section a comparison will be made with the inner tank localisation accuracy and the repeatability and sensitivity of the experiments will be discussed.

4.4.1 Localisation input determination

The outer tank signal's wave velocity can be found in [Table 4.8](#).

Table 4.8: Calculated mean outer tank wave velocity including standard deviation.

Test setup	Outer tank wave velocity [m/s]	
	Based on S0 waves	Based on A0 waves
Flexible support	4452 ± 857	2536 ± 142

As the inner and outer tank are made of the same material, it is expected that the inner and outer tank velocity are similar. The velocity difference between the outer tank and inner tank velocity for the flexible support is +9% and -8% for the S0 and A0 waves respectively.

4.4.2 Localisation accuracy experiment part 1

This subsection will first determine the 1D localisation accuracy with the calculated input values of part 1 of this experiment, where after these input values will be optimised. Finally the repeatability and sensitivity of part 1 of the experiment will be discussed.

Localisation accuracy based on calculated input values

Based on the velocity calculated in the previous section the PLBs can be localised as can be seen in [Figure 4.15](#).

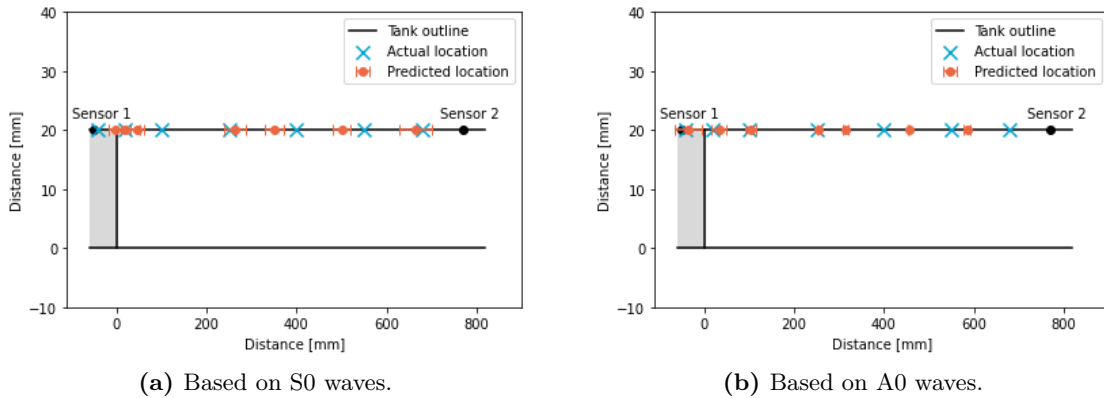


Figure 4.15: Localisation of PLBs on the outer tank using sensors 1 and 2.

The localisation accuracy can be seen in the first row of [Table 4.9](#).

Localisation optimisation

To optimise the localisation accuracy, the sensor arrangement and wave velocity is optimised as indicated in [subsection 3.8.3](#). This results in the localisation accuracy as indicated in [Table 4.9](#). It can be seen that the combination of the proposed optimisation methods has a positive effect on the localisation accuracy.

Table 4.9: Localisation accuracy of outer tank 1D localisation, including optimised localisation accuracy. The percentages refer to the relative change with respect to the RMSE using the calculated velocity and sensor 1 and 2 (row 1).

Sensors used	Velocity type	Based on S0 waves		Based on A0 waves	
		Velocity [m/s]	RMSE [mm]	Velocity [m/s]	RMSE [mm]
1 and 2	Calculated	4452	36.91	2536	60.06
1 and 2	Optimised	4571 (-2.7%)	36.34 (-1.5%)	2821 (+11.2%)	54.48 (-9.3%)
1, 2 and 4	Calculated	4452	42.39 (+14.8%)	2536	11.67 (-80.6%)
1, 2 and 4	Optimised	3551 (-20.2%)	27.42 (-25.7%)	2461 (-3.0%)	11.04 (-81.6%)

Inner tank and outer tank localisation accuracy comparison

Comparing the localisation using sensor 1 and 2 to the inner tank damage localisation method it can be seen that for localisation based on both S0 and A0 waves the inner tank localisation outperforms the outer tank localisation (by approximately a factor 2). This is due to:

- **Different optimisation variables.** For inner tank localisation accuracy optimisation both the support travel time and wave velocity can be optimised. For outer tank localisation only the wave velocity is being optimised to localise the PLBs (the different sensor arrangement only makes the area to look at smaller). This extra optimisation variable for the inner tank localisation makes that the accuracy can become better.
- **Different travel paths.** Due to the fact that the travel path for outer tank damage is different for that of inner tank damage (attenuation, curvature, support, etc.), it is expected that the received AE waves are also different. Differences in for example amplitude for the inner and outer tank waves while using the same threshold for both can result in setting the signal onset at a different part of the wave. Hence, influencing the localisation accuracy.

Experiment repeatability

A graphical representation of the localisation of the PLBs can be found in Figure 4.16. For this localisation the optimised method is used (hence using the optimised velocity in combination with sensor 1, 2 and 4). From the graphs it can be observed that localisation based on A0 waves gives a higher accuracy.

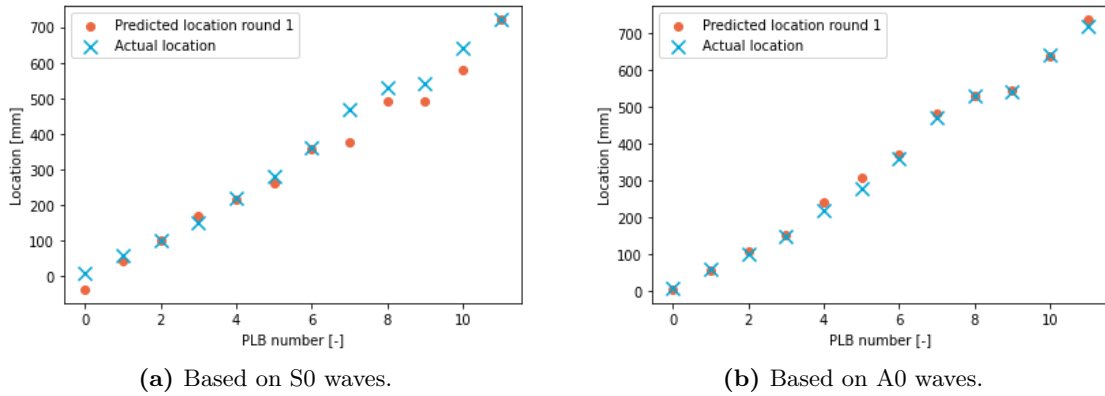


Figure 4.16: Localisation of PLBs on the outer tank using random PLBs at random locations. Every dot represents one PLB.

The quantified localisation **RMSE** can be found in [Table 4.10](#). The **RMSE** has increased with respect to the one calculated in the previous section. This is due to the same reasons as mentioned in [subsection 4.3.2](#).

Table 4.10: Localisation accuracy for randomly located PLBs.

Parameter	Based on S0 waves	Based on A0 waves
10 PLB (mean) dataset RMSE [mm]	27.42	11.04
10 separate PLBs dataset RMSE [mm]	29.67 (+8.2%)	13.21 (+19.7%)
Round 1 RMSE [mm]	33.75 (+23.1%)	12.44 (+12.7%)

Sensitivity study

The one-way sensitivity study reveals that again the accurate sensor placement has the the largest impact on the localisation accuracy. The inputs and results of the Monte Carlo simulation can be found in [Table 4.11](#). A summary of the results can be seen in [Table 4.11](#). The Monte Carlo simulation on localisation based on A0 waves shows that there is a more optimal configuration that can be used to improve the **RMSE**. This improvement would also bring the localisation **RMSE** closer to the one obtained for inner tank localisation.

Table 4.11: Results of the Monte Carlo simulations for experiment 4a part 1. The reference error refers to the error using the optimised values calculated in the previous subsections. The 90% RMSE refers to the value below which 90% of the calculated errors fall.

Parameter	Based on S0 waves	Based on A0 waves
Reference RMSE [mm]	29.67	13.21
Mean RMSE [mm]	71.42	28.42
90% RMSE [mm]	122.72	43.01
90% RMSE as percentage of inner tank length (=1000 [mm]) [%]	12.2	4.3

4.4.3 Localisation accuracy experiment part 2

Even though part 1 of this experiment allowed for comparison with the inner tank localisation, it is not necessarily an accurate representation of reality, as damage does not occur on a perfect line. Hence, 1D localisation on a 2D area will be investigated. This subsection will first determine the localisation accuracy with calculated input values, where after these input values will be optimised. Finally the repeatability and sensitivity of the experiment will be discussed.

Localisation accuracy based on calculated input values

An example of the 1D localisation performed using S0 waves can be seen in Figure 4.17.

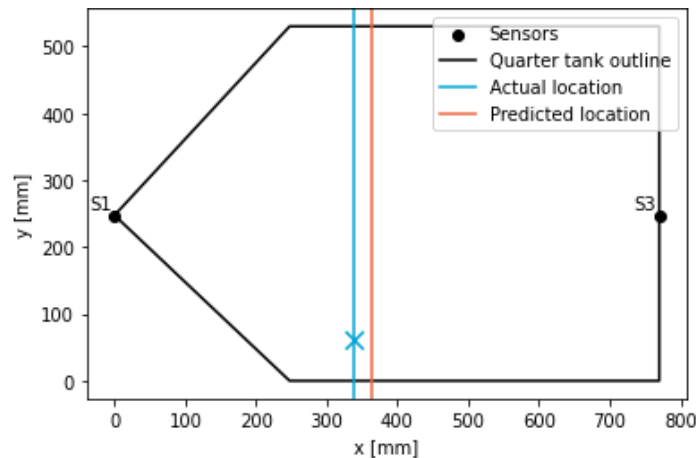


Figure 4.17: 1D localisation on a 2D area example using S0 waves.

The localisation accuracy for the 1D localisation on a 2D plane can be found in Table 4.12. It should be noted that the optimized velocity of part one of this experiment was used.

Table 4.12: Errors associated with the 1D on a 2D area localisation.

Parameter	Based on S0 waves	Based on A0 waves
Used velocity [m/s]	4671	2461
RMSE [mm]	58.25	64.35

Compared to part 1 of this experiment (Table 4.9), the RMSE is larger for this part of the experiment. This can be explained by the fact that the 2D area means that there is a second curvature present that is not taken into account for the data processing (where it is assumed to be a flat plate). This can induce extra errors. The errors are also higher closer to sensor 1 and sensor 3, which is most likely due to the difference in waves that arrive at the sensors when a PLB is placed close to one sensor. The received signal at the far away sensor will be quite attenuated and the S0 and A0 wave will have separated. Whereas for the close by sensor the wave will almost not be attenuated and the two wave types will not have separated yet. This causes the algorithm to identify the signal onset at different parts along the signal at the different sensors, hence reducing the localisation accuracy.

Localisation optimisation

The results of optimising the velocity to obtain the minimum RMSE can be found in Table 4.13.

Table 4.13: Errors associated with the 1D on a 2D area localisation. The percentages indicate the relative change with respect to the previously calculated (not optimised) values of those parameters.

Parameter	Based on S0 waves	Based on A0 waves
Optimized velocity [m/s]	3916 (-16.2%)	2941 (+19.5%)
Optimized RMSE [mm]	45.91 (-21.2%)	57.12 (-11.2%)

Figure 4.18 visually shows the localisation using the optimised wave velocity. It can be seen that especially PLBs located further away from sensor 1 have a less accurate localisation.

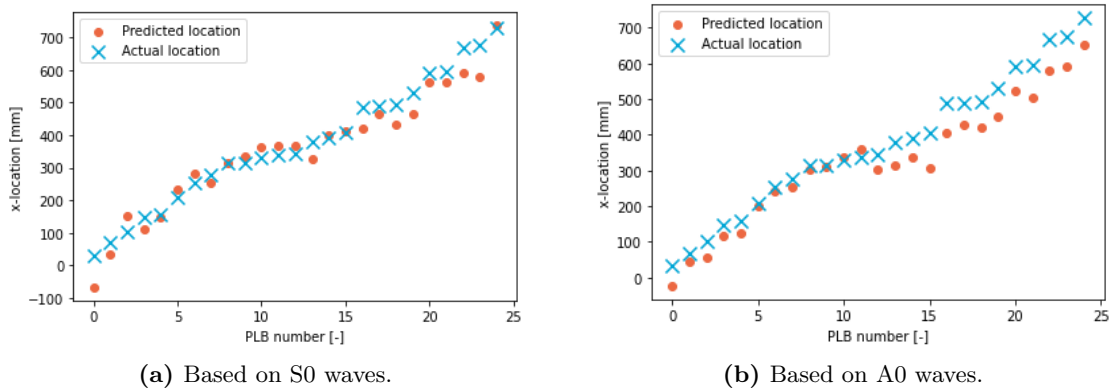


Figure 4.18: RMSE optimized 1D localisation error of the PLB on a 2D area.

Sensitivity study

The results of the Monte Carlo simulations can be found in section E.3. Localisation based on S0 and A0 waves show similar distributions and in both cases more optimal configurations were possible. Table 4.14 shows a summary of the Monte Carlo simulation results.

Table 4.14: Results of the Monte Carlo simulations for experiment 4a part 2. The reference error refers to the error using the optimised values calculated in the previous subsections. The 90% RMSE refers to the value below which 90% of the calculated errors fall.

Parameter	Based on S0 waves	Based on A0 waves
Reference RMSE [mm]	45.91	57.12
Mean RMSE [mm]	69.63	80.18
90% RMSE [mm]	102.14	112.75
90% RMSE as percentage of inner tank length (=1000 [mm]) [%]	10.2	11.3

4.5 Experiment 4b: Outer tank damage 2D localisation

Finally, because of the accessibility of the outer tank the 2D localisation accuracy will be investigated in this section. This will be done by first looking into the localisation accuracy with the calculated values, where after these values will be optimised for the 2D dataset. The section will be ended with a sensitivity study.

4.5.1 Localisation accuracy

For the localisation the optimised velocity of experiment 4a part 2 will be used (3916 [m/s] and 2941 [m/s] for S0 and A0 waves respectively), as that experiment also covered a 2D area. The results of this localisation can be seen in [Table 4.15](#).

Table 4.15: Optimized RMSE associated with 2D damage localisation on the outer tank of the flexible support test setup.

Parameter	Based on S0 waves	Based on A0 waves
Used velocity [m/s]	3916	2941
RMSE [mm]	102.57	68.33

The RMSE based on A0 waves is similar to the localisation accuracy in determined in [24] (and to a lesser extend in [23]). [Figure 4.19](#) visually shows the actual and predicted PLB locations.

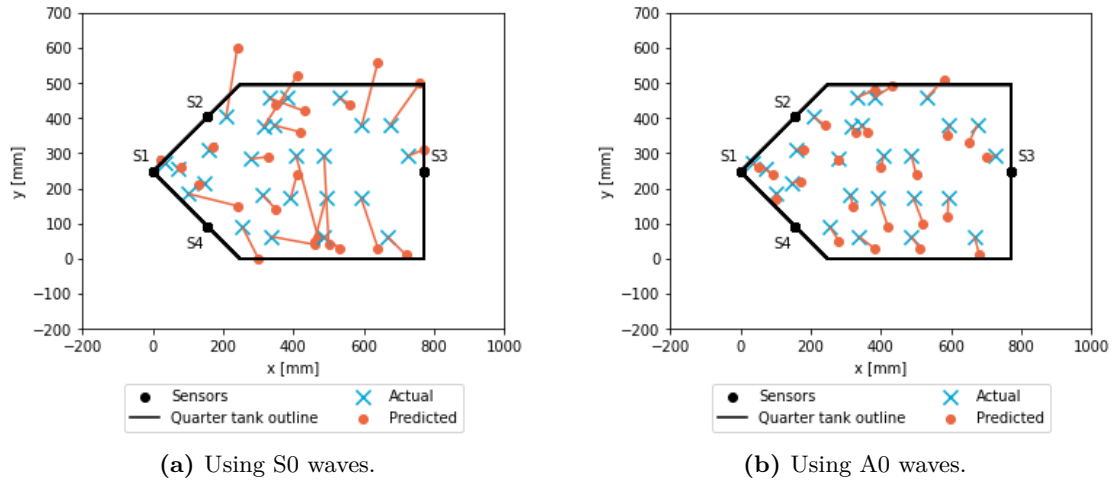


Figure 4.19: Optimised 2D localisation.

From Figure 4.19 it can be concluded that the A0 wave localisation has a lower accuracy than localisation based on S0 waves. Also the predicted locations are generally too low on the y-axis, whereas they are relatively accurate on the x-axis. For the localisation based on S0 waves on the other hand, there is a less clear deviation to a certain side. However, it could be observed that generally the PLBs in the sensor 1, 2 and 3 triangle have a relatively high localisation accuracy. This could be explained by the fact that these sensors are placed close to each other on a relatively flat area, hence less influence of the structure's curvature can be expected.

4.5.2 Localisation accuracy optimisation

The results of the optimisation of the velocity to minimise the RMSE can be seen in Table 4.16. The localisation accuracy based on A0 waves outperforms the S0 wave-based localisation by a factor 2.5.

Table 4.16: Optimized RMSE associated with 2D damage localisation on the outer tank of the flexible support test setup. The percentages indicate the relative change with respect to the previously calculated (not optimised) values of those parameters.

Parameter	Based on S0 waves	Based on A0 waves
Optimized velocity [m/s]	3540 (-10.6%)	2350 (-20.1%)
Optimized RMSE [mm]	100.37 (-2.1%)	41.13 (-39.8%)

4.5.3 Sensitivity study

The results of the Monte Carlo simulations can be found section E.4. The important results are summarised in Table 4.17. The 90% RMSE results are similar to those based on 1D localisation on a 2D area (experiment 4a part 2).

Table 4.17: Results of the Monte Carlo simulations for experiment 4a part 2. The reference error refers to the error using the optimised values calculated in the previous subsections. The 90% RMSE refers to the value below which 90% of the calculated errors fall.

Parameter	Based on S0 waves	Based on A0 waves
Reference RMSE [mm]	100.37	41.13
Mean RMSE [mm]	110.53	83.37
90% RMSE [mm]	126.58	127.12
90% RMSE as percentage of inner tank length (=1000 [mm]) [%]	12.7	12.7

4.6 Influence of experiment limitations

The results of the experiments discussed above are based on experiments that have physical limitations and are based on assumptions. In order to make conclusions based on those experiments it is important to understand the influence of those limitations and assumptions. This section discusses the effect of using a half-tank test setup instead of an entire tank, the effect of performing the experiments at room temperature rather than at the LH2 cryogenic storage temperature, the effect of using simulated damage rather than real damage and finally the effect of vacuum between the inner and outer tank.

4.6.1 Effect of an entire tank setup with respect to the half-tank test setup

First the effect using an entire tank with the sensor placement proposed in subsection 4.1.3 will be discussed with respect to the half-tank test setup that was used in the experiments. The effect on inner/outer tank distinction will be discussed, even as the effect on inner tank and outer tank localisation accuracy.

Inner and outer tank distinction accuracy

The effect of an entire tank with more available sensors on the distinction between simulated damage on the inner and outer tank is already briefly discussed in subsection 4.2.2. The conclusion from that subsection is that the addition of sensors is expected to make the distinction more accurate, as there are more sensors available to pinpoint the location of the simulated damage.

Inner tank simulated damage localisation accuracy

Both sensors that will be used for inner tank localisation (sensor 1 and 2 in Figure 4.6) will now be placed on the outer tank instead of one on the inner tank as was the case in experiment 3 (sensor 3 in subsection 3.7.1). This means that the AE wave has to travel through the support on both sides to reach the sensors, instead of just one side. Hence, the localisation algorithm proposed in subsection 3.7.3 needs to be changed to account for this change in travel path. The localisation equation would remain the same, but the determination of the

time-wise middle would become:

$$X_{middle} = V_{IT} \left(\frac{t_{support,1} + \frac{L_{IT}}{V_{IT}} + t_{support,2}}{2} - t_{support,1} \right) \quad (4.1)$$

Where $t_{support,1}$ and $t_{support,2}$ refer to the **AE** wave's travel time through the two inner tank supports. The location of X_{middle} is subsequently given in terms of distance to support number 1.

As mentioned, the **AE** wave has to travel through a support to reach both sensors. This means that the signals received by both signals will be significantly attenuated (in contrast to the signal received by sensor 3 in experiment 3 being much less attenuated than the signal received by sensor 1, as could be seen in [Figure 4.3](#)). If both supports influence the **AE** wave similarly. This could improve simulated damage localisation accuracy. This would mean that the signal received by the two sensors is similar. Hence, the signal onset determination method can better detect the same part of the wave at both sensors, which will improve the localisation accuracy.

On the other hand, in experiment 3 it was made sure that the line on which the **PLBs** were placed was as unobstructed as possible. However, in the entire tank scenario the damage will not happen on a perfect line, but can be located anywhere on the inner tank. On the inner tank here are pipes, sloshing baffles, etc. which can influence the **AE** wave or (partially) reflect/refract it. This unexpected behaviour could have a negative effect on the localisation accuracy.

Outer tank simulated damage localisation accuracy

On the localisation of simulated damage on the outer tank it is expected that the entire tank scenario has a positive impact on the localisation accuracy. Because of the availability of more sensors than were used in experiment 4a and b, the localisation accuracy is expected to improve. An issue could be, however, that experiment 4a and b are both performed on the flexible support test setup as the fixed support had a significant amount of pipes attached to it. The presence of these pipes and other fixtures could complicate the accurate localisation of damage on an entire tank setup.

4.6.2 Effect of experiments at room temperature with respect to cryogenic temperatures

All experiments discussed above are performed at room temperature. However, during most of its operating life the liquid hydrogen tank will contain **LH2** with a temperature of 20 [K]. As discussed in [subsection 1.7.3](#), the cryogenic temperature is expected to affect the material's Young's modulus and hence the wave speed. Therefore, it is important to take the change in wave speed into account when determining the inner and outer tank wave velocity and to correct for that.

In terms of noise it is argued that the sensor noise will go up [9](see [subsection 1.11.1](#)), but that the thermal noise will go down [69] (see [subsection 1.7.3](#)). A lower noise amplitude would result in a higher **SNR**, hence an improved localisation accuracy.

Finally, it is important to note that these cryogenic temperatures also need to be taken into account when designing the measurement system. For example in [subsection 1.10.1](#) the importance of choosing the right couplant for the sensors is discussed.

4.6.3 Effect of simulated damage with respect to real damage

To determine the effect of using [PLBs](#) in stead of real damage the frequency and amplitude of the two will be compared.

The frequency choice of 100 [kHz] is based upon the research performed in [subsection 1.10.2](#). However, a range of frequencies is expected for actual [AE](#) sources. If these frequencies are significantly higher, this could lead to a significant increase in attenuation, hence making it more difficult to detect the signal.

To amplitude ranges of representative [AE](#) signals can be found in [Appendix C](#). For aluminium the range was found to be between 30-70 [dB_{ae}] and for steel 44-75 [dB_{ae}]. These amplitudes were obtained by placing an [AE](#) sensor relatively close to the damage. Hence, it is determined that the best comparison can be made with the amplitude received by sensor 2 or 3 in the case of experiment 3 (inner tank damage localisation) or sensor 1 and 3 in experiment 4a (outer tank 1D damage localisation). These sensors received signals in the range of 75-85 [dB_{ae}]. Hence, in a real damage scenario the amplitude is lower than the simulated one used in the experiments in this research. An effect of this could be that the real damage becomes more difficult to detect, leading to false negatives, or when they are detectable the signal onset is difficult to find because of a low signal-to-noise ratio.

On the other hand, in [14] the threshold for an [AE](#) signal to be considered damage was set to 70 [dB_{AE}]. After inspection of the monitored tank it was concluded that the tank was not damaged, even though the threshold had been surpassed multiple times. Hence, the threshold was deemed too conservative. Hence, maybe in real life applications higher amplitudes can be expected related to damage.

Nevertheless, it is recommended for future research to further investigate the [AE](#) characteristics of damage in a [LH2](#) tank and whether the wave's energy is sufficient to travel through the support.

4.6.4 Effect of vacuum between the inner and outer tank

In all experiments discussed in the previous sections there was a vacuum between the inner and outer tank. However, for future research it would be of interest to see the influence of the vacuum on localisation accuracy. If the influence would be minimal, it could be argued that there is no need for a vacuum to perform experiments similar to the ones performed in this thesis. This could simplify future research. The results of the localisation of simulated damage on the inner tank where the vacuum was removed can be seen in [Appendix F](#). An overview of the localisation accuracy for the flexible support test setup and per wave mode used can be found in [Table 4.18](#).

Table 4.18: Results of the investigation into the influence of a vacuum between the inner and outer tank on the localisation accuracy of an PLB performed on the inner tank of the flexible support test setup.

Localisation accuracy	Based on S0 waves	Based on A0 waves
Vacuum between inner and outer tank RMSE [mm]	66.4	46.6
Air between inner and outer tank RMSE [mm]	84.3 (+27%)	38.2 (-18%)

From the graphs in [Appendix F](#) it can be concluded that for the flexible support the absolute difference between vacuum and air between the inner and outer tank in terms of localisation accuracy, especially for A0 waves, is little. Also, the difference in localisation accuracy based on S0 waves is mainly due to one outlier. The difference between air and vacuum could also just be due to the fact that these localisation accuracies are from two different datasets that will logically result in a difference in localisation accuracy.

In short, these initial results look promising in the sense that no vacuum is necessarily needed in the inner tank localisation experiment for the test setup as used in this experiment. However, it would be recommended to perform more experiments with more sensors to confirm the signal's travel path to be able to make a definitive conclusion.

Chapter 5

Conclusion

Liquid hydrogen (LH2) is often indicated as a fuel to enable the transition of the aviation industry into a more environmentally friendly future. However, utilizing LH2 requires safe storage, which is inhibited by the low storage temperature (20 [K]) which causes cryogenic embrittlement and the presence of hydrogen which causes of hydrogen embrittlement. These factors create a hazardous and unpredictable environment for which predictive maintenance is desired, hence necessitating continuous monitoring of the tank's structural integrity. The structural health monitoring method that is concluded to be the most suitable is acoustic emission (AE) monitoring. This method is sufficiently sensitive and operates passively in the sense that it listens to the structure for growing damage, hence only focusing on worsening damage. The focus of this research is on investigating the feasibility of monitoring the structural integrity of a metal double walled vacuum insulated tank using acoustic emission testing. This is a new application of an already proven method with great potential to monitor the structural integrity of LH2 tanks.

The first experiment discussed in this research dives into the location of sensor placement and whether the sensors can be placed outside of the tank to monitor the inner tank. It has been shown that simulated damage on the inner tank can be recorded with sensors on the outer tank for both the fixed and flexible support test setup. The measured attenuation did not prevent outside-the-tank sensor placement. However, extra attenuation experiments are recommended to exclude the influence of sensor attachment and investigate the influence of welds and curvatures. In short, experiment 1 resulted in the minimal sensor placement needed to cover an entire tank as shown in [Figure 5.1](#).

Experiment 2 focused on the research question regarding the accuracy that can be obtained in making a distinction between simulated damage on the inner and outer tank. Because of accessibility this experiment is only performed on the flexible support test setup. A distinction method based on A0 waves was able to obtain an accuracy of 80%, an inner and outer tank precision of 71% and 100% respectively and an inner and outer tank sensitivity of 100% and 60% respectively. A limitation of the used method was a 'grey area' between e.g. sensor 1 on the outer tank and the halfway point between that sensor and the guard sensor (e.g. sensor 1.2). In this area the algorithm mistakenly identified outer tank damage as inner

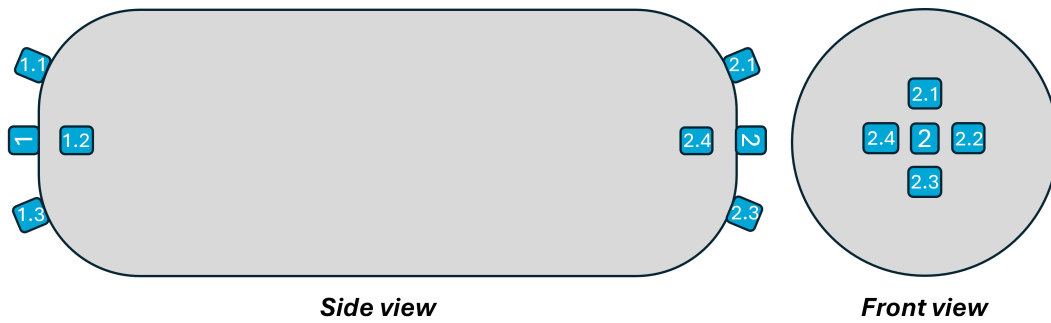


Figure 5.1: Graphical representation of sensor placement for the complete tank scenario (not to scale).

tank damage, because the wave would reach the sensor 1 before it would reach sensor 1.2. However, this limitation can be reduced by reducing the spacing between the center and the guard sensor and adding more sensors.

The next research question (and hence experiment) focused on how accurately the proposed sensor placement can localise simulated damages on the inner tank (only 1D). Only the type of wave (S0 or A0) resulting in the best localisation accuracy will be named here. For the flexible support an accuracy of 17.29 [mm] was obtained using A0 waves and for the fixed support 21.15 [mm] using S0 waves. The 90% RMSEs determined with Monte Carlo simulations (the error below which 90% of the Monte Carlo cases fell) were 58.16 [mm] and 73.36 [mm] for the flexible and fixed support based on A0 waves respectively. Additionally, the repeatability experiments have shown that too much or too little couplant and poor sensor attachment have a negative effect on localisation accuracy.

Finally, experiment 4 focused on the research question regarding the obtainable localisation accuracy for simulated damage on the outer tank. The 1D localisation accuracy of simulated outer tank damage is lower than that of inner tank damage. This can be attributed to the fact that the inner tank localisation accuracy optimisation had two input parameters (wave velocity and support travel time), whereas the outer tank optimisation only had one (wave velocity). Additionally, AE waves from the inner or outer tank travel different paths with different attenuation, curvatures and other obstacles (e.g. welds and piping), hence different localisation accuracies can be expected. The 1D localisation on a 2D area resulted in an optimal RMSE of 45.91 [mm] and a 90% RMSE of 102.14 [mm] using S0 waves. Finally, the last part of this experiment investigated the accuracy 2D localisation, because of the easily accessible outer tank. This resulted in an optimised RMSE of 41.13 [mm] and a 90% RMSE of 127.12 [mm] using A0 waves.

There were four main limitations in conducting the above mentioned experiments:

- **Simulate damage.** The frequency of the simulated damage is representative for expected tank damage. The amplitude of the simulated damage is, however, higher. Which means that there is a possibility that not all real damage is detectable. The lower signal-to-noise ratio (SNR) also results in a decrease in localisation accuracy. Experiment 2 showed that an SNR reduction to 2 decreased the inner/outer tank distinction accuracy by 20%.
- **Room temperature.** The material's temperature influences the wave speed, hence

the localisation accuracy.

- **Half a tank.** In an entire tank scenario it is expected that both the inner/outer tank distinction and the outer tank localisation is improved because of the presence of more sensors. Inner tank localisation becomes slightly more complex as damage will not be located on one unobstructed line (no piping, sloshing baffles etc., this is expected to decrease the localisation accuracy) and a wave has to travel through a support on both sides (increase of localisation accuracy if the localisation sensors now both receive a similarly attenuated signal).
- **Controlled environment (minimal amount of noise).** Especially structural noise is expected to significantly affect the ability to detect AE waves as the expected frequencies are similar to the expected AE frequencies. This can be minimised by vibrationally isolating the structure, using guard sensors or more advanced noise filters.

Based on the conclusions mentioned above, it can be said that acoustic emission testing can be used to detect and localise simulated damage in both the inner and outer tank with outside-the-tank sensor placement.

5.1 Recommendations for future work

The recommendations for future research based on the research provided here can be divided into four categories, which will be shortly discussed below.

AE source characterisation

For this thesis a frequency of interest is assumed (100 [kHz]). The AE waves created by a PLB are considered to be a valid representation of actual damage signals. However, it is recommended that more research is done on the signal characteristics (e.g. amplitude, frequency, rise time) of signals created by hydrogen induced cracking of different relevant materials.

Other tank geometries and/or materials

In this thesis only one tank is investigated. However, to create a more general image of the feasibility of acoustic emission-based structural health monitoring other support geometries and tank materials should be investigated. This could also allow the use of AE-based SHM systems on vacuum insulated tanks in other industries.

Influence of the tank in use (noise and temperature)

To validate the feasibility of the proposed method, the SHM system should be used in the environment it was intended for: An aircraft. This would validate whether the distinction between noise and damage signals can be made. Additionally, it is recommended to investigate the restrictions the temperature of the tank puts on the sensor selection and operation.

Structural integrity assessment

Being able to register AE signals created by growing damage is only part of the equation. The other part is the interpretation of those signals and to subsequently make an assessment of the structural integrity of the product. Hence, it is recommended to develop assessment criteria to determine whether the LH2 tank should be further inspected or taken out of service.

References

- [1] Airbus. How to store liquid hydrogen for zero-emission flight. <https://www.airbus.com/en/newsroom/news/2021-12-how-to-store-liquid-hydrogen-for-zero-emission-flight>, December 2021. Accessed: February 2024.
- [2] P. Boer, A. Wit, and R. Benthem. Development of a liquid hydrogen-based fuel cell system for the hydra-2 drone. 01 2022.
- [3] J. Glazer, S.L. Verzasconi, R.R. Sawtell, and J.W. Morris. Mechanical behavior of aluminum-lithium alloys at cryogenic temperatures. *Metallurgical Transactions A*, 18(10):1695–1701, October 1987.
- [4] G. Tzoumakis, K. Fotopoulos, and G. Lampeas. Multi-physics digital model of an aluminum 2219 liquid hydrogen aircraft tank. *Aerospace*, 11(2), 2024.
- [5] S. Pant, J. Laliberte, and M. Martinez. Structural health monitoring (shm) of composite aerospace structures using lamb waves. 07 2013.
- [6] J.C. Spannermand J.W. McElroy and American Society for Testing Materials. *Monitoring structural integrity by acoustic emission : conference, Fort Lauderdale, Jan. 1974, proceedings*. ASTM special technical publication ; 571. [s.n.], Philadelphia, 1975.
- [7] D.G. Aggelis and T.E. Matikas. Effect of plate wave dispersion on the acoustic emission parameters in metals. *Computers & Structures*, 98-99:17–22, 2012.
- [8] M.G.R. Sause and E. Jasiuniene. *Structural health monitoring damage detection systems for aerospace*. Springer Cham, September 2021.
- [9] Y. Xu, S. Ding, and F. Liu. Acoustic emission in-service detection of cryogenic storage tank floors. In *e-Journal of Nondestructive Testing (eJNDT)*, volume 13. 17th World Conference on Nondestructive Testing, 2008.
- [10] ASTM International. ASTM E976-15: Standard guide for determining the reproducibility of acoustic emission sensor response. December 2015.

- [11] Gary G. Martin. *In-Flight Acoustic Emission Monitoring*, pages 343–365. Springer US, Boston, MA, 1980.
- [12] Shm next. <https://shmnext.com/index.html>. Accessed: September 2024.
- [13] Physical Acoustic Corporation. R15a - 150 khz general purpose ae sensor. <https://www.physicalacoustics.com/by-product/sensors/R15a-150-kHz-General-Purpose-AE-Sensor>. Accessed: May 2024.
- [14] B. Binu, K.K. Purushothaman, and J. Philip. A study on the crack growth of aa2219 aluminium alloy material using acoustic emission signal analysis. In *e-journal of Non-destructive Testing (eJNDT)*, volume 22. Indian National Seminar and Exhibition on Non-Destructive Evaluation NDE 2015, 2017.
- [15] B. Binu, K.K. Purushothaman, and J. Philip. Acoustic emission signal analysis to study the yield behaviour of aa2219 aluminium alloy material. National seminar and exhibition on non-destructive evaluation, December 2014.
- [16] S. Tiwari, M.J. Pekris, and J.J. Doherty. A review of liquid hydrogen aircraft and propulsion technologies. *International Journal of Hydrogen Energy*, 57:1174–1196, 2024.
- [17] E.J. Adler and J.R.R.A. Martins. Hydrogen-powered aircraft: Fundamental concepts, key technologies, and environmental impacts. *Progress in Aerospace Sciences*, 141:100922, 2023. Special Issue on Green Aviation.
- [18] S. Choudhary, M. Vishwakarma, and S. Dwivedi. Evaluation and prevention of hydrogen embrittlement by ndt methods: A review. *Materials Proceedings*, 6:18, 05 2021.
- [19] A. Gomez and H. Smith. Liquid hydrogen fuel tanks for commercial aviation: Structural sizing and stress analysis. *Aerospace Science and Technology*, 95:105438, 2019.
- [20] A. Campari, F. Ustolin, A. Alvaro, and N. Paltrinieri. A review on hydrogen embrittlement and risk-based inspection of hydrogen technologies. *International Journal of Hydrogen Energy*, 48(90):35316–35346, 2023.
- [21] A. Nasrollahi, W. Deng, Z. Ma, and P. Rizzo. Multimodal structural health monitoring based on active and passive sensing. *Structural Health Monitoring*, 17(2):395–409, 2018.
- [22] R. Graue, M. Krisson, M. Erdmann, and A. Reutlinger. Integrated health monitoring approach for reusable cryogenic tank structures. *Journal of Spacecraft and Rockets*, 37(5):580–585, 2000.
- [23] J. Fu, Z. Cui, S. Yin, and T. Kundu. Acoustic source localization on the surface of a cylindrical pressure vessel. In Paul Fromme and Zhongqing Su, editors, *Health Monitoring of Structural and Biological Systems XIV*, volume 11381, page 113812S. International Society for Optics and Photonics, SPIE, 2020.
- [24] S. Kalafat and M.G.R. Sause. Acoustic emission source localization by artificial neural networks. *Structural Health Monitoring*, 14(6):633–647, 2015.
- [25] Fuel Cells and Hydrogen 2 Joint Undertaking. *Hydrogen-powered aviation - A fact-based study of hydrogen technology, economics, and climate impact by 2050*. Publications Office, 2020.

-
- [26] R. Meissner, P. Sieb, E. Wollenhaupt, S. Haberkorn, K. Wicke, and G. Wende. Towards climate-neutral aviation: Assessment of maintenance requirements for airborne hydrogen storage and distribution systems. *International Journal of Hydrogen Energy*, 48(75):29367–29390, 2023.
- [27] J. Moore, J. Durham, A. Eijk, E. Karakas, R. Kurz, J. Lesak, M. McBain, P. McCalley, L. Moroz, Z. Mohamed, B. Pettinato, G. Phillippi, H. Watanabe, and B. Williams. Chapter 9 - compressors and expanders. In Klaus Brun and Timothy Allison, editors, *Machinery and Energy Systems for the Hydrogen Economy*, pages 333–424. Elsevier, 2022.
- [28] G.U. Ingale, H.-M. Kwon, S. Jeong, D. Park, W. Kim, B. Bang, Y.-I. Lim, S.W. Kim, Y.-B. Kang, J. Mun, S. Jun, and U. Lee. Assessment of greenhouse gas emissions from hydrogen production processes: Turquoise hydrogen vs. steam methane reforming. *Energies*, 15(22), 2022.
- [29] S. Sadeghi and S. Ghandehariun. Environmental impacts of a standalone solar water splitting system for sustainable hydrogen production: A life cycle assessment. *International Journal of Hydrogen Energy*, 48(50):19326–19339, 2023.
- [30] M.-S Kim, T. Lee, Y. Son, J. Park, M. Kim, H. Eun, J.-W. Park, and Y. Kim. Metallic material evaluation of liquid hydrogen storage tank for marine application using a tensile cryostat for 20 k and electrochemical cell. *Processes*, 10(11), 2022.
- [31] T. Burschky, Y. Cabac, D. Silberhorn, B. Boden, and B. Nagel. Liquid hydrogen storage design trades for a short-range aircraft concept. *CEAS Aeronautical Journal*, 14:879–893, 2023.
- [32] E.W. Baumann, R.S. Becker, P.J. Ellerbrock, and S.W. Jacobs. DC-XA structural health-monitoring system. In Janet M. Sater, editor, *Smart Structures and Materials 1997: Industrial and Commercial Applications of Smart Structures Technologies*, volume 3044, pages 195 – 206. International Society for Optics and Photonics, SPIE, 1997.
- [33] S.E. Hosseini. Chapter 5 - hydrogen storage and delivery challenges. In S.E. Hosseini, editor, *Fundamentals of Hydrogen Production and Utilization in Fuel Cell Systems*, pages 237–254. Elsevier, 2023.
- [34] W. Xu, Q. Li, and M. Huang. Design and analysis of liquid hydrogen storage tank for high-altitude long-endurance remotely-operated aircraft. *International Journal of Hydrogen Energy*, 40(46):16578–16586, 2015.
- [35] CORDIS. Composite conformal liquid h2 tank. <https://cordis.europa.eu/project/id/101101404>, February 2023. Accessed: February 2024.
- [36] NLR. Case: Liquid hydrogen composite tanks for civil aviation. <https://www.nlr.org/case/case-liquid-hydrogen-composite-tanks-for-civil-aviation/>. Accessed: February 2024.
- [37] Composites World. Composites in hydrogen storage. <https://www.compositesworld.com/kc/cw-collections/composites-hydrogen-storage>. Accessed: February 2024.

- [38] D. Kang, S. Yun, and B. Kim. Review of the liquid hydrogen storage tank and insulation system for the high-power locomotive. *Energies*, 15(12), 2022.
- [39] C. Buyck. H2fly’s breakthrough flight demonstration bolsters the case for liquid hydrogen propulsion. <https://www.futureflight.aero/news-article/2023-09-13/h2fllys-breakthrough-flight-demonstration-bolsters-case-liquid-hydrogen>, September 2023. Accessed: February 2024.
- [40] Collins Aerospace. Collins aerospace to lead the development of thermoplastics for liquid hydrogen tanks. <https://www.collinsaerospace.com/news/news/2023/03/collins-aerospace-to-lead-the-development-of-thermoplastics-for-liquid-hydrogen-tank>, March 2023. Accessed: February 2024.
- [41] S.K. Manwatkar, M. Sunil, A. Prabhu, S.V.S. Narayana Murty, R. Joseph, and P. Ramesh Narayanan. Effect of grain size on the mechanical properties of aluminum alloy aa2219 parent and weldments at ambient and cryogenic temperature. *Transactions of the Indian Institute of Metals*, 72(6):1515–1519, Jun 2019.
- [42] N. Nayan, G. Singh, D. Baunthiyal, S.V.S. Narayana Murty, T.A. Prabhu, and S.K. Singh. Mechanical properties of cryo-rolled aluminium alloy aa2219 at 300, 77 and 20 k. *Materials Science and Engineering: A*, 881:145399, 2023.
- [43] H.J. Pasma and W.J. Rogers. Safety challenges in view of the upcoming hydrogen economy: An overview. *Journal of Loss Prevention in the Process Industries*, 23(6):697–704, 2010. Papers Presented at the 2009 International Symposium of the Mary Kay O’Connor Process Safety Center.
- [44] J. Leachman. Cryogenic hydrogen embrittlement. <https://hydrogen.wsu.edu/2019/02/18/cryogenic-hydrogen-embrittlement/>, February 2019. Accessed: February 2024.
- [45] M.-S. Kim and K.W. Chun. A comprehensive review on material compatibility and safety standards for liquid hydrogen cargo and fuel containment systems in marine applications. *Journal of Marine Science and Engineering*, 11(10), 2023.
- [46] Office of Safety and Mission Assurance. Safety standard for hydrogen and hydrogen systems: Guidelines for hydrogen system design, materials selection, operations, storage and transportation. Technical Report 97N29521, NASA, January 1997.
- [47] R.E. Smallman and R.J. Bishop. Chapter 7 - mechanical behaviour of materials. In R.E. Smallman and R.J. Bishop, editors, *Modern Physical Metallurgy and Materials Engineering (Sixth Edition)*, pages 197–258. Butterworth-Heinemann, Oxford, sixth edition edition, 1999.
- [48] J.A. Lee and S. Woods. Hydrogen embrittlement. Technical Report JSC-CN-36009, NASA, April 2016.
- [49] F. Qiu, Z.n Shen, Y. Bai, G. Shan, D. Qu, and W. Chen. Hydrogen defect acoustic emission recognition by deep learning neural network. *International Journal of Hydrogen Energy*, 54:878–893, 2024.

-
- [50] W.T. Chandler. Hydrogen embrittlement and its control in hydrogen-fueled engine systems. In *NASA. Langley Res. Center Recent Advan. in Structures for Hypersonic Flight, Pt. 1*. NASA, January 1978.
- [51] F.C. Rivet. *Hydrogen embrittlement of Aluminum-Lithium alloys*. PhD thesis, Virginia Tech, 1990.
- [52] J. Turner, S. Contaut, A. Tarantino, and A. Masson. Cryogenic hydrogen fuel system and storage: Roadmap report. March 2022.
- [53] R. Ahmad and S. Kamaruddin. An overview of time-based and condition-based maintenance in industrial application. *Computers & Industrial Engineering*, 63(1):135–149, 2012.
- [54] S.K. Al-Jumaili, M.R. Pearson, K.M. Holford, M.J. Eaton, and R. Pullin. Acoustic emission source location in complex structures using full automatic delta t mapping technique. *Mechanical Systems and Signal Processing*, 72-73:513–524, 2016.
- [55] J. Chen, B. Liu, and H. Zhang. Review of fiber bragg grating sensor technology. *Frontiers of Optoelectronics in China*, 4(2):204–212, Jun 2011.
- [56] L. Oluwole, A. Olanipekun, and O.O. Ajide. Design, construction and testing of a strain gauge instrument. *Int. J. Sci. Eng. Res. 6 1825-9*, 6:1825–1829, 04 2015.
- [57] H. Choi, S. Choi, and H. Cha. Structural health monitoring system based on strain gauge enabled wireless sensor nodes. In *2008 5th International Conference on Networked Sensing Systems*, pages 211–214, 2008.
- [58] F. Bu, L. Xue, M. Zhai, X. Huang, J. Dong, N. Liang, and C. Xu. Evaluation of the characterization of acoustic emission of brittle rocks from the experiment to numerical simulation. *Scientific Reports*, 12(1):498, Jan 2022.
- [59] J. Hensman, R. Mills, S.G. Pierce, K. Worden, and M. Eaton. Locating acoustic emission sources in complex structures using gaussian processes. *Mechanical Systems and Signal Processing*, 24(1):211–223, 2010.
- [60] S. Cantero-Chinchilla, G. Aranguren, J. Royo, M. Chiachio, J. Etxaniz, and A. Calvo-Echenique. Structural health monitoring using ultrasonic guided-waves and the degree of health index. *Sensors*, 21:993, 02 2021.
- [61] L.F. Friedrich, A.S. Cezar, A.B. Colpo, B.N.R. Tanzi, M. Sobczyk, G. Lacidogna, G. Niccolini, L.E. Kostaski, and I. Iturrioz. Long-range correlations and natural time series analyses from acoustic emission signals. *Applied Sciences*, 12(4), 2022.
- [62] T. Kundu. Acoustic source localization. *Ultrasonics*, 54(1):25–38, 2014.
- [63] A.-D. Nguyen and V. Godinez. 7 - integrated health and corrosion monitoring systems in the aerospace industry. In Samuel Benavides, editor, *Corrosion Control in the Aerospace Industry*, Woodhead Publishing Series in Metals and Surface Engineering, pages 151–171. Woodhead Publishing, 2009.

- [64] H. Speckmann and R. Henrich. Structural health monitoring (shm) - overview on technologies under development. 16th World Conference on NDT, 2004.
- [65] A. Ohmori K. Horikawa, K. Yoshida and K. Sakamaki. Acoustic emission caused by environmental embrittlement of an al-mg-si alloy. *Journal of Acoustic Emission*, 21:206–212, 2004.
- [66] Y. You, Q. Teng, Z. Zhang, and Q. Zhong. The effect of hydrogen on the deformation mechanisms of 2.25cr-1mo low alloy steel revealed by acoustic emission. *Materials Science and Engineering: A*, 655:277–282, 2016.
- [67] O. Shapovalov, M. Gaal, G. Hönig, T. Gradt, and S. Weiss. Temperature dependence of the propagation speed of a longitudinal wave in different solids for use as a wedge material in an extreme-temperature-resistant ultrasonic transducer. 09 2019.
- [68] J. Nunn. Measuring young’s modulus the easy way, and tracing the effects of measurement uncertainties. *Physics Education*, 50(5):538, aug 2015.
- [69] H. Nomura, K. Takahisa, K. Koyama, and T. Sakai. Acoustic emission from superconducting magnets. *Cryogenics*, 17(8):471–481, 1977.
- [70] M.T. Thompson. Chapter 16 - noise. In Marc T. Thompson, editor, *Intuitive Analog Circuit Design (Second Edition)*, pages 617–643. Newnes, Boston, second edition edition, 2014.
- [71] M. Ju, Z. Dou, J.-W. Li, X. Qiu, B. Shen, D. Zhang, F.-Z. Yao, W. Gong, and K. Wang. Piezoelectric materials and sensors for structural health monitoring: Fundamental aspects, current status, and future perspectives. *Sensors*, 23(1), 2023.
- [72] S. Jinachandran and G. Rajan. Fibre bragg grating based acoustic emission measurement system for structural health monitoring applications. *Materials*, 14(4), 2021.
- [73] K. Tada and H. Yuki. Detection of acoustic emission signals with the fabry-perot interferometer type optical fiber sensor. *Journal of Acoustic Emission*, 2017.
- [74] L. Jianxun, P. Zhao, P. Wei, H. Yuan, and H. Xu. 252.8 °c liquid hydrogen acoustic emission experiment in simulated aerospace fuel tank. *IEEE Transactions on Industrial Electronics*, 71(2):2122–2132, 2024.
- [75] P. Wei, X. Han, D. Xia, T. Liu, and H. Lang. Novel fiber-optic ring acoustic emission sensor. *Sensors*, 18(1), 2018.
- [76] V.G. Smirnov and Y.F. Solntsev. The use of acoustic emission for determination of fracture toughness at cryogenic temperatures. *Strength of Materials*, 22(11):1582–1586, Nov 1990.
- [77] A.J. Brunner. A review of approaches for mitigating effects from variable operational environments on piezoelectric transducers for long-term structural health monitoring. *Sensors*, 23(18), 2023.
- [78] S. Torkamani, S. Roy, M. Barkey, E. Sazonov, S. Burkett, and S. Kotru. A novel damage index for damage identification using guided waves with application in laminated composites. *Smart Materials and Structures*, 23:095015, 08 2014.

-
- [79] L. Draudviliene, R. Raišutis, E. Žukauskas, and A. Jankauskas. Validation of dispersion curve reconstruction techniques for the a₀ and s₀ modes of lamb waves. *International Journal of Structural Stability and Dynamics*, 14:1450024, 05 2014.
- [80] Y.I. Hwang, D. Sung, H.J. Kim, S.J. Song, K.B. Kim, and S.S. Kang. Propagation and attenuation characteristics of an ultrasonic beam in dissimilar-metal welds. *Sensors*, 2020.
- [81] K. Ono. A comprehensive report on ultrasonic attenuation of engineering materials, including metals, ceramics, polymers, fiber-reinforced composites, wood, and rocks. *Applied Sciences*, 10(7), 2020.
- [82] N. Seckel and A. Singh. Physics of 3d ultrasonic sensors, 07 2019.
- [83] Iowa State University. Theory behind acoustic waves. <https://www.nde-ed.org/NDETechniques/AcousticEmission/index.xhtml>. Accessed: May 2024.
- [84] E. Fjær, R.M. Holt, P. Horsrud, A.M. Raaen, and R. Risnes. Chapter 5 - elastic wave propagation in rocks. In *Petroleum Related Rock Mechanics*, volume 72 of *Developments in Petroleum Science*, pages 259–318. Elsevier, 2021.
- [85] D.G. Aggelis, M.G.R. Sause, P. Packo, R. Pullin, S. Grigg, T. Kek, and Y.-K. Lai. *Acoustic Emission*, pages 175–217. Springer International Publishing, Cham, 2021.
- [86] S. Hautala. *Physics across oceanography: Fluid mechanics and waves*. UW Pressbooks, 2020.
- [87] M. Metzenmacher, A. Beugholt, D. Geier, and T. Becker. Combined longitudinal and surface acoustic wave analysis for determining small filling levels in curved steel containers. *Sensors*, 2002.
- [88] F. Piñal Moctezuma, M. Delgado Prieto, and L. Romeral Martínez. Performance analysis of acoustic emission hit detection methods using time features. *IEEE Access*, 7:71119–71130, 2019.
- [89] G. Āšwit, A Adamczak, and A Krampikowska. Time-frequency analysis of acoustic emission signals generated by the glass fibre reinforced polymer composites during the tensile test. *IOP Conference Series: Materials Science and Engineering*, 251(1):012002, oct 2017.
- [90] A. Boniface, J. Saliba, Z.M. Sbartá, N. Ranaivomanana, and J.-P. Balayssac. Evaluation of the acoustic emission 3d localisation accuracy for the mechanical damage monitoring in concrete. *Engineering Fracture Mechanics*, 223:106742, 2020.
- [91] M.R. Pearson, M. Eaton, C. Featherston, R. Pullin, and K. Holford. Improved acoustic emission source location during fatigue and impact events in metallic and composite structures. *Structural Health Monitoring*, 16(4):382–399, 2017.
- [92] R. Unnthorsson. *Hit Detection and Determination in AE Bursts*, pages 1–19. 03 2013.
- [93] P. Li, K. Dai, T. Zhang, Y. Jin, Y. Liu, and Y. Liao. An accurate and efficient time delay estimation method of ultra-high frequency signals for partial discharge localization in substations. *Sensors*, 18(10), 2018.

- [94] S. Adrián-Martínez, M. Bou-Cabo, I. Felis, C.D. Llorens, J.A. Martínez-Mora, M. Saldaña, and M. Ardid. Acoustic signal detection through the cross-correlation method in experiments with different signal to noise ratio and reverberation conditions. In M. Garcia Pineda, J. Lloret, S. Papavassiliou, S. Ruehrup, and C.B. Westphall, editors, *Ad-hoc Networks and Wireless*, pages 66–79, Berlin, Heidelberg, 2015. Springer Berlin Heidelberg.
- [95] F. Piñal-Moctezuma, M. Delgado-Prieto, and L. Romeral-Martínez. An acoustic emission activity detection method based on short-term waveform features: Application to metallic components under uniaxial tensile test. *Mechanical Systems and Signal Processing*, 142:106753, 2020.
- [96] Q.-Q. Ni and M. Iwamoto. Wavelet transform of acoustic emission signals in failure of model composites. *Engineering Fracture Mechanics*, 69(6):717–728, 2002.
- [97] J. Jingpin, W. Bin, and H. Cunfu. Acoustic emission source location methods using mode and frequency analysis. *Structural Control and Health Monitoring*, 15(4):642–651, 2008.
- [98] L. Pazdera and J. Smutný. Identification and analysis of acoustic emission signals by cohen’s class of time frequency distribution. <https://www.ndt.net/article/wcndt00/papers/idn063/idn063.htm>. Accessed: March 2024.
- [99] W. Yang, X. Li, Y. Wang, Y. Zheng, and P. Guo. Novel method for detecting weak acoustic emission signals based on the similarity of time-frequency spectra. *Geophysics*, 87(2):V143–V154, 02 2022.
- [100] F. Hassan, A.K. Mahmood, N. Yahya, Z. Khan, and M. Rimsan. State-of-the-art review on the acoustic emission source localization techniques. *IEEE Access*, 9, 07 2021.
- [101] G.N. Morscher. Modal acoustic emission of damage accumulation in woven sic/sic at elevated temperatures. Technical Report 19990027825, NASA Lewis Research Center, August 1998.
- [102] L. Zhang, H. Ji, L. Liu, and J. Zhao. Time-frequency domain characteristics of acoustic emission signals and critical fracture precursor signals in the deep granite deformation process. *Applied Sciences*, 11(17), 2021.
- [103] G. Lacidogna, G. Piana, and A. Carpinteri. Acoustic emission and modal frequency variation in concrete specimens under four-point bending. *Applied Sciences*, 7(4), 2017.
- [104] H. Zheng, X. Zeng, J. Zhang, and H. Sun. *The Application of Carbon Fiber Composites in Cryotank*. 03 2018.
- [105] C. Wilkerson. Acoustic emission monitoring of the dc-xa composite liquid hydrogen tank during structural testing. Technical Report 97N11094, NASA, October 1996.
- [106] 22 - storage. In S. Mannan, editor, *Lees’ Loss Prevention in the Process Industries (Third Edition)*, pages 22/1–22/78. Butterworth-Heinemann, Burlington, third edition edition, 2005.

-
- [107] A. Prathuru, N. Faisal, J. Steel, and S. Jihan. Application of pencil lead break (plb) point source in the detection of interfacial defects in adhesive bonds. *Journal of Non-destructive Evaluation*, 41(4):65, Sep 2022.
- [108] M. Sause. Investigation of pencil-lead breaks as acoustic emission sources. *Journal of Acoustic Emission*, 29:184–196, 01 2011.
- [109] M. Hamstad. Acoustic emission signals generated by monopole (pencil lead break) versus dipole sources: Finite element modeling and experiments. *Journal of Acoustic Emission*, 25:92–106, 01 2007.
- [110] M. Innes, C. Davis, C. Rosalie, P. Norman, and N. Rajic. Acoustic emission detection and characterisation using networked fbg sensors. *Procedia Engineering*, 188:440–447, 2017. Structural Health Monitoring - From Sensing to Diagnosis and Prognosis.
- [111] F. Tanvir, T. Sattar, D. Mba, and G. Edwards. Identification of fatigue damage evaluation using entropy of acoustic emission waveform. *SN Applied Sciences*, 2(1), dec 2019.
- [112] D.B. Duthie and F. Gabriels. Acoustic emission noise sources during storage tank floor corrosion tests. In *e-Journal of Nondestructive Testing (eJNDT)*. 11th European Conference on Non-Destructive Testing (ECNDT 2014), October 2014.
- [113] A. Schroeder Pedersen. Materials for cryogenic storage of hydrogen and natural gas, Feb 1997.
- [114] V. Barat, Y. Borodin, and A. Kuzmin. Intelligent ae signal filtering methods. *Journal of Acoustic Emission*, 28:109–119, 01 2010.
- [115] D. Liu, H. Yang, B. Wang, and S. Grigg. Hydrogen induced cracks monitored with acoustic emission under the laboratory condition. In *e-Journal of Nondestructive Testing (eJNDT)*, volume 28. EWGAE35 & ICAE10 conference on acoustic emission testing, 2023.
- [116] D. Merson, S. Dement'ev, A. Ioffe, Pa. Suvorov, and A. Vinogradov. Acoustic emission during hydrogen charging of a pipeline steel. *ISIJ International*, 51(10):1682–1687, 2011.
- [117] C. Wachowski, J.-W. Biermann, and R. Schala. Approaches to analyse and predict slosh noise of vehicle fuel tanks. In *24th international conference of noise and vibration Engineering (ISMA2010)*. Belgium, 2010.
- [118] G. Siva Teja, C. Saurav Vara Prasad, B. Venkatesham, and K. Sri Rama Murty. Identification of sloshing noises using convolutional neural networka). *The Journal of the Acoustical Society of America*, 149(5):3027–3041, 05 2021.
- [119] G. Siva Teja and B. Venkatesham. Experimental study on the effect of centrally positioned vertical baffles on sloshing noise in a rectangular tank. *Applied Acoustics*, 176:107890, 2021.

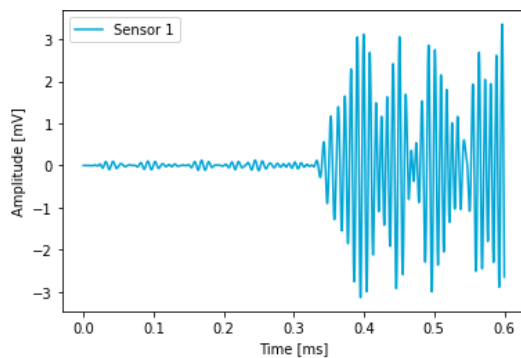
- [120] N. Zhao, C. Li, H. Jia, F. Wang, Z. Zhao, L. Fang, and X. Li. Acoustic emission-based flow noise detection and mechanism analysis for gas-liquid two-phase flow. *Measurement*, 179:109480, 2021.
- [121] S.Y. Chuang. Real-time aircraft structural monitoring using acoustic emission. In D.O. Thompson and D.E. Chimenti, editors, *Review of Progress in Quantitative Nondestructive Evaluation*, pages 371–377, Boston, MA, 1987. Springer US.
- [122] R.S. Geng. Application of acoustic emission for aviation industry - problems and approaches. 2004.
- [123] W.H. Lewis Jr., C.D. Bailey, and W.M. Pless. Acoustic emission structure-borne noise measurements on aircraft during flight. Technical Report AFML-TR-75-185, Lockheed-Georgia Company, May 1976.
- [124] S. L. S.L. McBride and J.W. Maclachlan. *Effect of Crack Presence on In-Flight Airframe Noises in a Wing Attachment Component*, pages 517–531. Springer US, Boston, MA, 1983.
- [125] E.v.K. Hill and C.L. Rovik. In-flight fatigue crack growth monitoring in a cessna t-303 crusader vertical tail. 2016.
- [126] G.G. Martin. Characteristics of noise attenuators for use in acoustic emission studies. *Ultrasonics*, 21(3):127–133, 1983.
- [127] S.K. Nayak and K.C. Biswal. Fluid damping in rectangular tank fitted with various internal objects - an experimental investigation. *Ocean Engineering*, 108:552–562, 2015.
- [128] G. Lackner and P. Tscheliesnig. Acoustic emission testing on flat-bottomed storage tanks: how to condense acquired data to a reliable statement regarding floor condition. *Journal of Acoustic Emission*, 2012.
- [129] Rigol. Rigol ds1104z plus 4ch, 100mhz, 1gsa/s digital oscilloscope – mso ready. <https://www.rigol-uk.co.uk/product/rigol-ds1104z-plus-100mhz-digital-oscilloscope-mso-ready/>. Accessed: May 2024.
- [130] M. Rosenblum, A. Pikovsky, A.A. Kühn, and J.L. Busch. Real-time estimation of phase and amplitude with application to neural data. *Scientific Reports*, 11(1):18037, Sep 2021.
- [131] C. Suhendi, M.R.P. Sudibyoy, I.F. Erlangga, and A.P. Arbad. Automatic event identification from tectonic earthquakes with modified akaike information criterion (maic). *IOP Conference Series: Earth and Environmental Science*, 258(1):012037, apr 2019.
- [132] R. Malaeb, E. Mahfoud, and M. Harb. Decomposition of fundamental lamb wave modes in complex metal structures using comsol®. 10 2018.
- [133] S.W. Ellingson. *Electromagnetics, Vol. 2*. Virginia Tech Publishing, 2020.

-
- [134] H. Carreón. Ultrasonic velocity testing of steel pipeline welded joints. In H. Felix Wu, Andrew L. Gyekenyesi, Peter J. Shull, and Tzu-Yang Yu, editors, *Nondestructive Characterization and Monitoring of Advanced Materials, Aerospace, and Civil Infrastructure 2017*, volume 10169, page 1016922. International Society for Optics and Photonics, SPIE, 2017.
- [135] H. Li, L. Geng, L. Zhang, and Y. Shi. The acoustic emission source localization in the pipeline network with consideration of radial position of defect. *Journal of Physics: Conference Series*, 2185(1):012019, January 2022.
- [136] Z.-L. Zhou, J. Zhou, L.-J. Dong, X. Cai, Y.-C. Rui, and C.-T. Ke. Experimental study on the location of an acoustic emission source considering refraction in different media. *Scientific Reports*, 7(1):7472, August 2017.
- [137] A. Hemmati-Sarapardeh, A. Larestani, M.N. Amar, and S. Hajirezaie. Chapter 1 - introduction. In A. Hemmati-Sarapardeh, A. Larestani, M.N. Amar, and S. Hajirezaie, editors, *Applications of Artificial Intelligence Techniques in the Petroleum Industry*, pages 1–22. Gulf Professional Publishing, 2020.
- [138] P.M. Reed, A. Hadjimichael, K. Malek, T. Karimi, C.R. Vernon, V. Srikrishnan, R.S. Gupta, D.F. Gold, B. Lee, K. Keller, T.B. Thurber, and J.S. Rice. *Addressing Uncertainty in Multisector Dynamics Research*. Zenodo, 2022.
- [139] H. Chang, E. Han, J.Q. Wang, and W. Ke. Acoustic emission study of corrosion fatigue crack propagation mechanism for ly12cz and 7075-t6 aluminum alloys. *Journal of Materials Science*, 40(21):5669–5674, November 2005.
- [140] X. Yao, B.S. Vien, C. Davies, and W.K. Chiu. Acoustic emission source characterisation during fatigue crack growth in al 2024-t3 specimens. *Sensors*, 22(22), 2022.
- [141] G. Shen, L. Li, and W. Zhang. Investigation on acoustic emission of hydrogen induced cracking for carbon steel used in pressure vessel. In *e-Journal of Nondestructive Testing (eJNDT)*, volume 13. 17th world conference on nondestructive testing, 2008.
- [142] B.B. Liao, D.L. Wang, M. Hamdi, J.Y. Zheng, P. Jiang, C.H. Gu, and W.R. Hong. Acoustic emission-based damage characterization of 70 mpa type iv hydrogen composite pressure vessels during hydraulic tests. *International Journal of Hydrogen Energy*, 44(40):22494–22506, 2019. Special Issue on Hydrogen Fire, Explosion and Safety Standards (ISHFESS2018).
- [143] R.S.M. Almeida, M.D. Magalhães, N. Karim, K. Tushtev, and K. Rezwan. Identifying damage mechanisms of composites by acoustic emission and supervised machine learning. *Materials & Design*, 227:111745, 2023.
- [144] P.J. de Groot, P.A.M. Wijnen, and R.B.F. Janssen. Real-time frequency determination of acoustic emission for different fracture mechanisms in carbon/epoxy composites. *Composites Science and Technology*, 55(4):405–412, 1995.

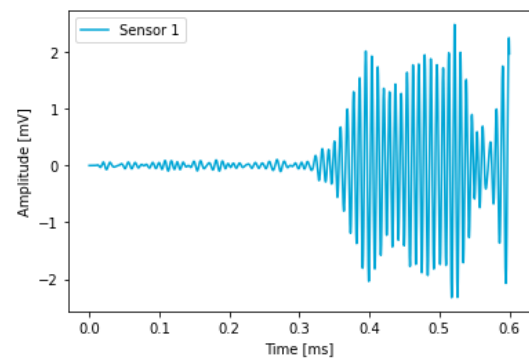
Appendix A

Examples of received **AE** waves

This appendix consists of visualisation of the received **AE** signals where the **PLB** is placed on the inner tank of the flexible support (Figure A.1, A.2), the inner tank of the fixed support (Figure A.3) and on the outer tank of the flexible support (Figure A.4).

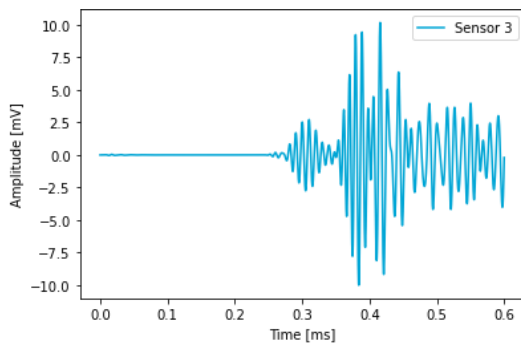


(a) **PLB** at 200.

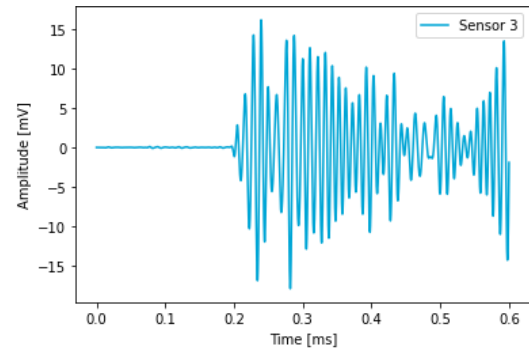


(b) **PLB** at 500.

Figure A.1: Examples of received waves by sensor 1 where the **PLB** is performed on the inner tank of the flexible support test setup.

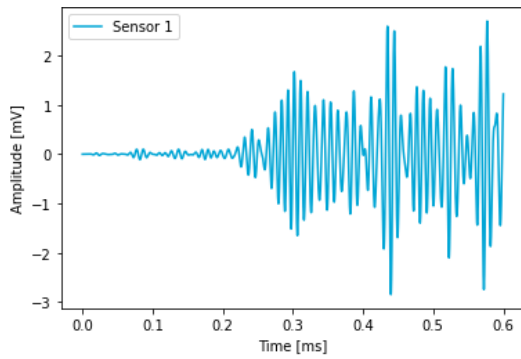


(a) PLB at 100 mm.

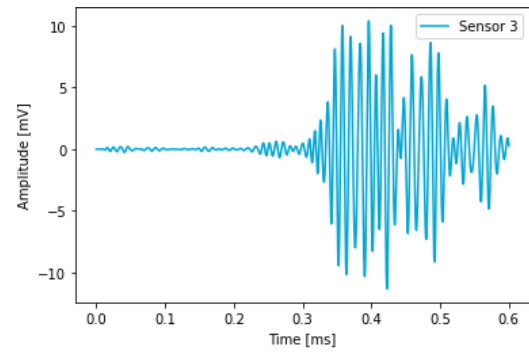


(b) PLB at 790 mm.

Figure A.2: Examples of received waves by sensor 3 where the PLB is performed on the inner tank of the flexible support test setup.

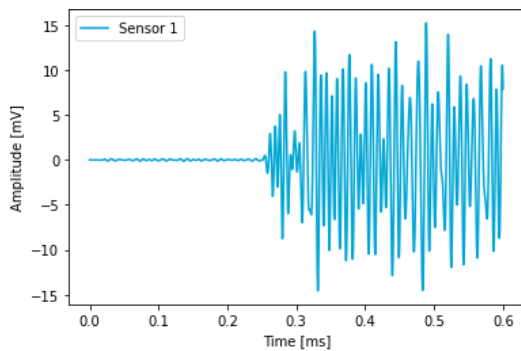


(a) Sensor 1, PLB at 30 mm.

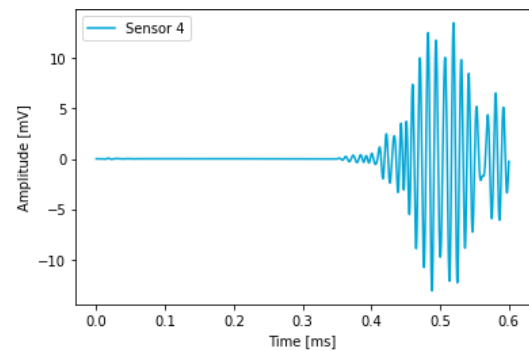


(b) Sensor 3, PLB at 150 mm.

Figure A.3: Examples of received waves by sensor 1 and 3 where the PLB is performed on the outer tank of the fixed support test setup.



(a) Sensor 1, PLB at 70 mm.



(b) Sensor 4, PLB at 730 mm.

Figure A.4: Examples of received waves by sensor 1 and 4 where the PLB is performed on the outer tank of the flexible support test setup.

Appendix B

Examples of signal onset determination

This appendix contains examples of signal onset determination for S0 and A0 waves (Figure B.1) and a visualisation of the improved onset determination using the AIC method in Figure B.2.

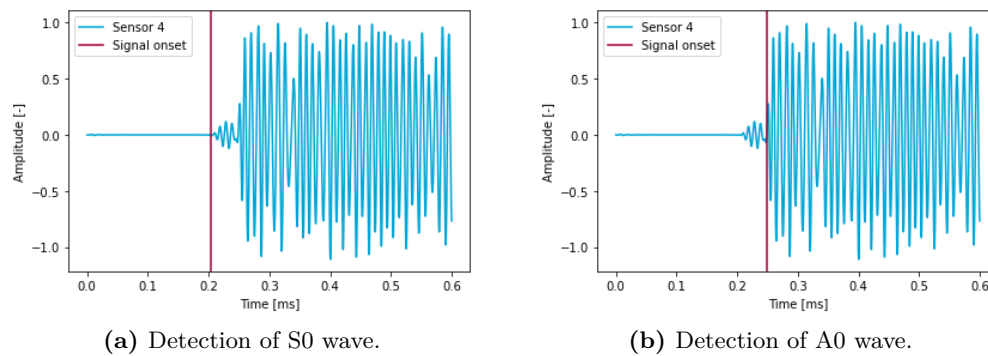


Figure B.1: Examples of signal onset detection (fixed support).

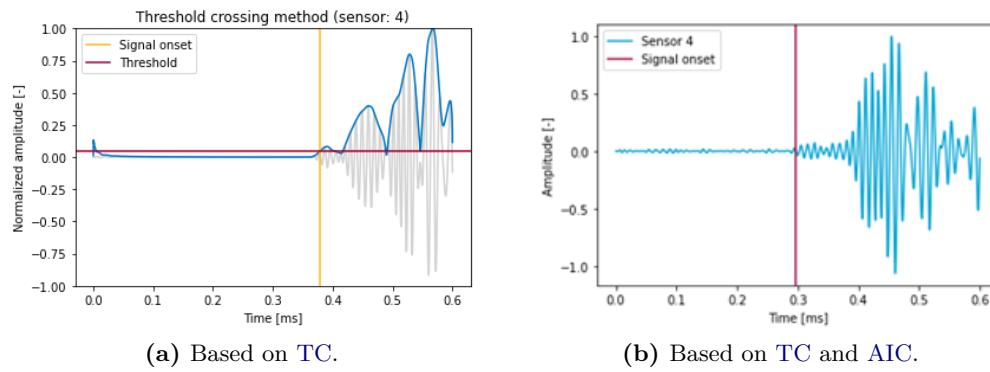


Figure B.2: The added accuracy (0.01 [ms]) of using AIC for signal onset determination (flexible support, S0 waves).

AE characteristics of crack growth in different materials

C.1 AE characteristics in aluminium

Table C.1: Waveform parameters of representative signals in aluminium.

Material	Event	Frequency [kHz]	Amplitude [dB]	Notes	Source
7076-T6	Fatigue crack growth	50-500 (peak at 100)	30-40 (pre-amp: 40)	Material tested in air	[139]
	Hydrogen induced cracking	50-700 (peak at 215)	30-40 (pre-amp: 40)	Material tested in aqueous solution, more activity than in air	
2024-T3	Crack extension	150-550	X	X	[140]
2219-T87	Fatigue crack extension	100-600	X	X	[6]
	Crack growth	X	>70	X	[14]
	Crack growth	X	59	X	[15]

C.2 AE characteristics in steel

Table C.2: Waveform parameters of representative signals in steel.

Material	Event	Frequency [kHz]	Amplitude [dB]	Energy [eV]	Notes	Source
4130X steel	Hydrogen permeation and diffusion causing dislocation propagation	250-350	44-58 (pre-amp: 40)	235	High counts	[49]
	Hydrogen induced cracking	50-150	50-68 (pre-amp: 40)	380	"Grain shedding and intergranular cracking"	
20R steel	Electrifying corrosion	80-180	45 (pre-amp: 40)	X	X	[141]
	"Cracking and peeling off of FeS layer during electrifying corrosion"	80-180	65 (pre-amp: 40)	X	X	
	Hydrogen induced cracking	80-180	75 (pre-amp: 40)	X	X	
A516 carbon steel	Corrosion	>250	X	X	X	[115]
	Hydrogen induced cracking	100-200	X	X	X	
09GSF pipeline steel	Formation of sulfide film on surface due to corrosion	100-150	X	X	X	[116]
	Hydrogen induced cracking	100-250	X	X	X	

C.3 AE characteristics in composites

Table C.3: Waveform parameters of representative signals in composites.

Material	Event	Frequency [kHz]	Amplitude [dB]	Energy [eV]	Notes	Source
High strength carbon fiber-epoxy layers wrapped on a polyamide liner	Matrix cracking	100-200	40-55 (pre-amp: 40)	0-12500	Tank (type IV) was used for hydrogen storage and subjected to AET after being onboard for 46500 [km]	[142]
	Fiber breakage	290-460	70-90 (pre-amp: 40)	>than the others		
	Fiber-matrix debonding	210-320	50-72 (pre-amp: 40)	12500-250000		
Ceramic matrix composite ("FW12 composite containing Nextel 610 DF-11 fiber fabric reinforcing an 85% Al ₂ O ₃ +15% 3YSZ matrix")	Matrix cracking	50-400	33-55	X	Experiments performed in lab conditions aiming to isolate different failure modes	[143]
	Fiber breakage	300-500	65-90	X		
	Fiber-matrix debonding	200-500	55-65	X		
Graphite/epoxy composites	Matrix cracking	50-150	X	X	X	[144]
	Fiber breakage	140-180	X	X	X	
Glass/polyester composites	Matrix cracking	30-150	X	X	X	[144]
	Fiber breakage	300-400	X	X	X	

Continued on next page

Table C.3 – continued from previous page

Material	Event	Frequency [kHz]	Amplitude [dB]	Energy [eV]	Notes	Source
	Fiber-matrix debonding	180-290	X	X	X	
Glass/polypropelene composites	Matrix cracking	X	40-55	X	X	[144]
	Fiber breakage	X	85-95	X	X	
	Fiber-matrix debonding	X	65-85	X	X	
Carbon/epoxy composites	Matrix cracking	< 300	X	X	X	[144]
	Fiber breakage	> 500	X	X	X	
	Fiber-matrix debonding	In the order of 300	X	X	X	

Appendix D

One-way sensitivity studies on inner tank damage localisation

This appendix contains the one-way sensitivity studies for simulated damage on the inner tank. The one-way sensitivity analysis is performed for the flexible support (Figure D.1) and for the fixed support (Figure D.2).

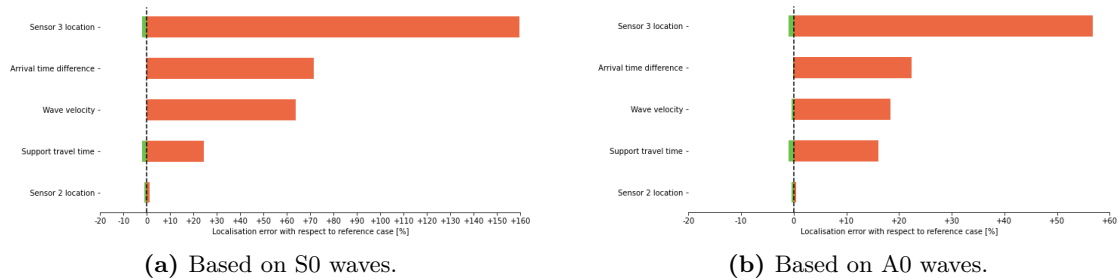


Figure D.1: One-way sensitivity study to determine the most influential input parameter on the average absolute localisation error of the flexible support test setup.

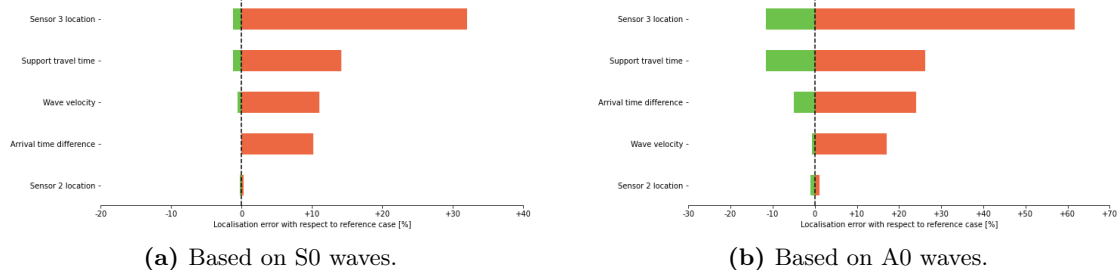


Figure D.2: One-way sensitivity study to determine the most influential input parameter for localisation on the fixed support test setup.

Appendix E

Monte Carlo simulations

In this appendix the Monte Carlo simulations will be discussed. This will be done per localisation experiment and subsequently per test setup and type of wave (S0 or A0). Two important errors that will be mentioned in this appendix are the reference error and the 90% error. The former refers to the error determined using the initial inputs and the latter refers to the error below which 90% of the determined errors fall.

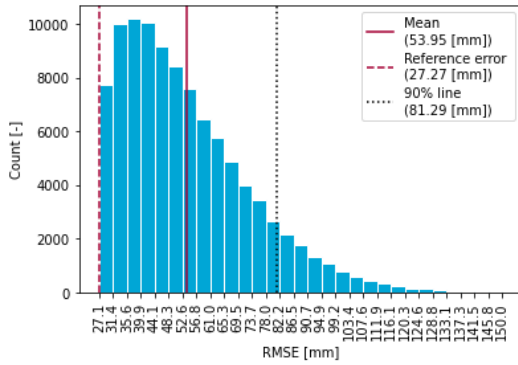
E.1 Experiment 3: Inner tank damage localisation

This section will show the inputs and the results of the Monte Carlo simulations on the localisation accuracy of PLBs performed on the inner tank.

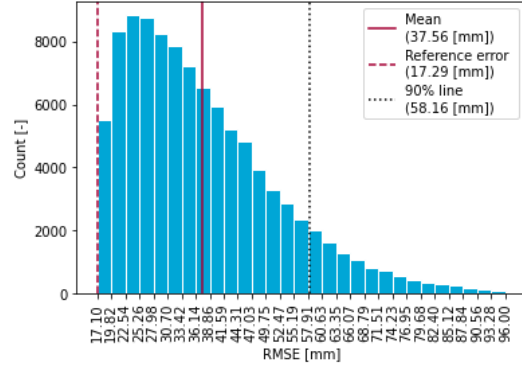
E.1.1 Flexible support test setup

Table E.1: Settings used in the Monte Carlo simulation for the inner tank damage localisation on the flexible support test setup.

Parameter	Based on S0 waves	Based on A0 waves
Support travel time [μs]	99.1 ± 14.49	87.5 ± 10.76
Wave velocity [m/s]	3691 ± 296.51	2711 ± 193.82
Location sensor 2 [mm]	10 ± 10	10 ± 10
Location sensor 3 [mm]	810 ± 10	810 ± 10
Wave arrival time difference sensor 1 and 3 [μs]	Calculated values ± 20	Calculated values ± 20
Number of iterations [-]	10^5	10^5



(a) Based on S0 waves.



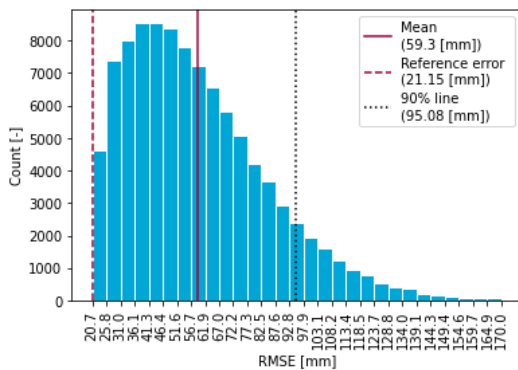
(b) Based on A0 waves.

Figure E.1: Results (RMSE) of the Monte Carlo simulation for the inner tank damage localisation on the flexible support test setup.

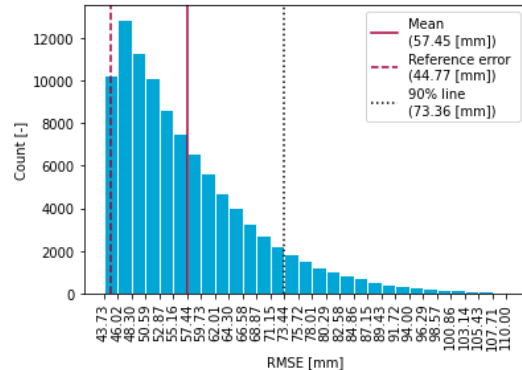
E.1.2 Fixed support test setup

Table E.2: Settings used in the Monte Carlo simulation for the inner tank damage localisation on the fixed support test setup.

Parameter	Based on S0 waves	Based on A0 waves
Support travel time [μs]	126.2 ± 24.40	134.8 ± 13.83
Wave velocity [m/s]	3411 ± 418.5	2641 ± 200.2
Location sensor 2 [mm]	10 ± 10	10 ± 10
Location sensor 3 [mm]	740 ± 10	740 ± 10
Wave arrival time difference sensor 1 and 3 [μs]	Calculated values ± 20	Calculated values ± 20
Number of iterations [-]	10^5	10^5



(a) Based on S0 waves.



(b) Based on A0 waves.

Figure E.2: Results (RMSE) of the Monte Carlo simulation for the inner tank damage localisation on the fixed support test setup.

E.2 Experiment 4a part 1: Outer tank 1D damage localisation

This section will show the inputs and the results of the Monte Carlo simulations on the 1D localisation accuracy of PLBs performed on the outer tank.

Table E.3: Settings used in the Monte Carlo simulation for the outer tank 1D damage localisation on the flexible support test setup.

Parameter	Based on S0 waves	Based on A0 waves
Wave velocity [m/s]	3551 ± 857	2461 ± 142
Location sensor 1 [mm]	0 ± 10	0 ± 10
Location sensor 2 [mm]	770 ± 10	770 ± 10
Location sensor 4 [mm]	220 ± 10	220 ± 10
Wave arrival time difference sensor 1 and 2 [μs]	Calculated values ± 20	Calculated values ± 20
Number of iterations [-]	10^5	10^5

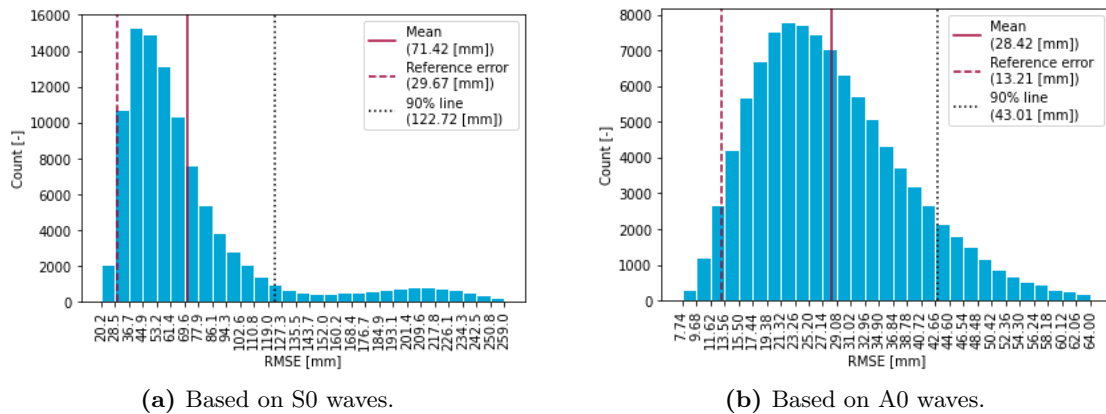


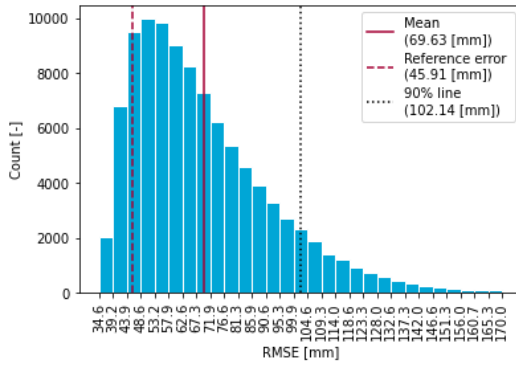
Figure E.3: Results (RMSE) of the Monte Carlo simulation for the outer tank 1D damage localisation on the flexible support test setup.

E.3 Experiment 4a part 2: Outer tank 1D damage localisation on a 2D area

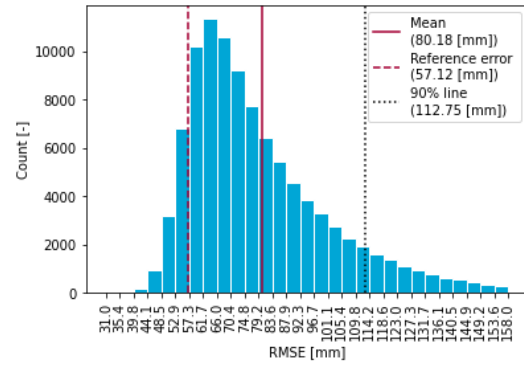
This section will show the inputs and the results of the Monte Carlo simulations on the 2D localisation accuracy of PLBs performed on the inner tank.

Table E.4: Settings used in the Monte Carlo simulation for the outer tank 1D damage localisation on a 2D area on the flexible support test setup.

Parameter	Based on S0 waves	Based on A0 waves
Wave velocity [m/s]	3916 ± 857	2941 ± 142
Location sensor 1 [mm]	0 ± 10	0 ± 10
Location sensor 2 [mm]	770 ± 10	770 ± 10
Location sensor 4 [mm]	220 ± 10	220 ± 10
Wave arrival time difference sensor 1 and 3 [μs]	Calculated values ± 20	Calculated values ± 20
Number of iterations [-]	10^5	10^5



(a) Based on S0 waves.



(b) Based on A0 waves.

Figure E.4: Results (RMSE) of the Monte Carlo simulation for the outer tank 1D damage localisation on a 2D area on the flexible support test setup.

E.4 Experiment 4b: Outer tank 2D damage localisation

Table E.5: Settings used in the Monte Carlo simulation for the outer tank 2D damage localisation on the flexible support test setup.

Parameter	Based on S0 waves	Based on A0 waves
Wave velocity [m/s]	3540 ± 857	2350 ± 142
X coordinate sensor 1 [mm]	0 ± 10	0 ± 10
X coordinate sensor 2 [mm]	156 ± 10	156 ± 10
X coordinate sensor 3 [mm]	770 ± 10	770 ± 10
X coordinate sensor 4 [mm]	156 ± 10	156 ± 10
Y coordinate sensor 1 [mm]	247 ± 10	247 ± 10
Y coordinate sensor 2 [mm]	403 ± 10	403 ± 10
Y coordinate sensor 3 [mm]	247 ± 10	247 ± 10
Y coordinate sensor 4 [mm]	92 ± 10	92 ± 10
Number of iterations [-]	200	200

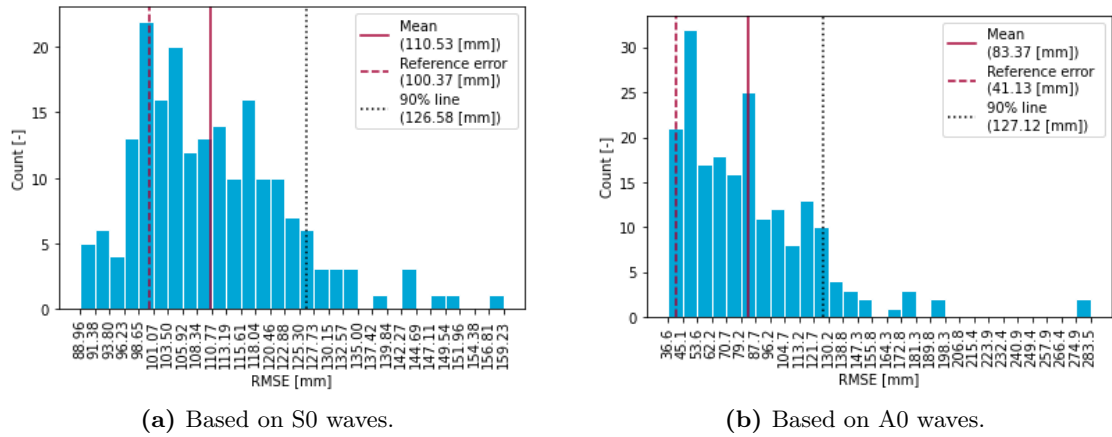
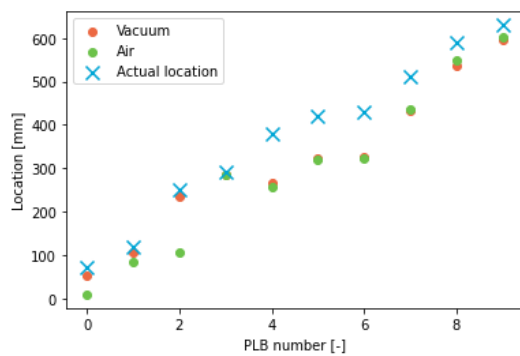


Figure E.5: Results of the Monte Carlo simulation for the outer tank 2D damage localisation on the flexible support test setup.

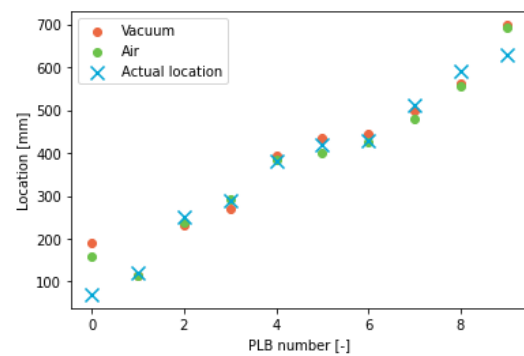
Appendix F

Influence of vacuum on the localisation accuracy

This appendix shows the influence of the vacuum between the inner and outer tank on the localisation of simulated damage on the inner tank of the flexible support test setup (Figure F.1).



(a) Based on S0 waves.



(b) Based on A0 waves.

Figure F.1: The effect of vacuum between the inner and outer tank on simulated damage on the inner tank of the flexible support test setup.